

User's Guide to the

HeatEx

Geothermal Reservoir Simulator

Final Technical Report:

Development of an Advanced Stimulation / Production Predictive Simulator for Enhanced Geothermal Systems

DOE Award Number DE-EE0002763

December 31, 2013

Prepared by:

John W. Pritchett Leidos, Inc. 10260 Campus Point Drive San Diego, California 92121

Tel: (858) 826-1628

E-mail: john.w.pritchett@leidos.com

Submitted to:

Department of Energy Golden Field Office 15013 Denver West Parkway Golden, Colorado 80401

DISCLAIMER

This report is based upon research supported in part by the U. S. Department of Energy under Award No. DE-EE0002763.

Any findings, opinions, conclusions and/or recommendations expressed in this report are those of the author alone and do not necessarily reflect the views of the Department of Energy.

ACKNOWLEDGEMENTS

This work was carried out by Leidos, Inc. in San Diego, California, assisted by subcontractor Geowatt AG of Zurich, Switzerland, under a research grant from the U. S. Department of Energy. The author expresses his deep appreciation to Prof. Thomas Kohl (now with the Karlsruhe Institute of Technology in Germany) and to Dr. Dieter Ollinger of Geowatt for their help with the fracture-modeling aspects of the work. Thanks are also due to Dr. Sabodh Garg of Leidos and to Prof. Ahmad Ghassemi of the University of Oklahoma in Norman for technical assistance and consultation. Two summer interns (Chakra Rawal and Xiaonan "Sonia" Wang), now completing their graduate studies at Texas A&M University, were also of considerable help in carrying out the research.

Financial support for this work was provided by the Geothermal Technologies Office of the U. S. Department of Energy (DOE-EERE) and by Leidos, Inc.

TABLE OF CONTENTS

1.	1. BACKGROUND			1
	1.1.	MOTIVA	TION	1
	1.2.	CENTRA	L TECHNICAL ISSUES	3
		1.2.1.	Fractures and Fracture Permeability	3 3 5 5
		1.2.2.	, C	5
		1.2.3.		5
		1.2.4.	Seismicity Issues	6
		1.2.5.		6
	1.3.	CODE DI	EVELOPMENT AND COMPUTING ENVIRONMENT	8
2.			TRUCTIONS	9
	2.1.		NICATING WITH THE SIMULATOR	9
	2.2.	-	UATION-OF-STATE	10
	2.3.		TOR PROBLEM SPECIFICATION	18
		2.3.1.	Minimum Input Specifications	20
		2.3.2.	The "VECTOR" Distribution Procedure	21
		2.3.3.	Setting the "World" Coordinate Context	23
		2.3.4.		24
		2.3.5.		33
		2.3.6.	Specifications of Initial Conditions	35
		2.3.7.	Specifying Formation Properties	37
		2.3.8.	Modeling Fracture Permeability	38
		2.3.9.	Modeling Subsurface Electrical Disturbances	41
		2.3.10.	Tracers Permanenting the Time History	46
		2.3.11.	1 0	48
		2.3.12.	1 1	51 51
		2.3.13.	1 &	
3.	3. ILLUSTRATIVE CALCULATIONS		55	
	3.1.		MENSIONAL ILLUSTRATIVE CASES 1, 2 AND 3	56
		3.1.1.		56
	2.2	3.1.2.	Computed Results for Cases 1 – 3	57
	3.2.		MENSIONAL ILLUSTRATIVE CASES 4 AND 5	64
		3.2.1	Problem Specifications	64
		3.2.2.		66
	2 2	3.2.3.	Computed results for Case 5 – central injection well DIMENSIONAL ILLUSTRATIVE CASE 6	70 80
	3.3.	3.3.1.		80
		3.3.1.	Case 6 Problem Specifications Computed Results for Case 6	94
	3.4.		OATA SETS FOR ILLUSTRATIVE CASES	105
	J. 4 .	3.4.1.	Case 1 Input Data Files	105
		3.4.1.	Case 2 Input Data Files Case 2 Input Data Files	103
		3.4.2.	Case 3 Input Data Files Case 3 Input Data Files	108
		3.4.3. 3.4.4.	Case 4 Input Data Files	108
		3.4.5.	Case 5 Input Data Files	115
		3.4.6.	Case 6 Input Data Files	116
1	DEBED		Case o Input Data I nes	
4.	REFER	LIVUE)		136

ILLUSTRATIONS

Fig. 1.1.	Examples of models with deterministic fracture zones subdivided into slip patches, and stochastically generated fractures.	4
Fig. 2.1.	Influence of pressure and temperature upon pure- H_2O fluid mass density ρ .	11
Fig. 2.2.	Influence of pressure and temperature upon pure- H_2O specific enthalpy H .	11
Fig. 2.3.	Influence of pressure and temperature upon pure- H_2O dynamic viscosity μ .	12
Fig. 2.4.	Influence of pressure and temperature upon pure- H_2O thermal conductivity κ .	12
Fig. 2.5.	Influence of pressure, temperature and salinity upon brine mass density ρ .	13
Fig. 2.6.	Influence of pressure, temperature and salinity upon brine specific enthalpy H .	14
Fig. 2.7.	Influence of pressure, temperature and salinity upon brine dynamic viscosity μ .	15
Fig. 2.8.	Influence of pressure, temperature and salinity upon brine thermal conductivity κ .	16
Fig. 2.9.	Effects of specified rotation angles upon the orientation of the thermohydraulic computational grid when viewed in the "World" coordinate system.	26
Fig. 2.10.	Geometry of a single "Conductive MINC" assembly of 15 concentric spherical "shells" solid rock surrounded by fluid.	of 29
Fig. 2.11.	Geometry of discretized "external aquifer" region adjoining one of the boundaries of the thermohydraulic grid.	e 32
Fig. 3.1.	Numerical smearing of sharp tracer fronts using conventional vs. second-order treatmer convection effects.	nt of 58
Fig. 3.2.	Distributions of fluid pressure and temperature at $t = 500$ days (Case 1).	60
Fig. 3.3.	Distributions of fluid pressure and temperature at $t = 500$ days (Case 2).	61
Fig. 3.4.	Distributions of fluid pressure and temperature at $t = 500$ days (Case 3).	62
Fig. 3.5.	Time-histories of tracer content and fluid temperature 0.5 km downstream from inlet – Cases 1, 2 and 3.	63
Fig. 3.6.	Horizontal problem geometry for two-dimensional Cases 4 and 5.	65
Fig. 3.7.	Case 4 – time-history of datum level pressure in central production well.	67
Fig. 3.8.	Case 4 – time-histories of pressure computed by HeatEx at sensor locations.	68
Fig. 3.9.	Case 4 – spatial distribution of pressure after 1000 days.	69

Fig. 3.10.	Case 5 – time-history of datum level pressure in central injection well as computed by	
	HeatEx.	71
Fig. 3.11.	Case 5 – time-histories of pressure computed by HeatEx at sensor locations.	72
Fig. 3.12.	Case 5 – time-histories of salinity computed by HeatEx at sensor locations.	73
Fig. 3.13.	Case 5 – time-histories of temperature computed by HeatEx at sensor locations.	74
Fig. 3.14.	Case 5 – spatial distributions of pressure, temperature and salinity after 100 days of injection.	76
Fig. 3.15.	Case 5 – spatial distributions of pressure, temperature and salinity after 200 days of injection.	77
Fig. 3.16.	Case 5 – spatial distributions of pressure, temperature and salinity after 400 days of injection.	78
Fig. 3.17.	Case 5 – spatial distributions of pressure, temperature and salinity after 800 days of injection.	79
Fig. 3.18.	Case 6 – overall problem geometry.	81
Fig. 3.19.	Case 6 – grid and wellfield geometry.	83
Fig. 3.20.	Case 6 – details of lower portion of well completions.	84
Fig. 3.21.	Case 6 – spatial distribution of fracture patches viewed from above.	92
Fig. 3.22.	Case 6 – spatial distribution of fracture patches viewed from south.	93
Fig. 3.23.	Case 6 – effectiveness of ten days of stimulation operations.	95
Fig. 3.24.	Case 6 – histories of well performance during first 60 days.	97
Fig. 3.25.	Case 6 – well diagnostic quantities during first 60 days.	100
Fig. 3.26.	Case 6 – histories of well performance.	103
Fig. 3.27.	Case 6 – well diagnostic quantities.	104

1. BACKGROUND

1.1. MOTIVATION

Reservoir engineering, whether practiced in the oil and gas industry, in the study of groundwater hydrology, or for the development of geothermal projects, has for many years depended upon numerical simulation techniques as a tool for the synthesis of diverse data sets and the development of predictive models for future reservoir performance. In all of these disciplines, the acquisition of pertinent data is expensive, difficult and time-consuming since the most valuable information can usually only be acquired by drilling. Geothermal projects suffer particularly from these difficulties, since the economic value of the resource being sought is relatively low on a per-unit-volume basis, the geological environments in which the resource is typically found are difficult to drill, and the resource usually lies at considerable depth.

Despite these difficulties, the development of the "conventional" geothermal power industry during the past century has been fairly encouraging, particularly during the last forty years or so after computer-aided reservoir engineering studies became feasible. Several computerized "geothermal reservoir simulator" programs have been developed and deployed such as TOUGH2 (*Pruess et al.*, 1997), TETRAD (*Shook and Renner*, 2002) and STAR (*Pritchett*, 1995), and geothermal reservoir engineers have been reasonably successful in using these tools together with field data acquisition campaigns to formulate forecasts and capacity estimates that have economic value. In this sense, it is probably fair to say that geothermal reservoir engineering is now finally beginning to catch up with the practice of reservoir engineering in the oil and gas industry.

But in terms of the overall electricity market, the geothermal power industry is only a very small player. In the United States (the world's leader in geothermal electricity generation), geothermal projects now total only about 3 gigawatts (GW) of installed generating capacity, while the annualized national electricity demand is about 470 GW. Worldwide, installed geothermal generating capacity totals less than 12 GW as compared to a worldwide annualized electricity consumption of about 2400 GW. Furthermore, despite the explosive growth in the demand for "clean", "renewable" and "carbon-free" electricity arising from looming fuel shortages, public safety concerns and the climate change threat, and exponential growth of both the wind and solar power industries, geothermal industry growth remains modest with an electricity market share (nationwide and worldwide) that is significantly less than 1%.

One of the main reasons for this disappointing performance is simply the scarcity of high-grade geothermal resources awaiting development. The U.S. Geological Survey recently estimated that perhaps 30 GW worth of conventional geothermal resources remain undeveloped in the United States (USGS, 2008), but even if the existing domestic industry were to increase in size by an order of magnitude by developing them all, geothermal generation would still be a relatively small component of the national electricity supply. The reason why geothermal systems that are suitable for electricity generation using conventional methods are hard to find is simply that the prerequisite combinations of natural high terrestrial heat flow, the presence of joints and faults, tectonic activity and volcanism, hot permeable rock at drillable depths capped

by an impermeable seal – as well as the presence of a nearby power market, since geothermal projects must be co-located with the resource – are relatively rare in nature.

As has been repeatedly pointed out by various authors, however (*Tester et al.*, 2006; *DOE*, 2008), if "Enhanced Geothermal Systems" (or "Engineered Geothermal Systems" – "EGS") were to become a practical alternative, it is highly likely that the role of geothermal in the nation's and the world's electricity supply would increase, perhaps substantially. Estimates as to how much improvement will occur are widely scattered (*Pritchett*, 2012) but it seems undeniable that there would be at least *some* improvement – so long as substantial amounts of electricity could be generated and brought to market at a reasonably competitive price.

There are several well-known obstacles to the successful deployment of EGS projects on a commercial scale, of course. EGS projects are expected to be deeper, on the average, than conventional "natural" geothermal reservoirs, and drilling costs are already a formidable barrier to conventional geothermal projects. Unlike conventional resources (which frequently announce their presence with natural manifestations such as geysers, hot springs and fumaroles), EGS prospects are likely to appear fairly undistinguished from the earth surface. And, of course, the probable necessity of fabricating a subterranean fluid circulation network to mine the heat from the rock (instead of simply relying on natural, pre-existing permeable fractures) adds a significant degree of uncertainty to the prospects for success.

As noted above, the presence of a decades-long tradition of geothermal reservoir engineering practice and of suitable computational tools to facilitate that discipline has undoubtedly played a major role in the success of the conventional geothermal industry as it exists today. But no comparable tools exist for EGS systems. Conventional hydrothermal reservoirs like The Geysers, Coso, Hatchobaru and Wairakei have relatively low pressures, often high *in-situ* steam contents and extraordinarily high temperatures at shallow depths due to gravity-driven upward thermal convection through natural vertical faults and fissures. The differences between such systems and what a "typical" EGS reservoir is likely to be like (if, indeed, anyone can say for certain what such a system would be like) are profound. Existing tools (like TOUGH2, TETRAD and STAR) that have provided such good service making forecasts for conventional systems are of little use for EGS systems.

Accordingly, the basic motivation for the work presented herein was to try to develop a new set of tools that would be more suitable for this purpose. Several years ago, the Department of Energy's Geothermal Technologies Office recognized this need and funded a cost-shared grant to our company (then SAIC, now Leidos) to partner with Geowatt AG of Zurich, Switzerland and undertake the development of a new reservoir simulator that would be more suitable for EGS forecasting than the existing tools. That project has now been completed and a new numerical geothermal reservoir simulator has been developed. It is named "HeatEx" (for "Heat Extraction") and is almost completely new, although its methodology owes a great deal to other previous geothermal software development efforts, including Geowatt's "HEX-S" code, the STAR and SPFRAC simulators developed here at SAIC/Leidos, the MINC approach originally developed at LBNL, and tracer analysis software originally formulated at INEL. Furthermore, the development effort was led by engineers with many years of experience in using reservoir simulation software to make meaningful forecasts for real geothermal projects, not just software designers. It is hoped that, as a result, HeatEx will prove useful during the

early stages of the development of EGS technology. The basic objective was to design a tool that could use field data that are likely to become available during the early phases of an EGS project (that is, during initial reconnaissance and fracture stimulation operations) to guide forecasts of the longer-term behavior of the system during production and heat-mining.

1.2. CENTRAL TECHNICAL ISSUES

1.2.1. Fractures and Fracture Permeability

Although most conventional "natural" geothermal reservoirs rely on permeable fractures through relatively hard rock to provide conduits for underground fluid flow (as contrasted to the intergranular permeability that predominates in sedimentary aquifers and typical oilbearing formations), in natural geothermal reservoirs these fractures are usually fairly closely spaced and are often propped open by continuous tectonic activity and microseismicity. They need little or no "maintenance" by the project operator. By contrast, with EGS it is anticipated that the stimulation and perhaps even the creation of fractures to serve as heat-exchanging fluid conduits will be a major technical challenge which will probably require continuous attention throughout the life of the project. Therefore, a suitable mathematical representation for the behavior of hard-rock fractures under these circumstances is an absolutely essential prerequisite to meaningful numerical reservoir simulation for EGS systems.

Biot (see e.g. *Biot*, 1941; *Biot and Willis*, 1957) was perhaps the first to develop a theoretical framework (i.e. theory of poroelasticity) for treating fluid diffusion through deformable geologic media. Later, the theory was extended by other workers to include nonlinear phenomena (see e.g. *Morland*, 1972; *Garg et al.*, 1977; *Garg*, 1987). The classical theory of Biot and its nonlinear extensions are limited to porous media with pore radii much smaller than the region of interest.

EGS applications typically involve fluid flow through fractured media. For these applications, it is necessary to extend the classical theory to dual media, i.e., high permeability fractured media embedded in low permeability matrix rock. Because of the complexity of the pertinent phenomena (e.g. nonlinear fracture opening and closing, fluid mass and heat exchange between the high permeability fractures and the surrounding low permeability rock matrix), it is possible to obtain analytical solutions only for highly simplified problems (see e.g. *Ghassemi et al.*, 2008). Several numerical models have also been developed to study the coupling of thermal, hydraulic, and mechanical response of an EGS reservoir (see e.g., *Kohl and Hopkirk*, 1995; *Kohl et al.*, 1995; *Noorishad and Tsang*, 1996; *Rutqvist et al.*, 2001). These numerical models have been used to simulate the response of a single fracture (or at most a few fractures) embedded in a porothermoelastic matrix, and are of limited utility for modeling the stimulation of an EGS reservoir.

More recently, *Kohl and Megel* (2005, 2007) developed the HEX-S code to simulate the transient hydro-mechanical response of an EGS reservoir to hydraulic injection. The code was used to successfully predict the pressure response and shearing locations for the September 2004 stimulation of the GPK4 well at the European Soultz-sous-Forets EGS site (*Kohl and*

Megel, 2007). The reservoir model used in the forecast was based on data analysis of the earlier May 2003 stimulation of Soultz well GPK3.

HEX-S was designed to compute the time-dependent evolution of fracture apertures and consequent development of anisotropic permeability, and of fluid pressure in the fractures as a result of injection. The permeability distribution in HEX-S depends on the location, orientation, aperture, and size of the fractures incorporated in the model. Both deterministic and stochastic fracture sets (see Figure 1.1) may be specified. Every fracture or fracture zone is represented by a circular plane subdivided into a large number of circular "patches" with radii defined on the basis of the interpretation of microseismic data. The initial aperture of each slip patch is assumed to be proportional to its radius, and is scaled to represent the transmissivity of the open borehole section. The code incorporates various aperture laws to allow for (1) normal compliance of fracture walls, (2) compliance and shearing, and (3) jacking and shearing. For the time-dependent pressure calculation, HEX-S employs an "overlay" grid. The hydraulic conductivity of each element of the "overlay" grid is computed from the apertures of the intersecting slip patches by a mapping procedure that results in strongly anisotropic permeability. The computed hydraulic conductivity is in turn used to update the pressure distribution. As discussed at length later in Section 2.3.8 of this report, HeatEx uses a "fracture patch" technique to represent the fracture system, to estimate temporal changes in fracture aperture and compute the resulting macroscopic reservoir permeability changes that is nearly identical to that originally developed for HEX-S. In fact, several hundred lines of HeatEx's Fortran source code (those that carry out the aperture-change calculations) were written at Geowatt in Switzerland by Thomas Kohl and Dieter Ollinger (the authors of the original HEX-S code) and subsequently incorporated directly into HeatEx in San Diego.

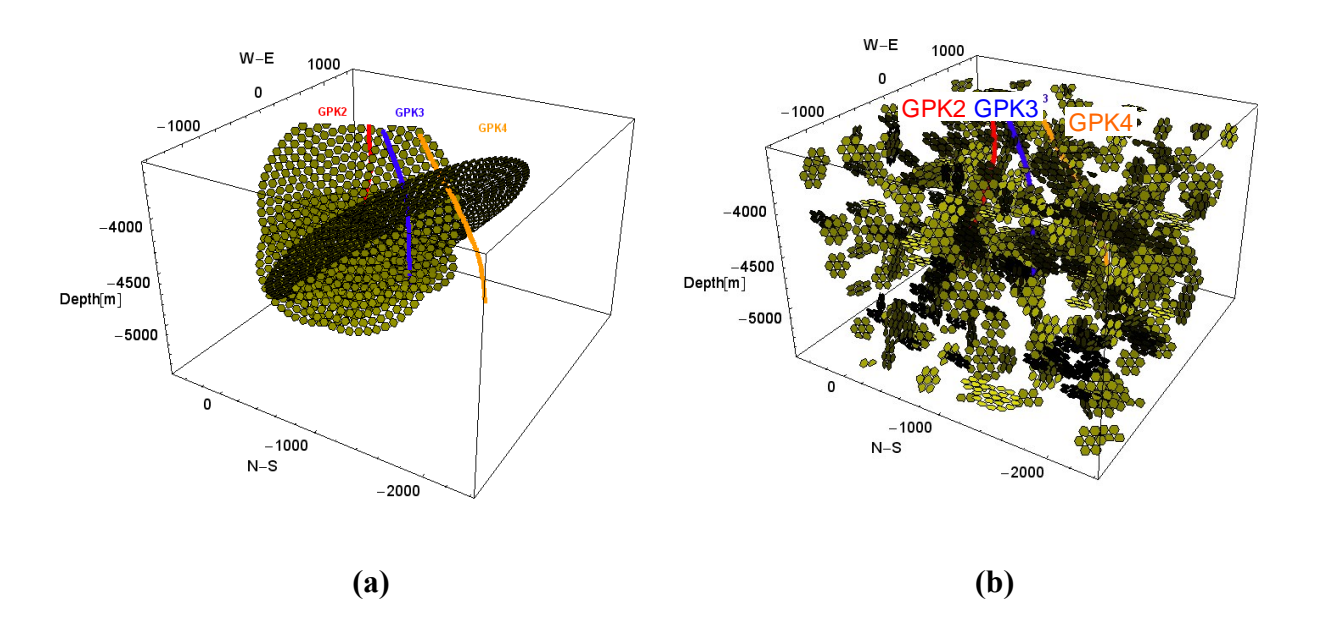


Figure 1.1. Examples of models with (a) deterministic fracture zones subdivided into slip patches, and (b) stochastically generated fractures for the 5-km-deep Soultz reservoir. GPK2, GPK3 and GPK4 are the boreholes. Figure from *Kohl and Megel* (2007)

1.2.2. Identifying Fracture Networks

Modeling of the locations of microearthquake events and the measured pressure and flowrate history in the injection well is at present the method of choice for inferring the properties of the fracture network created (or enhanced) as a result of hydraulic stimulation. The observed pressure response in the well is influenced in great part by the near-wellbore fractures. Matching of microearthquake locations can only discern fracture zones that actually produce detectable signals during pressurization. Moreover, microseismic surveys cannot discriminate among fractures of varying degrees of fluid transmissivity. Clearly, it would be desirable to supplement microearthquake and pressure data by other measurements that may be diagnostic of the fracture network.

In recent years, techniques have been devised to calculate the effects of subterranean reservoir evolution upon surface geophysical surveys, based on the results of conventional numerical reservoir simulation calculations. If repeated surveys exhibit systematic temporal changes that can be correlated with events taking place in the reservoir, additional constraints are provided for history-matching studies, resulting in more robust and reliable reservoir models. The Leidos STAR geothermal reservoir simulation system incorporates postprocessors that are capable of computing changes in these geophysical observables based on the results of numerical reservoir simulations. Geophysical techniques considered to date include microgravity surveys, active seismic surveys, DC resistivity surveys (Schlumberger type), magneto-telluric (MT and CSAMT) surveys, and self-potential (SP) surveys. The computational postprocessors that carry out these calculations of changes in geophysical observables have been extensively tested and verified (*Pritchett*, 2003) and have been applied in various field studies, mainly in Japan (see, for example, *Nakanishi, Pritchett and Tosha*, 2001).

Under a previous DOE grant, SAIC explored the use of the SP ("self-potential") technique for monitoring the growth of underground fractures in EGS stimulation experiments (*Pritchett and Ishido*, 2005; *Pritchett*, 2008) and developed the specialized SPFRAC simulator for this purpose. Conventional earth-surface SP surveys are not very helpful owing to the great depth and limited strength of the signals from hydrofracturing events, but continuous downhole SP monitoring (using electrodes in the uncased zones of nearby shut-in observation wells) can in principle sense the progress of the reservoir pressurization that results from stimulation operations. Data of this type could be used to supplement microseismic data to more completely characterize the fracture system. As discussed at greater length in Section 2.3.9 of this report, the new HeatEx simulator has the optional capability to carry out predictive forecasts of electrokinetic underground SP changes in much the same way as SPFRAC, but in the context of a unified simulation of the entire process, including fracture evolution, ongoing temperature change, etc. Section 3.3 of this report contains an example of a simulation carried out in this manner.

1.2.3. Flow Channel Continuity

As noted above, HeatEx provides a complete description of the fracture network created by hydraulic stimulation of the EGS system. Simultaneous matching of tracer test data and self-potential measurements will make it possible to discriminate permeable fractures (i.e. fluid

flow paths) created by hydraulic stimulation. As noted earlier, microseismic surveys and pressure response in the injection well are by themselves insufficient to determine the connected permeable fracture volume. A description of the permeable fracture network is essential for imaging the fluid flow through the EGS reservoir. Like any other reservoir model, HeatEx may be used to compute details of fluid flow in the reservoir. As discussed in Section 2.3.10, HeatEx can treat multiple tracers simultaneously, and can also treat various types of tracer interactions (radioactive decay, tracer-tracer chemical reactions, and absorption on the rock surfaces).

1.2.4. Seismicity Issues

In the future, HeatEx may also prove to be of use for evaluating seismic risks associated with the injection of highly pressured fluid in the subsurface. Experience from a M3.4 earthquake in Basel, Switzerland, has demonstrated that the environmental soundness of EGS techniques needs to be assured. An urban environment represents an optimum setting for heat utilization but is also most vulnerable to seismic damage. Results from HeatEx could potentially be used to compute the seismic moment associated with a shear displacement due to injection (*Bruel*, 2007).

1.2.5. Heat Sweep Efficiency and Short Circuits

An important distinction between geothermal reservoir engineering and the same discipline as practiced in the oil and gas industry arises from the character of the commodity being sought. Unlike oil and gas, with geothermal the objective is not to recover the subterranean fluids *per se*, but instead to recover the heat energy that the fluid carries up the production wells with it. Once the useful heat has been removed, the cooled geothermal fluid is either reinjected or discarded. In the reservoir itself, only a small fraction of the available heat is to be found in the *in-situ* geothermal fluid – most of the available heat energy is present in immobile hot rock. This is usually even more true for EGS reservoirs than it is for conventional hydrothermal systems.

It follows that before the heat energy in the rock can be put to use, it must be transferred from its initial location within the rock interior to the surface of a pore, fissure or fracture where flowing fluid may carry it toward a production well. This heat transfer from the solid rock to the flowing fluid takes place by means of heat conduction. If we consider a single fracture containing flowing water at a relatively low temperature (T_w) penetrating an unbounded volume of solid impermeable uniform rock which is initially at uniform temperature T_r , it is easy to show (e.g. *Carslaw and Jaeger*, 1959) that the subsequent temperature distribution (a function of lateral distance from the fracture x and time t) will be given by:

$$T(x, t) = T_w + (T_w - T_r) \times erf(x / \delta_T)$$

where *erf* is the error function and δ_T is the thermal boundary thickness, given by:

$$(\delta_T)^2 = 4 \kappa t / \rho c$$

and κ , ρ and c are the thermal conductivity, density and heat capacity of the rock, respectively. Thus, as time goes on, a "thermal boundary layer" containing cooled rock will penetrate more and more deeply from the fracture into the solid rock mass. The thickness of this boundary

layer will increase in proportion to the square root of the elapsed time since the onset of coldwater flow. Using values for κ , ρ and c that are representative of reservoir rocks, we may estimate:

```
t = 1 \text{ second}, \quad \delta_T = 1.7 \text{ millimeters}

t = 1 \text{ hour}, \quad \delta_T = 10 \text{ centimeters}

t = 1 \text{ day}, \quad \delta_T = 0.5 \text{ meters}

t = 1 \text{ month}, \quad \delta_T = 2.6 \text{ meters}

t = 1 \text{ year}, \quad \delta_T = 9.5 \text{ meters}

t = 30 \text{ years}, \quad \delta_T = 52 \text{ meters}
```

Traditional reservoir engineering practice in the past has been to assume that a state of "local thermodynamic equilibrium" (LTE) between the fluid and rock prevails, which is tantamount to assuming that the spatial separation between adjacent flow channels (pores and/or fractures) is small in comparison with the thermal boundary layer thickness at time-scales of interest. If the reservoir under consideration is a typical porous sandstone formation with intergranular separations of the order of a millimeter or so, this approximation is obviously justified. Even in an intensely fractured natural geothermal reservoir with average fracture separations less than one meter, LTE will provide reasonably good results so long as time-scales of interest are no shorter than a day or so.

But EGS reservoirs, which in effect require a man-made fracture system, are likely to have average fracture separations which are much larger. If cold water from an injection well enters the fracture system, passes through the reservoir, and then flows into a production well too rapidly, two adverse consequences will occur. First, in a reservoir with sparse fractures, the thermal boundary layer thickness will still be significantly smaller than the average fracture separation at the time that cold water reaches the production well, which means that much of the heat energy in the reservoir will have been left behind, giving rise to poor sweep efficiency. Second (as will be seen in "Illustrative Case 3"; see Section 3.1.2 of this report), as average fracture separation becomes larger the time of first arrival of cold water at the production well will become earlier and earlier, and in extreme cases the arrival of cold water may be nearly simultaneous with the "tracer arrival time". This is, in effect, a "thermal short circuit", in which cold injected water enters a single dominant fracture which is also penetrated by a production well. The cold water reaches the production well after only a short period of operation, resulting in production well abandonment at a time when the thermal boundary layer is still relatively thin and only a small fraction of the heat energy in the rock lying between the fractures has been recovered.

Avoiding "short circuits" and premature depletion of the resource will obviously be a primary goal of geothermal reservoir engineering as applied to EGS projects, but reservoir simulators that assume LTE are incapable of addressing problems of this kind. As discussed in Section 2.3.4.4, HeatEx uses a new generalization of the "conductive MINC" approach first proposed by *Pritchett* (1997) to treat nonequilibrium unsteady heat transfer between the rock and the interpenetrating fluids on a variety of spatial scales ("fracture separations") simultaneously. The approach poses little additional computational burden over an LTE approach, and permits unprecedented generality in the practical representation of the microstructure of the heatmining process.

1.3. CODE DEVELOPMENT AND COMPUTING ENVIRONMENT

HeatEx was written principally by the present author in San Diego, California between summer 2010 and autumn 2013 at a company once known as SAIC and now known as Leidos Inc., with considerable help from Prof. Thomas Kohl (now with the Karlsruhe Institute of Technology in Germany) and Dr. Dieter Ollinger of Geowatt AG in Zurich, Switzerland. Able assistance was also provided informally by Dr. Sabodh Garg of SAIC/Leidos and by Prof. Ahmad Ghassemi of Texas A&M University (and later the University of Oklahoma). Two summer interns (Chakra Rawal and Xiaonan "Sonia" Wang), at the time completing their graduate studies at Texas A&M, were also of considerable help in first identifying and then implementing the "Pardiso" equation-solver which is at the heart of HeatEx.

HeatEx was developed using a Dell Model T7400 Precision Workstation[®] which is now nearly six years old. The machine has a Quad Core Intel Xeon[®] X5482 processor (3.20 GHz) and 8 GB of main memory. The operating system is Red Hat Enterprise Linux[®] and the computer is equipped with the Intel Fortran[®] compiler with the Intel MKL[®] ("Math Kernel Library") which incorporates "Pardiso", a 'Parallel Direct Sparse Linear System Solver' (Schenk and Gärtner, 2004; 2006). Pardiso is essential to HeatEx operation.

HeatEx is written in the standard Fortran 90 language (see e.g. *Adams et al.*, 1992) with a few Fortran 95 language extensions in the portions of the code that were contributed by Geowatt. Altogether, the HeatEx simulator consists of a main program and 223 subroutines with, in aggregate, about forty-seven thousand lines of Fortran source code and 2.1 megabytes of source text. A special-purpose equation-of-state interrogator utility is also provided, which adds a further eighteen thousand lines and 1.1 megabytes of Fortran. Copies of all of the Fortran source code files are being provided separately in electronic form. In addition, executable files for both the simulator and the equation-of-state utility as compiled for use on the Dell T7400 development system are included, and simulator input and output files for the six illustrative calculations described later in this report are also included in the electronic delivery package.

Section 2 of this report amounts to a "User's Manual" for the HeatEx simulator (and the HeatEs equation-of-state utility program), with more detailed technical descriptions as appropriate. Instructions are provided for the preparation of input data files to operate the programs, and for the interpretation of the output files produced by the calculations. Then, Section 3 presents six illustrative calculations involving three different geometries, both as examples to help familiarize the user with program operation and as demonstrations of the character and quality of the results obtainable using HeatEx.

2. OPERATING INSTRUCTIONS

In this section, detailed directions are provided describing how to specify a particular problem to the HeatEx software for simulation. Specific examples with both sample input and output are provided later, in Section 3.

2.1. COMMUNICATING WITH THE SIMULATOR

All input data provided by the user to the HeatEx software is supplied using ordinary ASCII text files. These files all have "reserved names", as discussed below. Furthermore, all output from the software will appear on "reserved name" ASCII output text files. The user prepares the input files using any convenient text editor – the simulator will then create the output files. The input and output files all have twelve-character reserved names. The input file names are all of the form "in******.fil" (for "input file") and the output file names are all of the form "rp*****.fil" (for "report file"), where "******" represents a particular lower-case six-character text string that is unique to the topic addressed by the data file in question.

The user-prepared input files (the "in*****.fil" files) each consist of a sequence of "lines" of data. Some of these lines will contain strings of alphabetic characters, while others will contain one or more numerical values (real numbers or integers) in a particular order to specify the desired input problem parameter values. Numerical values provided by the user to HeatEx will be both integers and double-precision real numbers. The variable "type" of which the value is being sought by HeatEx will be indicated by the "name" used for the variable in the instructions below. The long-standing Fortran variable-naming convention will be adhered to here: numerical variables whose names begin with the letters I, J, K, L, M or N (or i, j, k, l, m or n) are type "integer" and if the value supplied has a fractional part, the input value will be rounded to the nearest integer. All other numerical variables are type "double precision real". Lines containing input character strings are interpreted as case-insensitive – HeatEx converts all such strings to upper case upon input before interpretation.

"Free-field" formatting may be used to specify the required numerical values on each input text line. Values may be separated by blanks, commas, colons, or any other desired delimiter character *except* any of the following:

The "#" character plays a special role in HeatEx input syntax. If "#" appears in the *first column* of any input line, *that entire line will be disregarded* by HeatEx. In other words, if "#" is present in the first column of any line in the file, behavior will be the same as if the entire line were missing from the file. If the "#" character appears *anywhere else* in a line, the "#" character itself *and all characters appearing to the right of* "#" within that line will be disregarded. Behavior will be the same as if the "#" and all characters to the right of the "#" were instead replaced by blanks; only the portion of the line to the left of the "#" will be read by the program. These conventions were adopted to facilitate the inclusion of "comment" fields within input data files. Examples of input files prepared in this manner are provided in Section 3.4 of this report.

2.2. THE EQUATION-OF-STATE

A central component of HeatEx is the built-in fluid "equation of state" which provides the physical properties of the hot, high-pressure brine within the geothermal reservoir. This physical description is preset and cannot be changed by the user, but the user will frequently find it useful to have direct access to the equation of state to help with problem design. For this purpose, an auxiliary program ("HeatEs") has been developed. Instructions for operating HeatEs are provided later in this section.

The equation-of-state describes the constitutive behavior of a mixture of H₂O with dissolved NaCl. This description provides quantitative relations among the physical properties of this material. The properties involved include mass fraction of dissolved NaCl ("salinity"), pressure, temperature, specific internal energy, specific enthalpy, mass density, dynamic viscosity, and thermal conductivity.

The description is limited to all-liquid states (no steam, ice or solid salt precipitate). Input parameters are [pressure, specific internal energy, salinity]. Alternatively, input may consist of [pressure, specific enthalpy, salinity] or [pressure, temperature, salinity]. The description is valid for temperatures from the freezing point to 320°C and for salinities from zero to 0.25 (seven times more concentrated than ordinary seawater). For low salinities, the valid pressure range extends from the vapor pressure to 300 MPa. For higher salinities, the verified range of validity is limited to 100 MPa pressure due to the absence of adequate measured data at higher pressures for concentrated saline brines. Internally, given pressure, specific internal energy and salinity, the equation-of-state package calculates temperature, specific enthalpy, fluid mass density, fluid dynamic viscosity and thermal conductivity, and also the partial derivatives of these quantities with respect to pressure, specific internal energy, and salinity.

The accompanying figures illustrate calculated results obtained from the HeatEs equation-of-state software package, expressed as functions of pressure P, temperature T and salinity S over the ranges for which the description has been verified by comparisons with measured data. First, consider the pure-water case (no NaCl – zero salinity). Figure 2.1 illustrates the pure-water mass density in kilograms per cubic meter for temperatures from 0°C to 320°C and for pressures from the vapor pressure (an increasing function of temperature) to 300 MPa as calculated by the equation-of-state. Similarly, Figure 2.2 displays enthalpy (kilojoules per kilogram), Figure 2.3 displays the reciprocal of fluid dynamic viscosity (1/pascal-seconds), and Figure 2.4 displays thermal conductivity (milliwatts per meter per degree Celsius) for pure H_2O over the same range of pressures and temperatures.

The next four figures illustrate the influence of non-zero salinity on these same properties, but with the pressure range restricted to 100 MPa as discussed above. Each of these figures consists of six frames, for salinity values equal to 0% (same as pure water, above), 5%, 10%, 15%, 20% and 25% (the upper salinity bound on the range of HeatEs validity). Figure 2.5 shows fluid density (kg/m³), Figure 2.6 shows specific enthalpy (kJ/kg), Figure 2.7 displays reciprocal dynamic viscosity (1/Pa-s) and Figure 2.8 illustrates thermal conductivity (mW/m-°C) for these increasingly hypersaline brines.

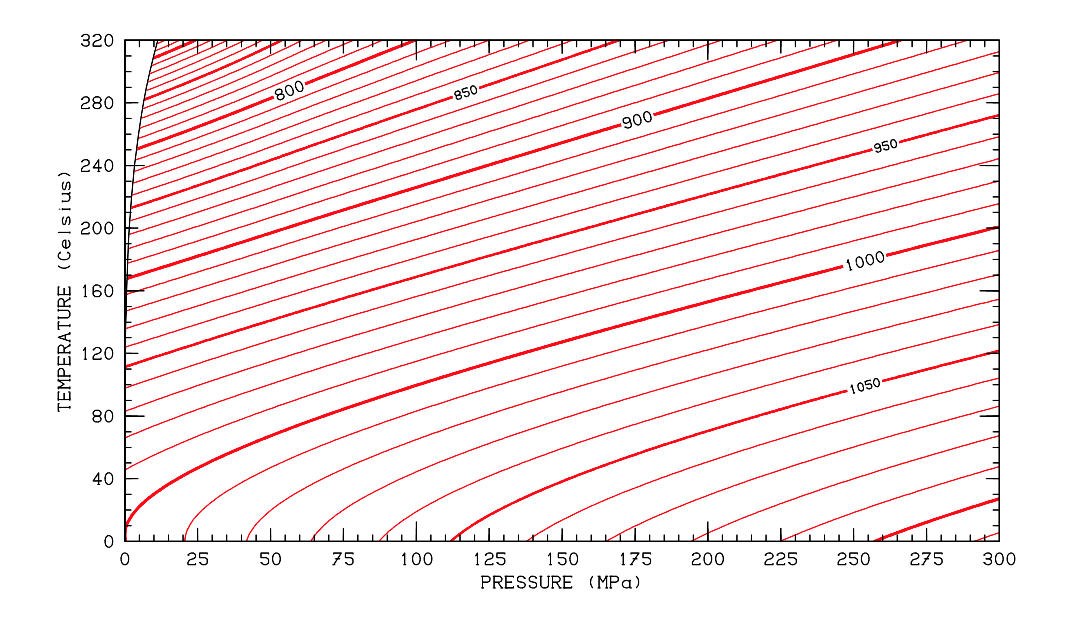


Figure 2.1. Influence of pressure and temperature upon pure- H_2O fluid mass density ρ . Contour values are expressed in kilograms per cubic meter.

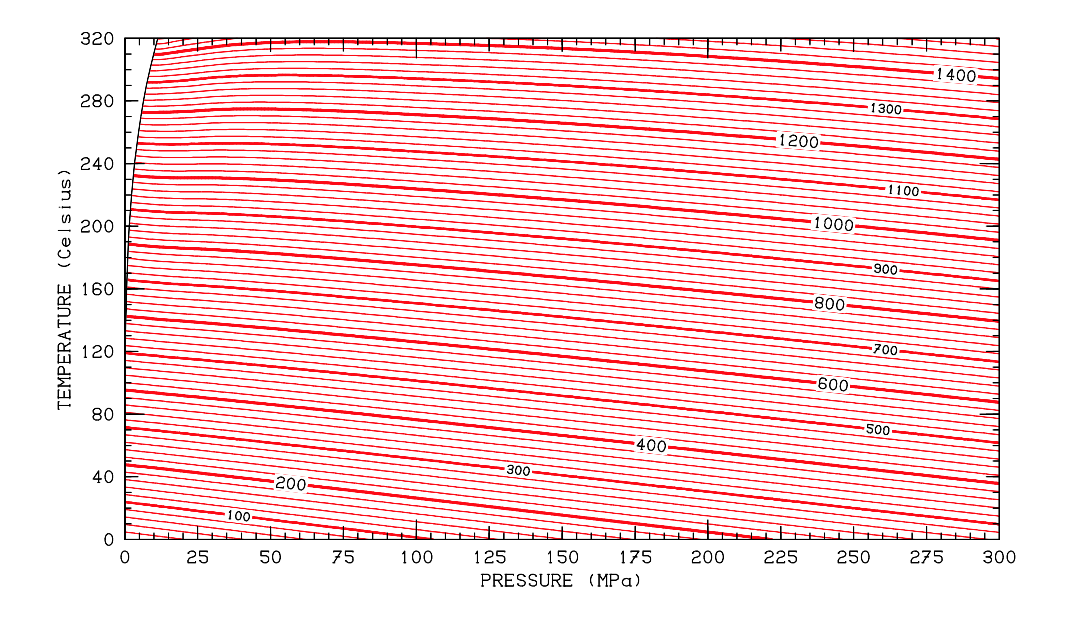


Figure 2.2. Influence of pressure and temperature upon pure-H₂O specific enthalpy *H*. Contour values are expressed in kilojoules per kilogram.

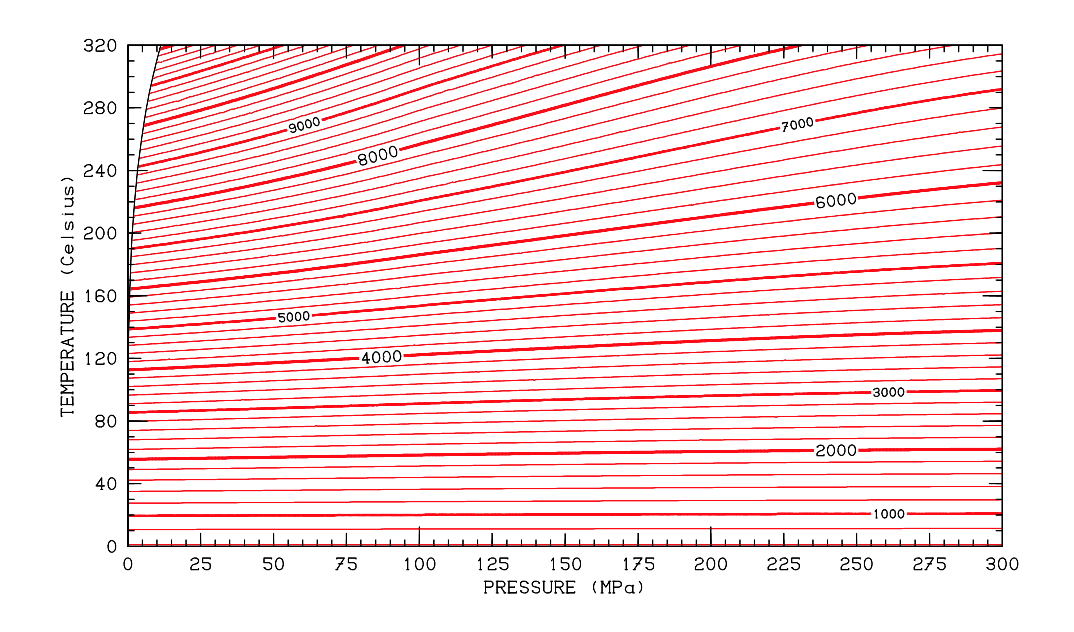


Figure 2.3. Influence of pressure and temperature upon pure- H_2O dynamic viscosity μ . Reciprocal of viscosity $(1/\mu)$ plotted, with values expressed in (1/Pa-s).

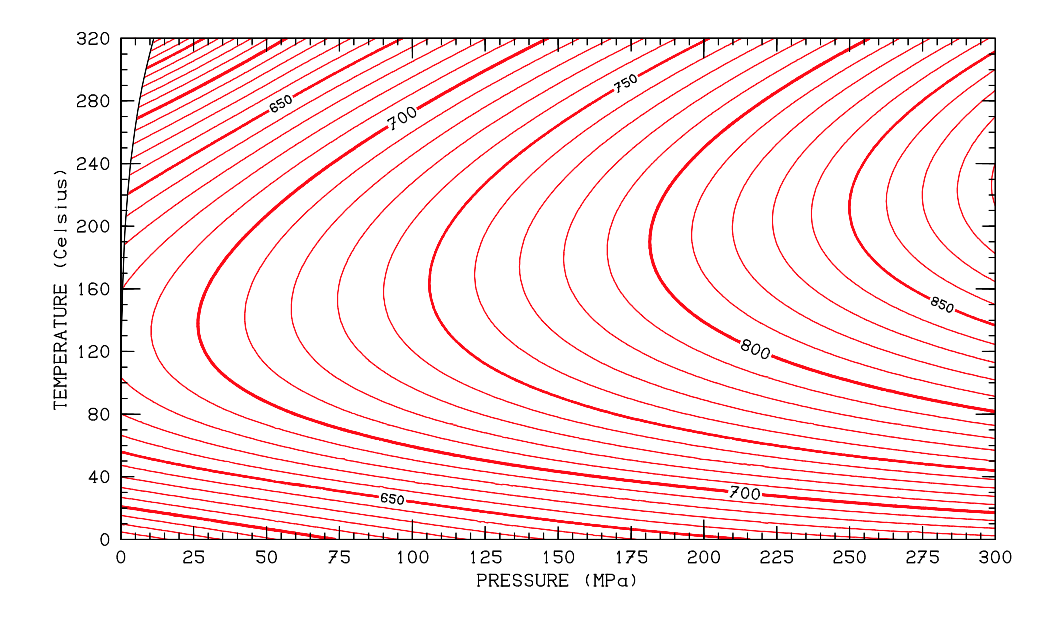


Figure 2.4. Influence of pressure and temperature upon pure- H_2O thermal conductivity κ . Values are expressed in milliwatts per meter per degree Celsius.

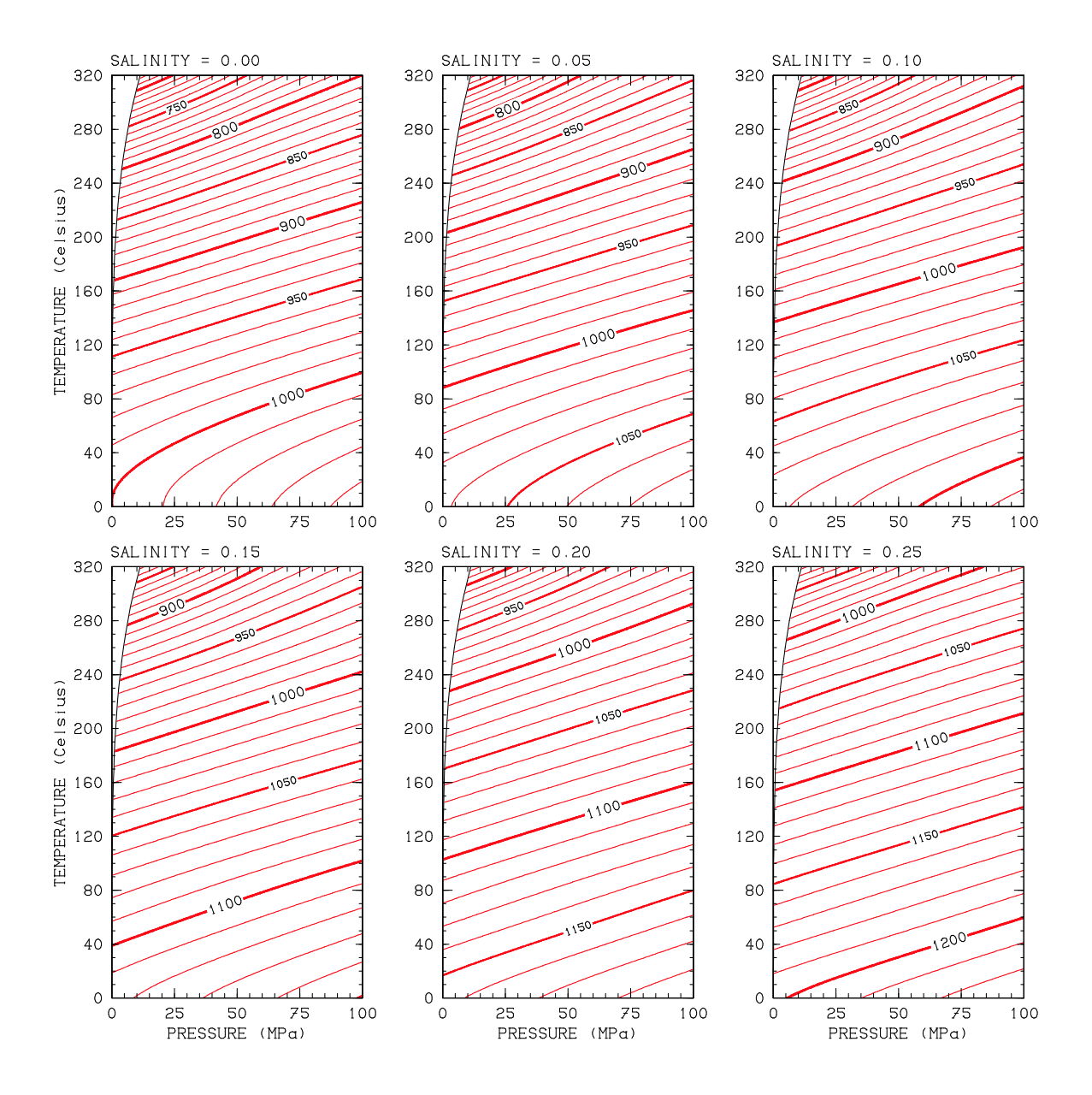


Figure 2.5. Influence of pressure, temperature and salinity upon brine mass density ρ . Contour values are expressed in kilograms per cubic meter.

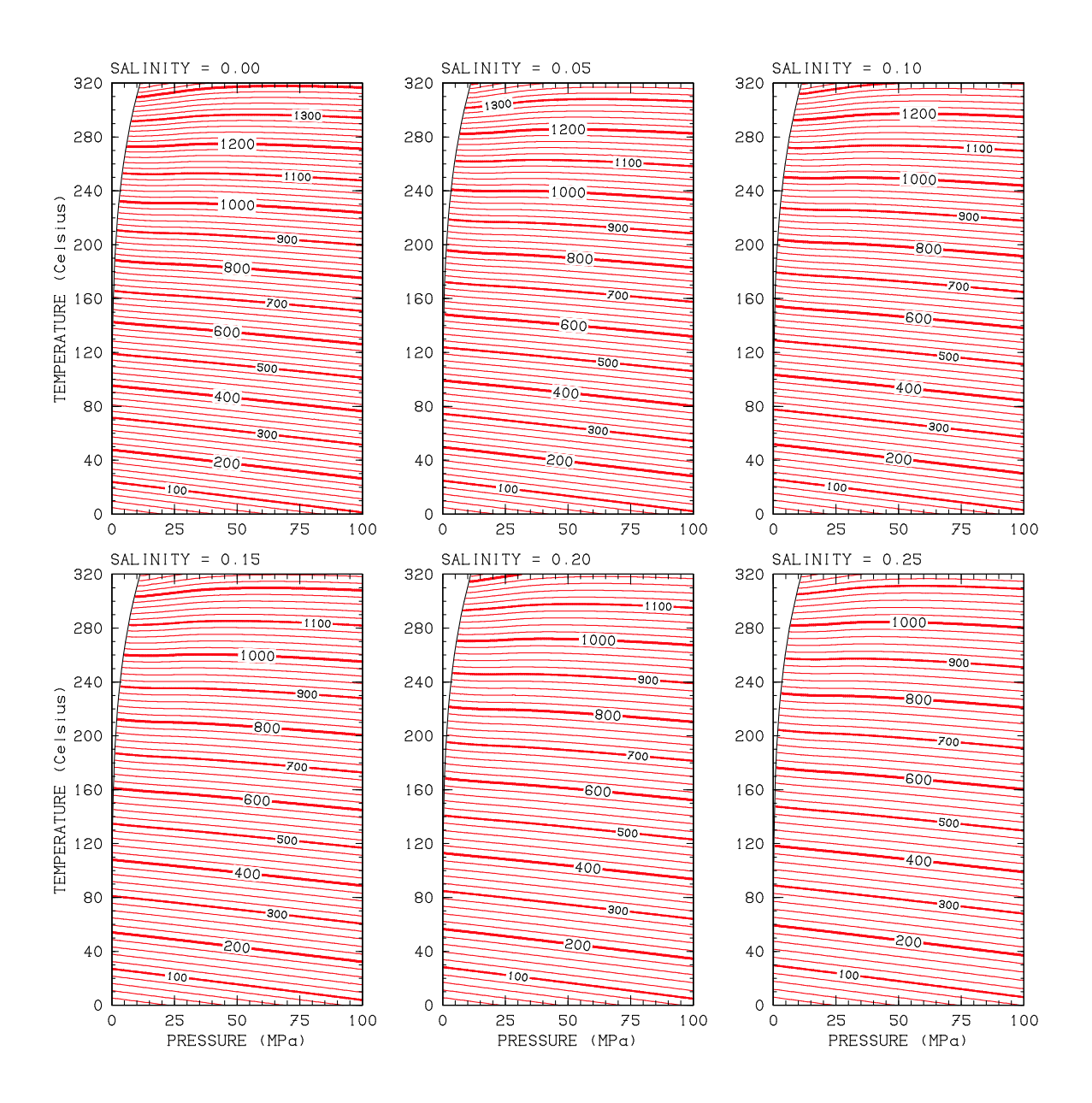


Figure 2.6. Influence of pressure, temperature and salinity upon brine specific enthalpy *H*. Contour values are expressed in kilojoules per kilogram.

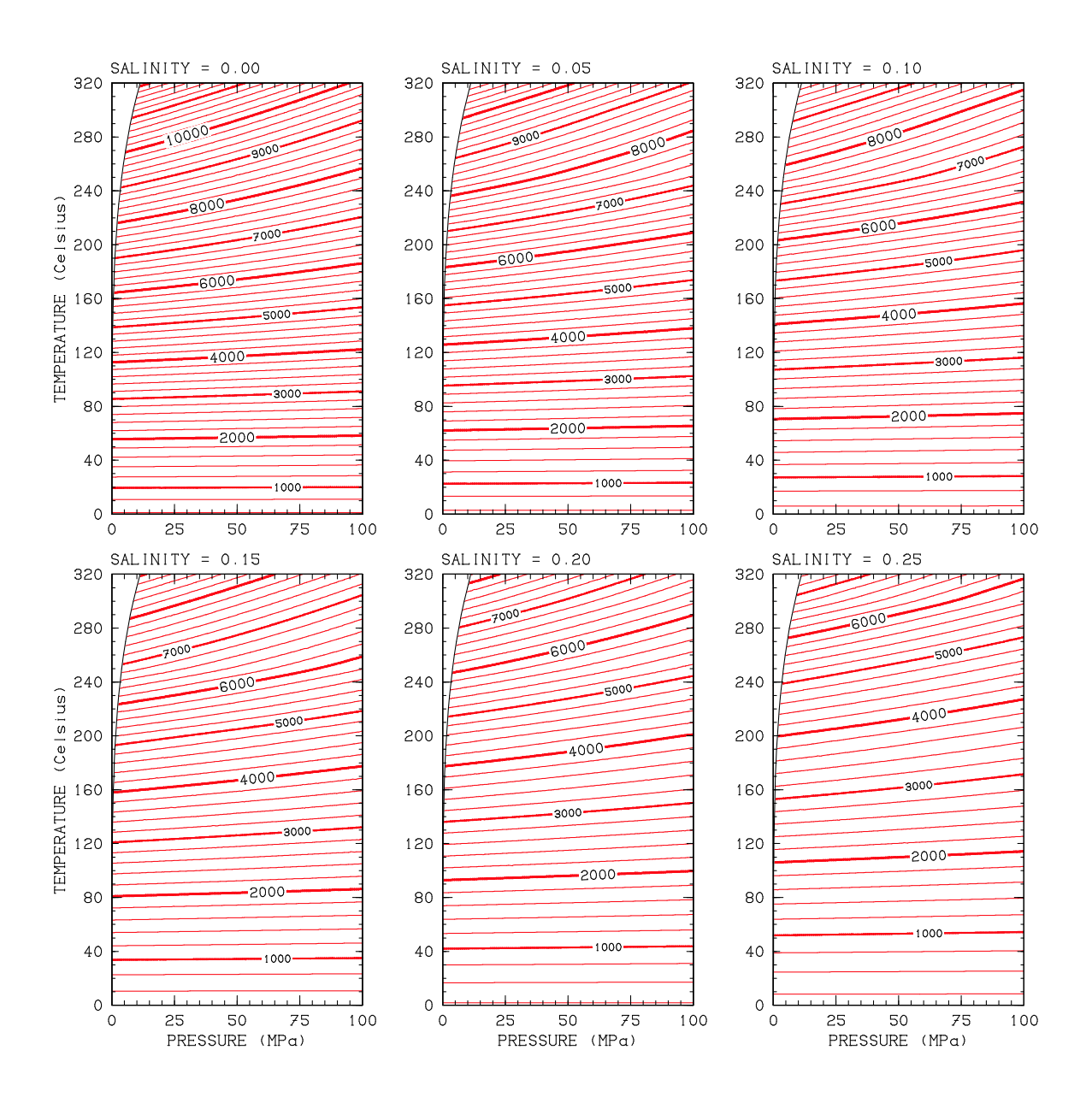


Figure 2.7. Influence of pressure, temperature and salinity upon brine dynamic viscosity μ . Reciprocal of viscosity (1 / μ) plotted, with contour values expressed in (1/Pa-s).

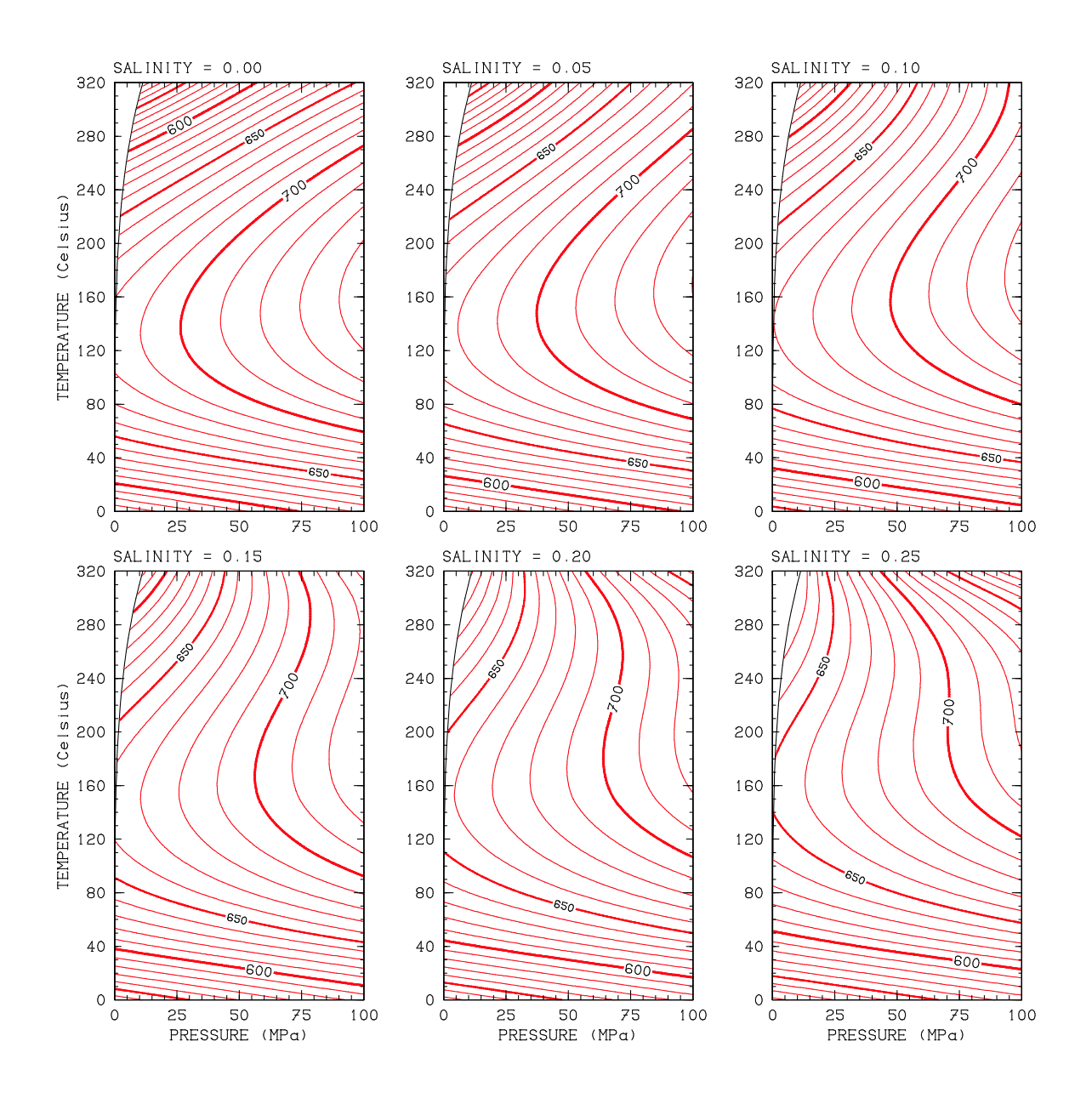


Figure 2.8. Influence of pressure, temperature and salinity upon brine thermal conductivity κ . Contour values are expressed in milliwatts per meter per degree Celsius.

The user may obtain numerical values from the equation-of-state by creating an appropriate "inestate.fil" input data file and then executing the HeatEs.exe utility program, which will read inestate.fil and then write computed results on a new output file named "rpestate.fil". Note: if a data file named "rpestate.fil" is already present in the local directory (for example, from a prior run of HeatEs.exe), the old data file will be overwritten. The inestate.fil file must consist of a series of line pairs (of indefinite length), with the first line of the pair containing a character string and the second line of the pair containing from one to eight numerical values:

```
Line 1: KEYWORD
Line2: VALUE(1), VALUE(2), ..., VALUE(last)
```

The "KEYWORD" character string is case-insensitive, but must be one of the following:

```
pressure
salinity
temperature
energy
enthalpy
```

and designates which kind of information is being specified by the subsequent "VALUE" entries. Before calculations can proceed, it is essential that at least one "pressure" value and at least one "salinity" value must be provided, and in addition the heat content of the system must be established, which can be done by either specifying "temperature", "energy" or "enthalpy". For example, if an "inestate.fil" is prepared as follows:

```
pressure
100000.
temperature
0 10 20 30 40 50
salinity
0.
```

then the resulting "rpestate.fil" file will contain:

```
Total
                           Specific
    NaCl
                   Temper-
                                    Internal
                                                 Mass
                                                       Dynamic
                                                                Thermal
                                                                           Elec.
Salinity
                            Enthalpy
                                                                         Conduc.
         Pressure
                    -ature
                                      Energy
                                              Density
                                                         Visc.
                                                                Conduc.
            (MPa) (Celsius)
                             (kJ/kg)
                                      (kJ/kg)
                                             (kg/m^3) (micPa-s)
                                                                (mW/m-C)
                                                                           (S/m)
   (ppm)
0.0000000 0.1000000 0.0000000 0.1000066 0.0000000 999.93370 1727.6800 560.63894 0.0000000
0.0000000 0.1000000 10.000000 42.000046 41.900023 999.77955 1276.0400 580.32432 0.0000000
0.0000000 0.1000000 20.000000 83.900587 83.800415 998.28250 987.51900 598.44470 0.0000000
0.0000000 0.1000000 30.000000 125.80273 125.70230 995.72584 791.06444 615.05611 0.0000000
0.0000000 0.1000000 50.000000 209.62208 209.52087 988.12416 546.72320 643.41782 0.0000000
```

If "inestate.fil" is instead:

```
pressure

1.e+06

enthalpy

100.e+03

salinity

0. 0.05 0.10 0.15 0.20
```

then the output "rpestate.fil" output will be:

```
NaCl
              Total
                               Specific
                      Temper-
                                          Internal
                                                                          Thermal
                                                                                      Elec.
                                                        Mass
                                                               Dynamic
 Salinity
           Pressure
                       -ature
                                Enthalpy
                                            Energy
                                                     Density
                                                                 Visc.
                                                                          Conduc.
                                                                                    Conduc.
              (MPa) (Celsius)
                                (kJ/kg)
                                           (kJ/kg)
                                                    (kg/m^3) (micPa-s)
                                                                         (mW/m-C)
                                                                                      (S/m)
    (maga)
0.0000000 1.0000000 23.641092 100.00000 98.997864 997.86826 907.99390 605.08556 0.0000000
50000.000 1.0000000 24.613628 100.00000 99.032342 1033.4234 956.20365 597.43590 7.5611235
100000.00 1.0000000 25.668359 100.00000 99.065038 1069.5623 1033.2937 590.04180 12.999047
150000.00 1.0000000 26.816316 100.00000 99.096282 1106.5395 1144.4259 582.91812 17.514529
200000.00 1.0000000 28.070566 100.00000 99.126360 1144.6361 1297.3027 576.07757 22.203296
```

The "VALUE" entries in file "*inestate.fil*", like all physical data supplied to HeatEx by the user, must be provided in standard SI units. This means that pressures are in pascals, salinities are dimensionless mass fractions, temperatures are in Celsius degrees, and both specific enthalpies and specific internal energies are to be supplied in joules per kilogram. Output quantities are sometimes provided in other, more convenient, units (*e.g.* pressures in megapascals – MPa – enthalpies in kJ/kg, etc.), but input is always pure SI.

2.3. SIMULATOR PROBLEM SPECIFICATION

Posing a problem to the HeatEx simulator entails the preparation of numerous "in*****.fil" input files and then executing "HeatEx.exe". Thirty different input-file reserved names are available for various purposes, but it will ordinarily not be necessary to use them all for a particular problem. Their names are (in alphabetical order):

	<u>File</u>	<u>Specifies</u>	See Section
1.	inaquifr.fil	"aquifer" boundary conditions	2.3.4.5
2.	inblintr.fil	individual detailed block output	2.3.12.2
3.	incondrk.fil	rock thermal conductivity distribution	2.3.7.1
4.	inecnbgr.fil	distant electrical conductivity distribution	2.3.9.3
5.	inelpram.fil	electrical property library entries	2.3.9.1
6.	inelprds.fil	spatial distribution of electrical property data	2.3.9.2
7.	infpdata.fil	properties of individual fracture patches	2.3.8.3
8.	infpprms.fil	fracture patch class properties	2.3.8.2
9.	ingravty.fil	acceleration of gravity	2.3.3.2
10.	ingridek.fil	electrokinetic grid geometry	2.3.4.2
11.	ingridte.fil	thermoelastic grid geometry	2.3.4.3
12.	ingridth.fil	thermohydraulic grid geometry	2.3.4.1
13.	ininhydr.fil	initial hydrostatic conditions	2.3.6.4
14.	ininpres.fil	initial pressure distribution	2.3.6.1
15.	ininsalt.fil	initial salinity distribution	2.3.6.3
16.	inintemp.fil	initial temperature distribution	2.3.6.2
17.	inintrcr.fil	initial tracer distribution	2.3.10.2
18.	inmincnd.fil	fluid/rock thermal equilibration	2.3.4.4
19.	inoutfrq.fil	output frequency requests	2.3.11.2
20.	inrgstrs.fil	regional earth stress distribution	2.3.8.1
21.	inrkigpr.fil	intergranular permeability distribution	2.3.7.3
22.	inrkvolp.fil	volumetric rock properties	2.3.7.2
23.	insnsors.fil	sensor assembly locations	2.3.12.1
24.	insorcen.fil	distributed energy sources	2.3.5.2
25.	insorcms.fil	distributed mass sources	2.3.5.1
26.	intimscl.fil	time-discretization	2.3.11.1
27.	intopogr.fil	earth-surface topography	2.3.3.1
28.	intrchem.fil	reactive tracer chemistry	2.3.10.1
29.	inwelflo.fil	well flow rate histories	2.3.13.2
30.	inwelgeo.fil	well geometries	2.3.13.1

Running HeatEx can produce various different "reserved-name" output files. Some of these simply amount to "echo-print" output files that acknowledge and interpret the instructions found on the corresponding input files. Any input errors encountered will also be reported on these files. They include the following:

rpaquifr,fil	(echoes inaquifr.fil)	rpintrer.fil	(echoes inintrer.fil)
rpblintr.fil	(echoes inblintr.fil)	rpmincnd.fil	(echoes inmincnd.fi)l
rpcondrk.fil	(echoes <i>incondrk.fil</i>)	rpoutfrq.fil	(echoes inoutfrq.fil)
rpecnbgr.fil	(echoes <i>inecnbgr.fil</i>)	rprgstrs.fil	(echoes inrgstrs.fil)
rpfpdata.fil	(echoes <i>infpdata.fil</i>)	rprkigpr.fil	(echoes inrkigpr.fil)
rpfpprms.fil	(echoes <i>infpprms.fil</i>)	rprkvolp.fil	(echoes inrkvolp.fil)
rpgravty.fil	(echoes <i>ingravty.fil</i>)	rpsnsors.fil	(echoes insnsors.fil)
rpgridek.fil	(echoes <i>ingridek.fil</i>)	rpsorcen.fil	(echoes insorcen.fil)
rpgridte.fil	(echoes <i>ingridte.fil</i>)	rpsorcms.fil	(echoes insorcms.fil)
rpgridth.fil	(echoes <i>ingridth.fil</i>)	rptimscl.fil	(echoes intimscl.fil)
rpinhydr.fil	(echoes ininhydr.fil)	rptopogr.fil	(echoes <i>intopogr.fi</i>)l
rpinpres.fil	(echoes <i>ininpres.fil</i>)	rptrchem.fil	(echoes intrchem.fil)
rpinsalt.fil	(echoes ininsalt.fil)	rpwelflo.fil	(echoes inwelflo.fil)
rpintemp.fil	(echoes <i>inintemp.fil</i>)		

Furthermore, output file *rpelprop.fil* provides an acknowledgement for the data found on both input files *inelpram.fil* and *inelprds.fil*, and both output files *rpwelgeo.fil* and *rpwelcas.fil* provide acknowledgements for data found on input file *inwelgeo.fil*.

Other "reserved-name" output files are produced automatically without direct user instructions. These include:

rpscreen.fil: This file will contain a permanent record (*i.e.* "cataloged file") containing all text information sent to the computer screen (*i.e.* "standard output) by HeatEx during the simulation run.

rptotals.fil: As the calculation proceeds forward in time, a single line will be written to this file at the end of each computational time-step containing, for the entire thermohydraulic grid volume, the total mass of H₂O present, the total mass of dissolved NaCl present, the total heat energy present in the liquid phase, and the total heat energy present in the solid phase (rock).

rptottra.fil: In a similar fashion, this file will contain step-by-step values of the total mass of each tracer species present in the grid volume.

In addition to the *rptotals.fil* and *rptottra.fil* continuous-record output, for each injection or production well involved in the problem (and specified by input file *inwelgeo.fil* – see below), an output file will be created (with name *rpwellNN.fil*, where "NN" is the well number – files will be named *rpwell01,fil*, *rpwell02.fil*, etc.). Each time step, the following instantaneous values will be recorded on the file: well flow rate (injection or production), datum level (downhole) flowing pressure, dissolved salt content, and the concentration of each tracer present. Also, for each "sensor assembly" specified by input file *insensor.fil* (see below), an output file with a name of the form *rpsnsrNN.fil* will record step-by-step values of local pressure, fluid temperature, rock temperature, salinity, and as appropriate, electrokinetic self-

potential (SP) and tracer concentrations. For each "grid block of interest" specified by input file *inblintr.fil* (see below), the following quantities will be recorded each computational timestep on an output file named *rpblocNN.fil*: grid block fluid pressure, specific enthalpy, salinity, fluid density, fluid temperature, average rock temperature and, for each concentric spherical "shell" in each pertinent MINC assembly, the instantaneous rock temperature of the shell.

Finally, as many as seven additional "snapshot" output files may be created at user-prescribed preset time intervals as specified by input file *inoutfrq.fil*. These are:

rpdispts.fil: For each block in the thermohydraulic grid, the porosity, fluid pressure, fluid specific enthalpy, fluid temperature, rock average temperature, and fluid salinity are reported.

rpdistra.fil: Lists the fluid mass fraction of each tracer present in each block in the thermohydraulic computational grid.

rpfpaper.fil: For each "fracture slip patch" represented in the thermohydraulic grid, this file provides the instantaneous values of (1) minimum aperture value, (2) maximum aperture value, (3) mean aperture value, (4) aperture due to compliance, (5) aperture due to shearing, (6) aperture due to jacking, and (7) shearing offset.

rprkperm.fil: For each block in the thermohydraulic grid, the instantaneous values of the tensor permeability components k_{xx} , k_{yy} , k_{zz} , k_{xy} , k_{yz} , and k_{zx} due to intergranular permeability and fracture permeability acting together are listed.

rprstart.fil: Records data suitable for program restart.

rpvoltge.fil: For each "conductive artifact" (continuous section of metallic well casing pipe), the instantaneous net current in/out of the conductor and the voltage on the conductor are provided. Also, for each computational block in the electrokinetic grid, the instantaneous electrical conductivity, drag current divergence, and electrical potential are listed.

rpwelsum.fil: For each production, injection or shut-in well, the datum level pressure, production or injection rate, flowing enthalpy, flowing fluid salinity and tracer concentrations and cumulative total production, total injection, and net production of fluid, salt, and each tracer are recorded. Also, for wells with multiple feedblocks, this file reports the contribution of each grid block to the total well flow.

2.3.1. Minimum Input Specifications

Of the thirty different input files listed above, some are always required for simulator operation, some are optional, and some may or may not be required depending on the character of the problem under study. These six input files are always required:

incondrk.fil ingridth.fil inrkigpr.fil inrkvolp.fil intimscl.fil intopogr.fil
These eight input files are always optional:

inaquifr.fil inblintr.fil ingravty.fil inmincnd.fil inoutfrq.fil insnsors.fil insorcen.fil insorcms.fil

and the remaining sixteen may or may not be needed, depending upon the circumstances. If the problem under consideration involves the calculation of electrokinetic potential, four files will be needed.

inecnbgr.fil inelpram.fil inelprds.fil ingridek.fil

If production or injection wells are involved, we must include:

inwelflo.fil inwelgeo.fil

Use of the "fracture patch model" for fracture permeability will require:

infpdata.fil infpprms.fil ingridte.fil inrgstrs.fil

If tracers are to be incorporated in the study, we must add:

inintrcr.fil intrchem.fil

And, in all cases, to specify the initial conditions, we will need either:

ininpres.fil and ininsalt.fil and inintemp.fil

or ininhydr.fil or inrstart.fil

2.3.2. The "VECTOR" Distribution Procedure

While describing a particular problem to the simulator for calculation, it is frequently necessary to specify the spatial distribution of a particular quantitative physical attribute (or collection of attributes) within a three-dimensional array of computational grid blocks. Assigning individual values to each grid block one at a time would require that the user prepare very large input files and will ordinarily not be necessary.

As an alternative, the "VECTOR" procedure has been adopted for HeatEx. This procedure is an input data syntax which will usually permit relatively complicated spatial distributions of attributes to be assigned to the various grid blocks using only a few input lines. It is used for assigning initial conditions (input files *ininpres.fil*, *ininsalt.fil*, *inintemp.fil* and *inintrcr.fil*) and material properties (files *incondrk.fil*, *inrkigpr.fil* and *inrkvolp.fil*) to the various blocks within the HeatEx thermohydraulic grid, and the same general procedure is used for all of these input files. The general structure of such a file is as follows:

Line 1: DEFAULT ATTRIBUTES

Line 2: COORDINATE DESIGNATOR

Line 3: LOCATION 1

Line 4: LOCATION 2

Line 5: LOCATION 3

Line 6: "SET"

Line 7: ATTRIBUTES

Line 8: LOCATION 1

Line 9: LOCATION 2

Line 10: LOCATION 3

Line 11: "SET"

Line 12: ATTRIBUTES

etc.

etc.

Line N-4: **LOCATION 1** *Line N-3:* LOCATION 2 *Line N-2:* **LOCATION 3**

Line N-1: "SET"

Line N: **ATTRIBUTES**

[end-of-file]

The first line in each such input file will always contain "default" values of the attribute(s) in question which will be applied initially to all of the blocks in the grid. These will be supplied as a simple list of numerical values in a specified order on the first line of the file (or a single value, for a single attribute). If a uniform distribution of the attribute(s) is desired, then the input file will consist of only this single first line. Examples of input files of this type may be found in Sections 3.4.4.8, 3.4.6.3 and 3.4.6.17.

If, however, a nonuniform distribution of the attribute is desired, more information must be provided. Following the "default" value on the first line, the second line may contain a twocharacter designator for the coordinate system in which the spatial coordinates specifying the modified attribute distribution will be provided. If the spatial information will be provided in "world" coordinates (meters East, meters North and meters ASL), Line 2 (above) must be deleted. Otherwise, the coordinate system employed is designated by the two-character string entered on Line 2:

Line 2 entry = "TH" means data in thermohydraulic grid coordinates (x_{th}, y_{th}, z_{th}) . Line 2 entry = "TE" means data in thermoelastic grid coordinates (x_{te} , y_{te} , z_{te}).

Line 2 entry = "**EK**" means data in electrokinetic grid coordinates (x_{ek}, y_{ek}, z_{ek}) .

Line 2 **absent** means data in "world" coordinates (*East, North, ASL*).

Following Line 2 (or Line 1, if "world" coordinates are selected) is a series of indefinite length of five-line data sets. These consist of three "LOCATION" lines, followed by a "SET" line, and then an "ATTRIBUTES" line. The "LOCATION lines refer to the x-, y- and z-location of the subregion within which the attribute value is to be modified. The "SET" line simply contains the three-character string "set" and serves to notify the program that the next line in the sequence will contain revised attribute values. The three "LOCATION" lines refer to the pertinent x, y and z coordinates:

> LOCATION 1: x_{th} , x_{te} , x_{ek} or East y_{th} , y_{te} , y_{ek} or North LOCATION 2:

LOCATION 3: z_{th} , z_{te} , z_{ek} or ASL

and the syntax for each of these lines must be one of the following four admissible possibilities:

1. "all"

2. "<[value]"

3. "> [value]"

4. "from [value] to [value]"

where [value] represents a coordinate location, in meters. For example, if Line 2 were absent and one of the subsequent five-line data sets were as follows:

```
> 1456.2
all
from 350.4 to 858.6
set
3.1416
```

the effect would be, for all thermohydraulic grid blocks whose centers lie farther east than +1456.2 meters, above 350.4 m ASL elevation and below 858.6 meters ASL elevation, to reset the attribute value from the "default" value to 3.1416.

Finally, note that the effects of these five-line data sets are order-dependent. If the "LOCATION" regions of more than one such data set overlap, then the value that appears last in the input file will supersede the earlier value(s).

2.3.3. Setting the "World" Coordinate Context

Location information in HeatEx is often expressed in "World" coordinates (i.e. meters Eastward, meters Northward and meters Above Sea Level or ASL) for purposes of input and output, even though, internally, several other coordinate systems are used for the calculations themselves.

<u>2.3.3.1.</u> Topography and geography – input file "intopogr.fil". This input file serves to establish the origin of the "World" coordinate system and the location of the earth surface in the area of interest. It is required for HeatEx operation. We assume that a topographic map is available with coordinates corresponding to north-south and east-west, with these horizontal coordinates measured relative to some suitable local surveyed benchmark. An example of a typical detailed *intopogr.fil* file is provided in Section 3.4.6.21.

The *intopogr.fil* file consists of four parts, to be provided in the following order:

- 1. Size declaration.
- 2 Eastward coordinates
- 4. Northward coordinates.
- 4. Surface elevation data.

The "Size declaration" is a single data input line containing two integers, both of which must be at least 2 and no greater than 128. These two integers ("NETOPO" and "NNTOPO") represent the size of the digital arrays forming the topographic map, in the Eastward and Northward directions respectively. Next, NETOPO "Eastward coordinate" real-number values must be provided in increasing order – multiple lines may be used for this purpose if needed. These represent horizontal distance in the eastward direction as measured on the map, in meters. NNTOPO "Northward coordinate" values are then required as well. Usually the coordinate values will be equally spaced, but this is not a requirement. Finally, the earth surface elevation (in meters above sea level) for the entire 2-D map region is provided, using NNTOPO lines of values each containing NETOPO elevation values. Multiple input data lines may be used as needed. The program first reads the elevation values for the southernmost row

of points, starting in the west and working to the east. When completed, the next line of points to the north is entered, and so on. This continues until all NNTOPO east-west lines of elevation information have been provided.

<u>2.3.3.2.</u> Gravity acceleration – input file "ingravty.fil". Ordinarily, HeatEx uses the standard handbook value for the acceleration due to gravity (9.80665 m/s², directed downward). If this value suffices, file ingravty.fil is not needed. To change the value of the gravity acceleration, add ingravty.fil with a single line containing a single real-number input constant "FACTOR". The acceleration of gravity will be reset to (9.80665×FACTOR) m/s².

2.3.4. Spatial Discretization Specifications

At least one (and as many as five) different types of superimposed spatial grids may be The most fundamental of these is the involved in a single HeatEx simulation. "thermohydraulic grid", used to solve the fluid mass and total energy conservation relations. In addition, there may also be an overlying "electrokinetic grid". used to solve for the distribution of electrokinetic self-potential as the hydraulic solution evolves. Furthermore, if the "dynamic fracture patch" model is used to represent the temporal evolution of "fracture permeability" in the reservoir, a "thermoelastic grid" will also be required (overlying the others), to represent the regional distribution of rock stress. Next, if "aguifer-type" boundary conditions are called for at one or more external surfaces of the thermohydraulic grid, then it will be necessary to make provision for the one-dimensional discretized grid extensions used to solve for the approximate pressure distribution changes in these external regions. Finally, if the non-equilibrium "conductive MINC" model is used to treat the unsteady exchange of heat between the fluids in the pores and fractures and the intervening solid rock, additional spherically-symmetric one-dimensional discretized representations will be required for these models as well.

<u>2.3.4.1.</u> Thermohydraulic grid geometry – input file "ingridth.fil". Of these various overlapping spatial discretization networks, the thermohydraulic grid is the only one which is indispensible to HeatEx operation. Examples may be found in Sections 3.4.4.2 and 3.4.6.11 of this report. In general, the file will consist of five parts, in the following order:

GRID SPACING IN THE X-DIRECTION

[blank line]

GRID SPACING IN THE Y-DIRECTION

[blank line]

GRID SPACING IN THE Z-DIRECTION

[blank line]

LOCATION AND ORIENTATION INFORMATION

SPECIFICATION OF VOID REGIONS

[end of file]

Each of the first three parts ("GRID SPACINGS") consists of an ordered list of grid block sizes (meters) in the pertinent coordinate direction. The first group provides $\Delta x_1, \Delta x_2, ..., \Delta x_{last}$, with the group terminated with a blank line. The second group provides $\Delta y_1, \Delta y_2, ..., \Delta y_{last}$ followed with another blank line and the third provides $\Delta z_1, \Delta z_2, ..., \Delta z_{last}$. Each of these groups may consist of multiple input lines if needed. These data specify the dimensions of a

computational region shaped like a rectangular prism with dimensions $X_{max} \times Y_{max} \times Z_{max}$. where $X_{max} = \sum \Delta x_i$, $Y_{max} = \sum \Delta y_j$ and $Z_{max} = \sum \Delta z_k$.

The next three input lines in the file each contain three real numbers, and serve to specify the location of the thermohydraulic grid and its orientation with respect to the "World" coordinate system. These variables are:

First line: GRID0X GRID0Y GRID0Z
Second line: W0EAST W0NRTH W0ASL
Third line: ROTCXY ROTCXZ ROTCYZ

The first and second lines specify six linear distances in meters, and the third specifies three angles of rotation, in degrees. The interpretation of these quantities is as follows. The spatial point (in "grid" coordinates) given by x = GRID0X meters, y = GRID0Y meters and z = GRID0Z meters coincides with the "World" location (W0EAST m East, W0NRTH m North, W0ASL m ASL). The data on the third line provides the three angles by which the "grid" coordinate system is rotated relative to the "World" coordinate system, around the z-axis, y-axis and x-axis respectively. See Figure 2.9.

If the entire spatial grid volume specified so far participates in the calculation, the *ingridth.fil* file will end here. But sometimes, to represent regions of space that are not well-approximated as a rectangular prism, the user will desire to describe more irregular study volume shapes. This can be accomplished by declaring some of the grid blocks as "void" using the final part of the *ingridth.fil* input file. This part consists of a sequence of indefinite length (including, of course, zero length) of input lines containing six integers each:

ILOV IHIV JLOV JHIV KLOV KHIV

Each such line will mark all grid blocks [i, j, k] with index values ILOV $\leq i \leq$ IHIV, JLOV $\leq j \leq$ JHIV and KLOV $\leq k \leq$ KHIV as "void", and such blocks will not participate further in the calculation (for an example, see Section 3.4.4.2 of this report).

2.3.4.2. Electrokinetic grid geometry – input file "ingridek.fil".

Not all HeatEx simulations undertaken will involve calculations of electrokinetic self-potential (only one of the six examples presented in Section 3 involves such calculations), but for those that do an "electrokinetic grid" must be specified by the user. This is done using input file *ingridek.fil*. Instructions for constructing this grid are identical to those for assembling *ingridth.fil* (see Section 2.3.4.1, directly above), with three groups of (x, y, z) "grid spacing" data separated by blank lines, location and orientation parameters, and the possibility of the presence of "void" regions.

Ordinarily, although the grid spacings and axis orientations are likely to differ between the two grid systems, a substantial volume of overlap between the two is to be expected. The electrokinetic drag current and its divergence (which drives the self-potential distribution) is actually calculated within the thermohydraulic grid and then interpolated into the electrokinetic grid. Likewise, regions where the electrical conductivity distribution is changing with time (due to changes in subsurface temperature and fluid salinity) are first characterized in the thermohydraulic grid and then interpolated for the SP calculations.

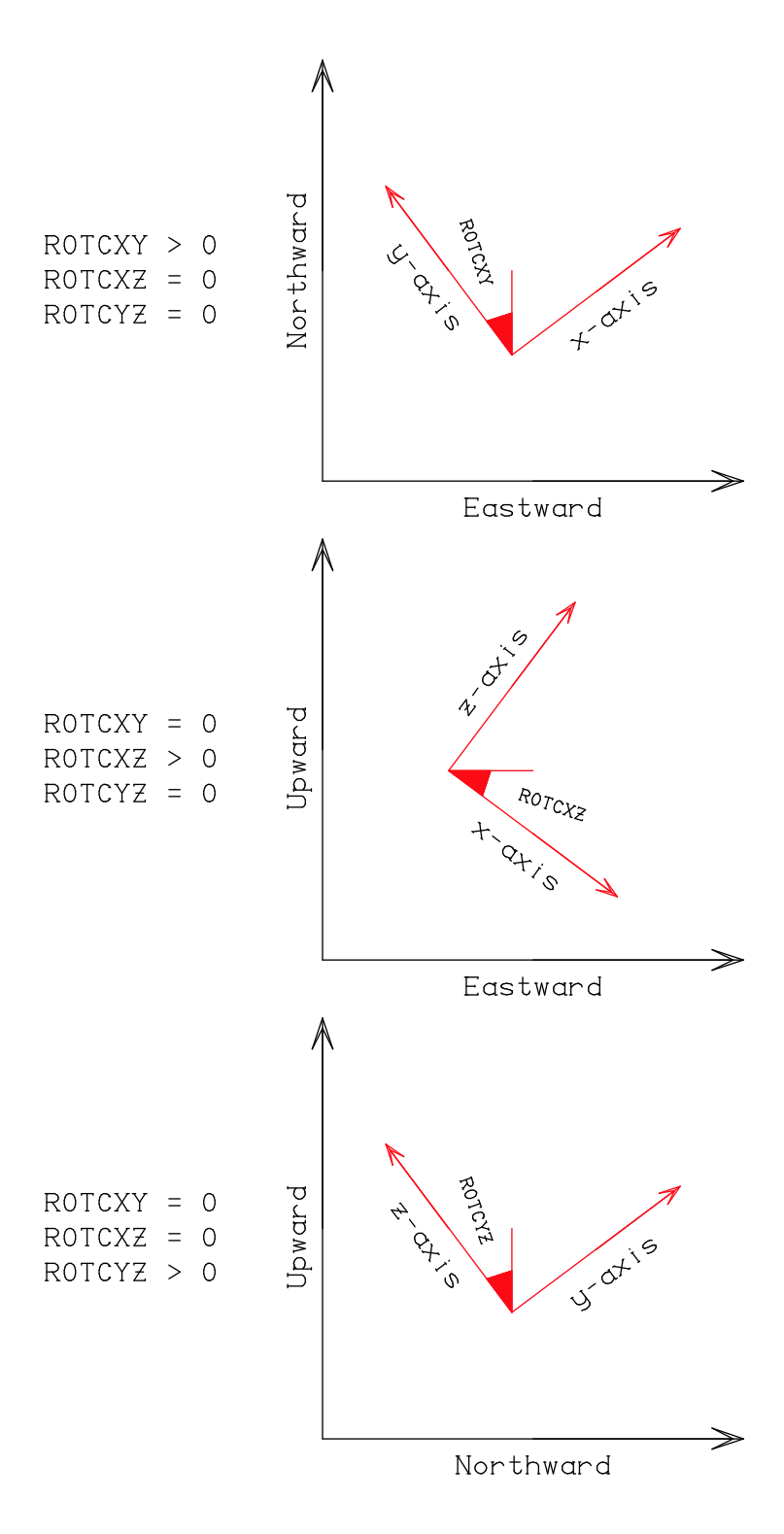


Figure 2.9. Effects of specified rotation angles (ROTCXY, ROTCXZ and ROTCYZ) upon the orientation of the thermohydraulic computational grid when viewed in the "World" coordinate system.

2.3.4.3. Thermoelastic grid geometry – input file "ingridte.fil".

Similarly, a "thermoelastic" grid will not always be required, but it will be essential if the dynamic "fracture permeability" model involving slip patches with changing apertures is to be incorporated in the simulation. The "thermoelastic grid" serves to store the distribution of regional rock stress in and around the region of interest, which is an essential part of the fracture patch model. Again, the instructions for the creation of the pertinent *ingridte.fil* input data file are the same as for both the "thermohydraulic grid" and the "electrokinetic grid" (see Section 2.3.4.1 above) and there is liable to be a substantial volume overlap among all three grids, but it is also likely that the thermoelastic grid will be substantially greater in spatial extent than the others. In this connection, compare Section 3.4.6.10 to Section 3.4.6.11. Once again, in this case there will be three groups of (x, y, z) "grid spacing" data separated by blank lines, location and orientation parameters, and possibly "voids".

2.3.4.4. Nonequilibrium fluid/rock heat exchange — input file "inminend.fil". An important HeatEx feature is its ability to go beyond the traditional geothermal reservoir modeling assumption of "local thermodynamic equilibrium", in which it is assumed that fluids and rocks, once brought into proximity, will quickly exchange heat conductively so that they will reach the same temperature on time-scales that are small compared to those of interest for fluid and heat production. This so-called "porous medium" approach is usually justified when the reservoir is hosted in sedimentary rocks where the fluid flow paths through the rock are on the intergranular scale, but for geothermal reservoirs which depend on widely-spaced permeable fractures to provide the fluid conduits, the time-scales required to mine the heat out of the relatively large fragments of intact rock between the fractures by means of heat conduction alone may not be negligible, and assuming instantaneous thermal equilibration under those circumstances can give rise to serious errors.

Pritchett (1997) is one of several authors who identified this difficulty and devised suitable mathematical approaches to treat reservoirs in which the spacing between the fractures is significant. His "conductive MINC" approach models the process as equivalent to the problem of conductive heat transfer from the interior of a solid sphere of rock to its surface, which is being maintained at a different temperature by fluid flowing past (in a fracture or other conduit). When the process starts, the heat transfer will be very rapid, but as time goes on and the cooling front penetrates deeper into the solid rock, the outward heat flux will decline. The process can be described using the following partial differential equation for T(r, t):

$$\partial T/\partial t = \alpha \left[\partial^2 T/\partial r^2 + (2/r) \times (\partial T/\partial r) \right]$$

where T is temperature, r is radius (which varies from zero to $(\lambda/2)$; λ is the diameter of the sphere of solid rock, taken as the "average fracture separation") and t is time. The quantity α is the solid rock "thermal diffusivity", defined as [(thermal conductivity) / (density × heat capacity)]. and is typically of the order of 10^{-6} m²/s for most geological materials. The problem may be non-dimensionalized using the dimensionless group $(\alpha t/\lambda^2)$, whence we obtain a "dimensionless time" t/τ_{eq} and a dimensionless radius r/λ , where $\tau_{eq} = \lambda^2/\alpha$.

This characteristic equilibration time-scale τ_{eq} is mathematically meaningful, but can cause misunderstandings about typical heat transfer rates. If we consider the problem of an initially

uniformly hot rock sphere being cooled by a constant (lower) temperature imposed at its outer boundary, as shown by *Carslaw and Jaeger* (1957) the time that will be required to remove 50% of the available heat energy will be only $\tau_{50\%} = (\tau_{eq}/32.4)$.

Using the "conductive MINC" approach as outlined by Pritchett (1997), each computational grid block in the mesh has a "representative spherical fragment" of solid rock associated with it, and heat transfer within the spherical fragment is treated as linear heat conduction, solving the above heat transfer equation subject to a time-dependent boundary temperature which is numerically equal to the instantaneous temperature of the fluid flowing in the fractures within the grid block. Pritchett's approach is a finite-difference method which subdivides the representative sphere into concentric spherical "shells" which are all of the same volume, as indicated in Figure 2.10. Since the above heat conduction problem is linear, a superposition technique may be used to make the task of keeping track of numerous different subgrid temperature values (the temperature in each of the "shells" is an unknown function of time) a fairly straightforward matter which imposes a negligible computational burden compared to that of solving the "outer" nonlinear reservoir equations governing the global behavior of the system. This approach of assigning a "representative sphere" of solid rock to each grid block was used in Pritchett's original 1997 paper, and is also employed in Illustrative Case 3 of the present study (see Section 3.1, below).

For the development of HeatEx, however, this approach was taken one step further. Instead of assigning a single "representative sphere" of rock to each grid block (with a single particular value of τ_{eq}), in HeatEx it is permissible to subdivide each grid block into several different "subvolumes" and then to describe each "subvolume" with a different "representative sphere" with its own value of τ_{eq} . In fact, one of the subvolumes may be treated using the classical "porous medium" model (equivalent to $\tau_{eq} = 0$) if desired. In this way, virtually any kind of cooling behavior can be mimicked. Illustrative Case 6 (see Section 3.3, below) uses this approach, subdividing each grid block into five different "subvolumes" for purposes of appraising the heat transfer between the solid rock and the reservoir brine.

Input file *inmincnd.fil* is used by HeatEx (1) to populate a "library" of "representative rock spheres" (each with a different value of τ_{eq}) and then (2) to subdivide the various blocks in the thermohydraulic grid into subvolumes and assign one of the model spheres in the "library" to each of the subvolumes. Examples of *inmincnd.fil* files may be found in Section 3.4.3.1 (for Case 3) and Section 3.4.6.14 (for Case 6). The first line in *inmincnd.fil* must contain a single integer:

NSHELL

which is the number of concentric, equal-volume spherical "shells" that will be used to discretize each "representative rock sphere". This first line is then followed by one or more lines which provide the various values for τ_{eq} that are to be represented in the "library" (real numbers, one per line, in increasing order, provided in seconds):

TAUEQ (1)
TAUEQ (2)
...
TAUEQ (last)
[blank line]

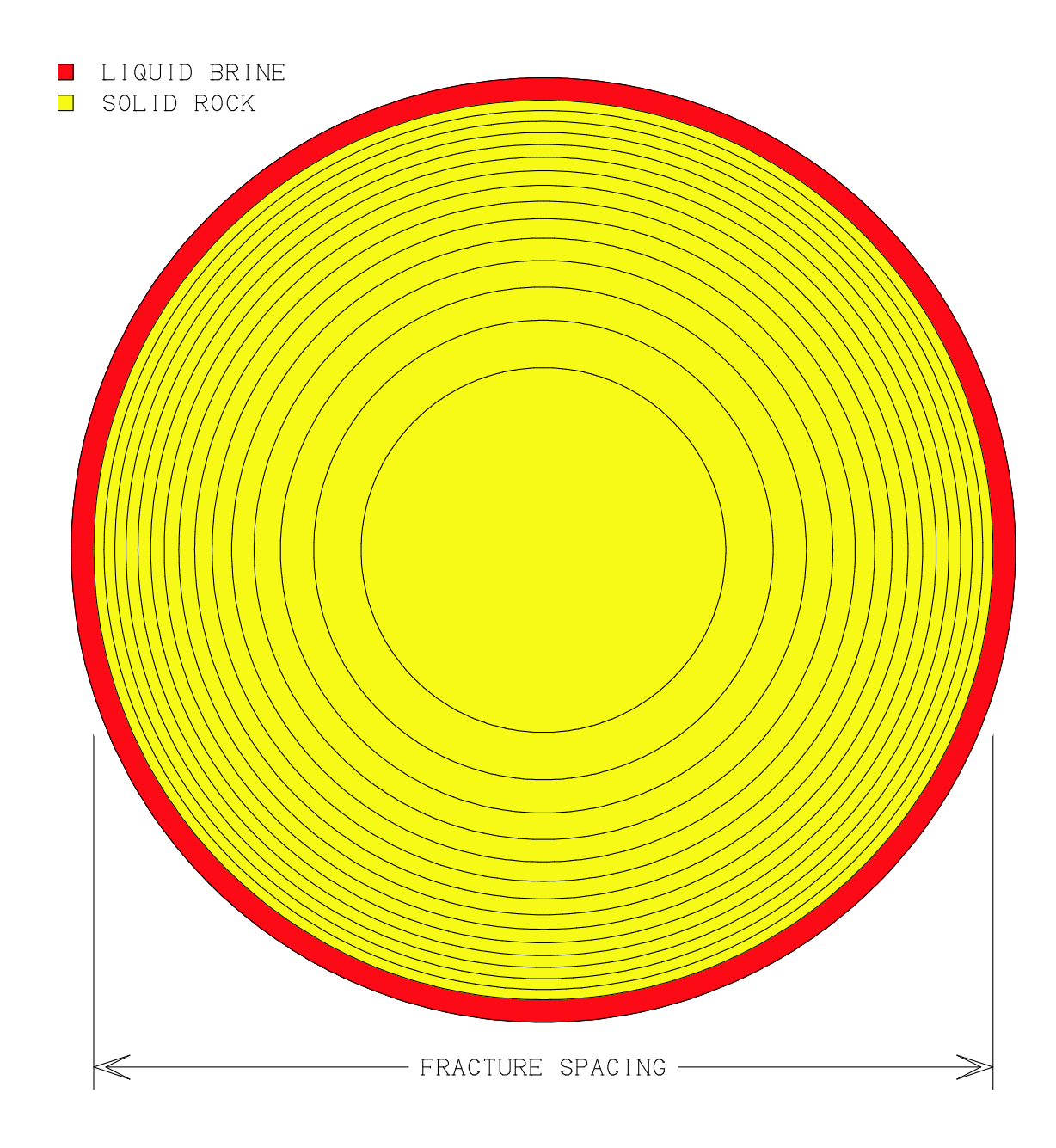


Figure 2.10. Geometry of a single "Conductive MINC" assembly of 15 concentric spherical "shells" of solid rock (*yellow*) surrounded by fluid (*red*). Each rock "shell" represents the same volume.

The terminal "blank line" is used to notify HeatEx that the end of the list has been reached. After this "blank line" another data line must be provided, containing a list of (last + 1) non-negative real numbers:

V(0) represents a "weighting factor" for the "porous medium" model ($\tau_{eq} = 0$); the others are "weighting factors" for the spherical assemblies for each of the τ_{eq} values listed above (the TAUEQ values). The above V distribution is used to compute volume fractions, for each block in the grid, to be associated with each of the τ_{eq} values:

[subvolume(n)] = [total block volume]
$$\times$$
 V(n) / Σ V

If this distribution of the τ_{eq} values (which is, so far, the same for all grid blocks) suffices, the *inmincnd.fil* may end at this point. Otherwise, however, any number of additional line pairs like the following may be appended as needed:

Each such line pair will have the effect of resetting, for all thermohydraulic grid blocks [i, j, k] with ILO $\leq i \leq$ IHI, JLO $\leq j \leq$ JHI, KLO $\leq k \leq$ KHI, the "weighting factors" for those blocks to the new V values.

<u>2.3.4.5.</u> "Aquifer" boundary conditions – input file "inaquifr.fil". Several types of boundary conditions for application to fluid flow at the perimeter of the thermohydraulic grid volume are feasible using HeatEx. By default, at the interfaces between "void" and "non-void" grid blocks (and in this connection the entire region beyond the grid is considered "void"), a "no-normal-flow" (or "Neumann") condition is imposed. As noted in Section 2.3.5 (below), distributed sources and sinks of mass/energy can also be applied within grid blocks adjacent to the boundary to generate such effects as fixed heat flow, fixed temperature, and/or fixed pressure (i.e. "Dirichlet") boundary conditions. Sometimes, however, it will be desirable to apply intermediate kinds of conditions at the exterior surfaces of the grid, to allow fluid to flow in and out of the computational volume in a "natural" manner.

For this purpose, some engineers have found so-called "aquifer" boundaries useful. Using this approach, at the perimeter of the simulation grid itself, another specialized representation of fluid flow in the unsteady but one-dimensional and linearized approximation is imposed to extend the computing region to greater distances in an approximate manner. Consider the single-phase fluid mass conservation relation in this one-dimensional approximation:

$$\partial p/\partial t = \beta \partial^2 p/\partial s^2$$

where $p = P(x, y, z, t) - P(x, y, z, t = 0) = P - P_o$ = the pressure disturbance relative to the (presumably steady) initial pressure, s represents linear distance away from the grid surface (s = -x, +x, -y, +y, -z or +z), and t is time. The "kinematic pressure diffusivity" β is taken to be constant, and equal to the average value of $(k/\varphi\mu c)$ in the region beyond the boundary, where k is rock permeability, φ is rock porosity, μ is fluid dynamic viscosity, and c is total compressibility (fluid compressibility + pore compressibility). Being linear in p, this partial differential equation may be solved using techniques similar to those used for solving the heat conduction equation for the "conductive MINC" model (Section 2.3.4.4 above).

The overall approach is illustrated by the accompanying sketch (Figure 2.11). Extending outward from each boundary face of the thermohydraulic grid boundary is a discretized one-dimensional spatial grid that extends a considerable distance further away. Each of these one-dimensional "strips" is solved independently (despite their appearance in Figure 2.11, the "yellow" region is not a two-dimensional grid, but is instead an array of independent one-dimensional grids, each oriented perpendicular to their boundary with the thermohydraulic grid). The above linear pressure diffusion equation is solved for p within each of these 1-D "strips" subject to (a) initial conditions of p = 0 everywhere, and (b) boundary conditions on either end, which are (1) a matching condition to the nonlinear solution for pressure evolving from the general-purpose simulation results within the thermohydraulic grid just adjacent to the boundary, and (2) either a Dirichlet (p = 0) or Neumann ($\partial p/\partial s = 0$) condition applied at the end farthest from the thermohydraulic grid boundary. Numerical experiments have shown that this approach can yield quite satisfactory results so long as care is taken that (1) the spatial discretization varies smoothly at the transition from the nonlinear to the linear region, and that (2) a sufficiently good estimate for β is used to avoid spurious reflections from the boundary.

To implement "aquifer boundaries" (of either the Neumann or Dirichlet type) in HeatEx, input file *inaquifr.fil* should be structured as follows (see Section 3.4.6.1 for an example). The file contains six "data blocks", each of which applies to one of the six exterior faces of the thermohydraulic computational grid:

```
Block 1: y-z face at x = x_{min} (s = -x)
Block 2: y-z face at x = x_{max} (s = +x)
Block 3: x-z face at y = y_{min} (s = -y)
Block 4: x-z face at y = y_{max} (s = +y)
Block 5: x-y face at z = z_{min} (s = -z)
Block 6: x-y face at z = z_{max} (s = +z)
```

and are incorporated into *inaquifr.fil* in the above order. The structure of each "data block" is the same, and is as follows.

The first line in the block must contain a character string, either "none", "all" or "some" (case insensitive):

```
Line 1: NONE or ALL or SOME (text string)
```

If Line 1 contains "none", then aquifer boundary conditions will not be applied to this grid face. Proceed to the next "data block".

If Line 1 contains "all", then aquifer boundary conditions will be applied to all of the grid block surfaces on this grid face. Skip to Line 3.

If Line 1 contains "some", then aquifer boundary conditions will be applied to just some of the block surfaces on this grid face. Line 1 will then be followed by a series (of indefinite length) of Line(s) 2, terminated with a blank line:

Line 1:	SOME				
Line 2:	MLO	MHI	NLO	NHI	(4 integers)
Line 2:	MLO	MHI	NLO	NHI	(4 integers)
Line 2:	MLO	MHI	NLO	NHI	(4 integers)



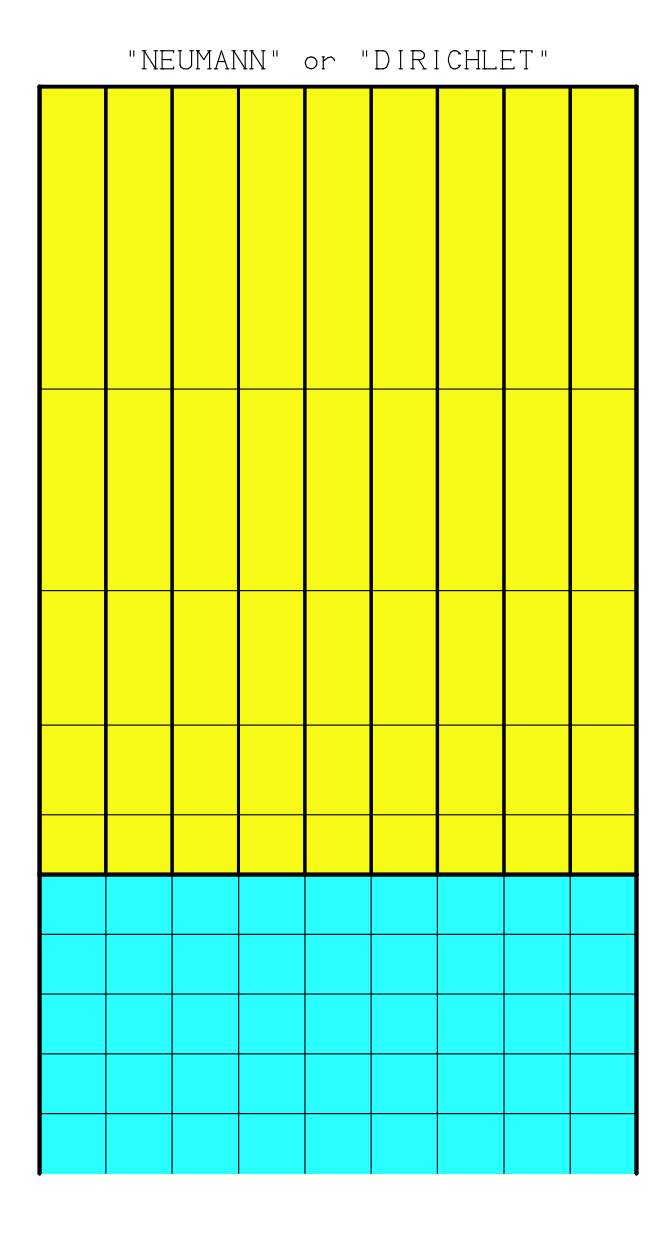


Figure 2.11. Geometry of discretized "external aquifer" region (*yellow*) adjoining one of the boundaries of the thermohydraulic grid (*cyan*). User must select distant boundary condition to apply at perimeter of aquifer region – "Neumann" (no flow) or "Dirichlet" (no pressure change).

```
Line 2: MLO MHI NLO NHI (4 integers)
...
Line 2: MLO MHI NLO NHI (4 integers)
[blank line]
```

The "blank line" signals HeatEx that this completes the input sequence of Line(s) 2. Each Line 2 contains four integers (MLO, MHI, NLO, NHI). All grid block surfaces with grid block indices "M, N" will have aquifer boundary conditions applied to them, where MLO \leq M \leq MHI and NLO \leq N \leq NHI, and where M and N represent:

```
for Blocks 1 and 2, "M" = "j" and "N" = "k" for Blocks 3 and 4, "M" = "i" and "N" = "k" for Blocks 5 and 6, "M" = "i" and "N" = "j"
```

Next, Line 3 designates the type of outer boundary condition to be applied to pressure changes at the distant end of the 1-D "strips", and consists of a single case-insensitive text string:

```
Line 3: DIRICHLET or NEUMANN (text string)
```

Finally, Line 4 completes the "data block" and provides nine input constants (one integer and eight real numbers), as follows:

```
Line 4: NBLOCK (integer), SIZE, PBAR, TBAR, SBAR, BMOD, SMOD, PORSTY, PERMBL (real numbers)
```

NBLOCK is the number of exterior grid blocks to be appended in the *s*-direction to the exterior of the thermohydraulic grid, and SIZE is the total *s*-direction length of the row of additional blocks. HeatEx always uses a geometric progression of exterior grid block sizes (as suggested in Figure 2.11 above):

$$\Delta S_{i+1} / \Delta S_i = \text{constant}$$

and the constant is chosen such that (1) the total length of the strip $(\Sigma \Delta s_i)$ equals SIZE (to be provided in meters) and (2) the interval closest to the thermohydraulic grid (Δs_{i-1}) is the same size as the adjacent principal grid block interval within the thermohydraulic grid. The remaining input constants on Line 4 are used to calculate an estimate for the "pressure diffusivity" β with the help of the HeatEs equation-of-state, and are:

PBAR	average pressure, pascals
TBAR	average temperature, degrees Celsius
SBAR	average fluid salinity, mass fraction
BMOD	average solid rock bulk modulus, pascals
SMOD	average solid rock shear modulus, pascals
PORSTY	average rock porosity, volume fraction
PERMBL	average rock permeability, square meters

2.3.5. Sources and Sinks

Provision has been made in HeatEx for the specification of distributed sources and sinks of fluid mass and of thermal energy within the thermohydraulic grid. One of the principal purposes for these features is in the application of boundary conditions on fluid mass and heat flow at the grid perimeter. All six illustrative cases presented in Section 3 use distributed sources and sinks in this manner, albeit in different ways.

<u>2.3.5.1.</u> Distributed mass sources/sinks – input file "insorcms.fil". This file assigns prescribed fluid mass sources and sinks to specified groups of grid blocks, and consists of a series of indefinite length of line pairs. The first line of each pair contains six integers, and the second contains a minimum of six (and perhaps more) real numbers:

The integers on the first line designate the volume of space affected by the mass source/sink described by the line pair – it consists of all non-void thermohydraulic grid blocks [i, j, k] with ILO $\leq i \leq$ IHI, JLO $\leq j \leq$ JHI and KLO $\leq k \leq$ KHI. It is of course required that ILO \leq IHI, JLO \leq JHI and KLO \leq KHI. Within this region, the imposed inward flow rate of fluid (kilograms per second per cubic meter) will be:

$$Q = RT0 + RPR \times P$$

but restricted to

$$RMN \le Q \le RMX$$

where P is local instantaneous pressure (grid block pressure), the input constants RT0, RMN and RMX are provided in kilograms per cubic meter per second, RMN \leq RMX, and RPR (which of course must not be positive) is provided in kg/m³-s-Pa. If the net flow is inward (that is, Q > 0), the enthalpy of the fluid flowing into the grid blocks will be ENT Joules per kilogram and its salinity will be SLT. The TR's are the tracer mass fractions in the inflowing fluid. Note that these sources/sinks may be overlapped – that is, a particular grid block may lie within the range of multiple line pairs. Thus, for example, it is possible to use these features to maintain the enthalpy (and salinity, and tracer content) of a particular grid block I*, J*, K* at desired values H*, S*, TR* by using two line pairs, both addressing that block:

where "large" represents a suitably chosen large positive constant. As another example, it is possible to use these mass sources to maintain the fluid pressure at a fixed value P^* at a particular grid block (located along a boundary, for example) by setting RT0 to a suitably chosen large positive value, and then setting RPR = $(-RT0/P^*)$. As will be seen, this was the approach taken to establishing the outer fixed-pressure boundary conditions in illustrative cases 4 and 5 (see Section 3.4.4.11).

2.3.5.2. Distributed energy sources/sinks – input file "insorcen.fil". The procedure is similar for heat sources/sinks. File insorcen.fil consists of a series of line pairs of indefinite length, with the first line of each pair containing six integers and the second line containing four real numbers:

The integers on the first line designate the volume of space affected by the heat source described by the line pair – it consists of all non-void thermohydraulic grid blocks [i, j, k] with ILO $\leq i \leq$ IHI, JLO $\leq j \leq$ JHI and KLO $\leq k \leq$ KHI. Within this region, the imposed heating rate (watts per cubic meter) will be:

$$e = PW0 + PWP \times T$$

but restricted to

$$PMN \le e \le PMX$$

where T is local instantaneous grid-block fluid temperature, the input constants PW0, PMN and PMX are provided in watts per cubic meter, PMN \leq PMX, and PWP (which must not be positive) is provided in watts/m³- $^{\circ}$ C.

2.3.6. Specifications of Initial Conditions

Specification of the starting conditions for a HeatEx reservoir simulation involves establishing the spatial distributions of fluid pressure P, fluid salinity S and fluid temperature T that prevail throughout the thermohydraulic grid volume at t=0. It will be assumed that the local solid rock temperature is initially equal to the local fluid temperature. If fluid tracers are involved in the calculation, the initial distributions of tracer concentrations will also be required.

Three different procedures are available to specify the initial distributions of P_0 , T_0 and S_0 (the initial values of pressure, temperature and salinity in each non-void thermohydraulic grid block). First, each of these quantities may be specified separately on a block-by-block basis, using input files *ininpres.fil*, *inintemp.fil* and *ininsalt.fil* as discussed in Sections 2.3.6.1 – 2.3.6.3 below. This is the approach taken in illustrative cases 1-5 discussed in Section 3. Second, it can be assumed that the system is initially in hydrostatic equilibrium; the user specifies the initial pressure at a particular point within the grid (and also specifies temperature and salinity as functions of vertical elevation), and HeatEx will then automatically calculate initial pressures in the various grid blocks assuming that a state of hydrostatic equilibrium prevails. This is done using input file *ininhydr.fil* (Section 2.3.6.4 below) and is the approach taken in illustrative case 6 (Section 3). Finally, instead of starting a new calculation, the user may wish to simply carry an already-completed simulation out further in time by "restarting" the run – this may be accomplished using input file *inrestrt.fil* as discussed in Section 2.3.6.5 below.

- <u>2.3.6.1.</u> Initial pressure distribution input file "ininpres.fil". Assigning initial pressure values to the various blocks in the thermohydraulic grid in this fashion involves the user creating an input file named ininpres.fil and writing it according to the specifications of the "VECTOR" distribution procedure (see Section 2.3.2 above). In this case, a single "attribute" is distributed, namely the desired initial pressure value, expressed in pascals.
- <u>2.3.6.2.</u> Initial temperature distribution input file "inintemp.fil". In a similar fashion, this file may be used to assign initial temperature values to the thermohydraulic grid blocks using the "VECTOR" procedure (Section 2.3.2). The "attribute" being distributed in this case is a single scalar the initial temperature value in degrees Celsius.

- <u>2.3.6.3.</u> Initial salinity distribution input file "ininsalt.fil". Again, file ininsalt.fil uses the "VECTOR" procedure (Section 2.3.2) to assign initial brine salinity values to each block in the thermohydraulic grid. The "attribute" in this case is "salinity" or dissolved NaCl mass fraction in the fluid phase; that is, [NaCl mass] / {[NaCl mass] + [H₂O mass]}.
- 2.3.6.4. Initial hydrostatic conditions input file "ininhydr.fil". As an alternative to ininpres.fil, inintemp.fil and ininsalt.fil above, file ininhydr.fil may be used to assign "hydrostatic" initial conditions to the thermohydraulic grid. Of course, for such an assignment to be meaningful a hydrostatic solution must exist, which means in practice that the initial distributions of pressure, temperature and salinity $(P_0, T_0 \text{ and } S_0)$ must be one-dimensional functions of elevation with respect to sea level only.

If these conditions are satisfied, input file *ininhydr.fil* will consist of two parts. The first part is a single line containing four real numbers:

PPEAST PPNRTH PPAASL PRSZRO

The first three entries designate a single spatial location in "World" coordinates (meters East, meters North and meters ASL respectively). *It is essential that this location lie within the non-void volume of the thermohydraulic computational grid!* The fourth entry (PRSZRO) is the desired t = 0 value of the fluid pressure at this particular location, expressed in pascals.

The second part of the file consists of a sequence of input lines (containing three data values each) of the form:

ELEV TEMP SALT

These three real numbers represent, respectively, vertical elevation with respect to sea level expressed in meters ASL, initial temperature in degrees Celsius at that elevation, and initial fluid salinity as a mass fraction at that elevation. As many of these lines may be supplied as desired (at least one is required), but they must be entered in order of increasing elevation (decreasing depth). These data prescribe the initial vertical profiles of temperature and salinity. For levels below the deepest (first) of these entries, the temperature and salinity will be assumed to be constant, and similarly for points above the last (shallowest) ELEV value.

Based upon the single fixed pressure value, these vertical profiles of temperature and salinity and the internal equation-of-state, HeatEx will compute the appropriate interpolated initial temperature and salinity values for each grid block, calculate the initial hydrostatic pressure distribution, and assign P_0 , T_0 and S_0 to each non-void block in the thermohydraulic grid.

2.3.6.5. Restarting a simulation – input file "inrestrt.fil". The final way that P_0 , T_0 and S_0 may be initially assigned to the thermohydraulic grid blocks to initialize a HeatEx simulation amounts to a "restart" procedure – that is, the objective is to carry a prior simulation further forward in time. As discussed below in Section 2.3.11.2, one of the output options available with HeatEx is to create a special-purpose output file called **rprestrt.fil**. From time to time during the simulation, the entire current state-of-the-system will be written on this file. To avoid overwhelming the computer's storage capacity, each time such a record is written, the prior such record is deleted. Thus, this file will always contain the most recent information available. At the end of the simulation if no "restarts" are planned, **rprestrt.fil** may be deleted to save disk space.

But to restart the simulation, all that is required is to create a new problem directory, copy all input files ('in******.fil" files) from the original problem directory to the new one, delete the "initial conditions" files (ininpres.fil, inintemp.fil, ininsalt.fil and/or ininhydr.fil), and then change the name of the old rprestrt.fil file to "inrestrt.fil", copy it into the new problem directory, and then start HeatEx. The run will pick up from the point in the prior calculation when the most recent record was written on rprestrt.fil.

2.3.7. Specifying Formation Properties

2.3.7.1. Thermal conductivity model – input file "incondrk.fil". The purpose of this input file is to specify, for each non-void block in the thermohydraulic grid, (1) the thermal conductivity (watts per meter per degree Celsius) of the solid rock within the block, and (2) how the overall effective thermal conductivity of the block is to be calculated by combining this value with the time-dependent fluid-phase thermal conductivity obtained from the equation-of-state (a function of local pressure, temperature and salinity; see Figures 2.4 and 2.8.). This input file is to be constructed using the "VECTOR" procedure described in Section 2.3.2 (above). Each "attribute" line will contain two numerical values – (1) a positive real number TCNDRK representing the desired value of the solid-rock thermal conductivity κ_r (which must lie between 0.1 W/m-°C and 10 W/m-°C) and (2) an integer which lies between 0 and 3 inclusive and which designates the "conductivity mixing model":

The significance of the value supplied for MIXCND is as follows:

- MIXCND = 0: The fluid-phase thermal conductivity obtained from the equation-of-state will be ignored. The grid block thermal conductivity will be simply set equal to TCNDRK and will not change with time.
- MIXCND = 1: The specified solid-phase thermal conductivity (κ_r = TCNDRK) will be combined with the fluid-phase conductivity from the equation-of-state (κ_f) using the "parallel rule":

$$\kappa_p = \varphi \times \kappa_f + (1 - \varphi) \times \kappa_r$$

where φ is rock porosity.

MIXCND = 2: The thermal conductivity values will instead be combined using the "series rule":

$$[1/\kappa_s] = [\varphi / \kappa_f] + [(1 - \varphi) / \kappa_r]$$

MIXCND = 3: The thermal conductivity values will be combined using Budiansky's Rule (*Budiansky*, 1970): κ_b is found by solving

$$[(3 \varphi \kappa_b) / (2 \kappa_b + \kappa_f)] + [(3 (1 - \varphi) \kappa_b) / (2 \kappa_b + \kappa_r)] = 1$$

for κ_b and then enforcing the restriction:

smaller of
$$[\kappa_p, \kappa_s] \leq \kappa_b \leq \text{larger of } [\kappa_p, \kappa_s]$$

<u>2.3.7.2.</u> Volumetric rock properties – input file "inrkvolp.fil". The purpose of this input file is to assign values for (1) rock grain density, (2) rock grain heat capacity, (3) initial rock porosity, (4) rock pore compressibility, (5) hydrodynamic dispersion coefficient for solutes and (6) hydrodynamic dispersion coefficient for heat convection to each non-void block in the

thermohydraulic computational grid. The input file is to be structured using the "VECTOR" procedure described in Section 2.3.2, and each "attribute" line will contain six real numbers:

RKDENS RKHTCP PORSTY COMPOR DSSOLU DSHEAT representing the assigned values for the above six parameters:

RKDENS = ρ_r = rock grain density in kg/m³,

RKHTCP = c_r = rock grain heat capacity in J/kg-°C,

PORSTY = φ = initial rock porosity,

COMPOR = $(\partial \varphi / \partial P) / \varphi$ = rock pore compressibility in Pa⁻¹,

DSSOLU = dispersion coefficient for solute convection in meters, and

DSHEAT = dispersion coefficient for thermal convection in meters.

<u>2.3.7.3.</u> Intergranular permeability – input file "inrkigpr.fil". In HeatEx, rock permeability is treated as being made up of two components. The "intergranular permeability" does not change with time, is isotropic, and may be regarded as an intrinsic rock property. The "fracture permeability", by contrast, is unsteady and anisotropic, and is a property of the instantaneous state of the fracture system which penetrates through the rock formations. The total permeability, which governs fluid flow through the system according to Darcy's Law, is the sum of the intergranular permeability and the fracture permeability. Since the fracture permeability is in general anisotropic, it requires a tensor representation, and therefore the total permeability must also be represented as a tensor. But the intergranular permeability (k^{ig}) , being isotropic, can be treated as a simple scalar function of position. Its contribution to the total permeability tensor is simply:

$$\Delta k_{xx} = k^{ig}$$
 $\Delta k_{xy} = 0$
 $\Delta k_{yy} = k^{ig}$ $\Delta k_{yz} = 0$
 $\Delta k_{zz} = k^{ig}$ $\Delta k_{zx} = 0$

Values for k^{ig} are assigned to the various thermohydraulic grid blocks using file *inrkigpr.fil*, which uses the "VECTOR" protocol (Section 2.3.2) with a single "attribute" (k^{ig}) which must be provided in square meters. Note that one millidarcy (usually a more suitable unit for expressing rock permeabilities) is equal to 10^{-15} m².

2.3.8. Modeling Fracture Permeability

In HeatEx, fracture permeability is assumed to arise from the presence of explicit fractures distributed through the reservoir volume, and represented by a collection of circular "fracture slip patches" distributed in space with user-specified center locations, orientations, sizes, and physical properties. The technique borrows heavily from the Geowatt "Hex-X" approach (*Kohl and Megel*, 2005; 2007).

If a portion of a slip patch intersects a particular thermohydraulic grid block volume, its presence will contribute to the rock permeability tensor describing the grid block. The distribution of the contribution among the various components of the permeability tensor (k_{xx} , k_{yy} , k_{zz} , k_{xy} , k_{yz} and k_{zx}) will depend upon the orientation of the fracture patch relative to the thermohydraulic grid coordinates, and the magnitude of the contribution will increase in direct

proportion to (1) the area of the fracture patch's intersection with the grid block (A) and (2) the aperture of the fracture raised to the third power (λ^3).

The aperture of a fracture depends on (1) the mechanical properties of the rock hosting the fracture, (2) the fluid pressure P in the fracture, and (3) the effective normal and shear stresses on the fracture plane. The effective normal and shear stresses are computed from the total regional stress tensor and the fluid pressure P. The fracture aperture will change with time because of a combination of the following three mechanical processes:

1. Normal compliance: For low effective shear stress, only a compliant reaction of the fracture walls will affect the aperture. The compliant aperture λ_c is given by:

$$\lambda_{\rm c} = \lambda_0 / (1 + 9 \varepsilon_n / \varepsilon_{90\%})$$

where λ_0 is the zero-stress aperture value ("AP0" below), ε_n is the instantaneous normal effective stress, and $\varepsilon_{90\%}$ is the "90% closure" effective stress ("CS90" below). The conditions for compliant behavior are (1) the normal stress is compressive and (2) the Mohr-Coulomb criterion is satisfied. Aperture increases caused by compliant response are treated as reversible.

2. Compliance and shearing: If the effective shear stress at the fracture walls exceeds the friction resistance and the effective normal stress is compressive, then the fracture will fail in shear. The aperture change (λ_s) due to shear offset U is given by

$$\lambda_{\rm s} = U \tan (\Phi_{dil})$$

where Φ_{dil} is the shear dilation angle of the fracture wall. The aperture change due to shear slippage is irreversible and results in a permanent change to the permeability distribution.

3. Jacking and shearing: If the effective normal stress becomes tensile, then the fracture walls will separate and the friction forces acting upon them will vanish. In this case, a reversible increase in aperture due to jacking (λ_j) must be considered in addition to the irreversible change arising from shearing (see above).

Even though the shear-induced aperture change is the only permanent effect of hydraulic stimulation, the contributions from jacking and compliance are obviously important in a transient sense during the stimulation process and must, therefore, be taken into account when simultaneously considering the short- and long-term effects of reservoir stimulation.

<u>2.3.8.1.</u> Specifying the regional stress distribution – input file "inrgstrs.fil". The purpose of this input file is to populate the thermoelastic grid (Section 2.3.4.3 above) with regional earth stress data for subsequent use by the fracture dynamics model. The input file consists of a series of arbitrary length of nine-line groups, each of which specifies the distribution of the six independent stress components within a user-prescribed rectangular prism by linear interpolation among the prescribed values at the corners of the prism. The user must take care that the entire thermoelastic grid volume is populated in this fashion. The nine input lines each contain six real numbers, as follows:

```
Line 1:
        CE1
                 CE2
                          CN1
                                  CN2
                                           CA1
                                                    CA2
Line 2: SEE111
               SNN111
                        SAA111
                                 SEN111
                                          SEA111
                                                   SNA111
Line 3: SEE211
               SNN211
                        SAA211
                                 SEN211
                                          SEA211
                                                   SNA211
Line 4: SEE121
               SNN121
                        SAA121
                                 SEN121
                                          SEA121
                                                   SNA121
Line 5: SEE221
               SNN221
                        SAA221
                                 SEN221
                                          SEA221
                                                   SNA221
Line 6: SEE112
               SNN112
                        SAA112
                                 SEN112
                                          SEA112
                                                   SNA112
Line 7: SEE212
               SNN212
                        SAA212
                                 SEN212
                                          SEA212
                                                   SNA212
Line 8: SEE122
               SNN122
                        SAA122
                                 SEN122
                                          SEA122
                                                   SNA122
Line 9: SEE222
                        SAA222
                                 SEN222
               SNN222
                                          SEA222
                                                   SNA222
```

The first line contains the locations of the eight corners of the prism; the units of the entries are [m East, m East, m North, m North, m ASL and m ASL] respectively. The location of corner ijk is [CEi meters East, CNj meters North and CAk meters ASL]. The remaining eight lines provide the stress components in pascals, each line providing values for one of the ijk corners. Here, the normal stresses are denoted by SEE, SNN and SAA (ε_{ee} , ε_{nn} and ε_{aa} respectively) and the shear stresses by SEN, SEA and SNA (ε_{en} , ε_{ea} and ε_{na} respectively).

<u>2.3.8.2.</u> Specifying fracture class properties – input file "infpprms.fil". Many pertinent physical property values of the numerous "fracture slip patches" are likely to be shared by many different individual patches. Accordingly, to reduce repetitive input, the various patches have been categorized into "classes" which share common properties. This procedure is somewhat arbitrary and the number of different "classes" involved for a particular problem is up to the user – there is no reason in principle why each individual patch could not constitute its own unique "class", for example, permitting all of the properties to be independently assigned.

Input file *infpprms.fil* begins with two lines specifying the elastic moduli which are used in the deformation model for all fracture patches:

```
Line 1: YOUNG (real number)
Line 2: SHEAR (real number)
```

These are, respectively, the Young's and shear modulus: they must be positive and are to be provided in pascals. These are to be followed by N additional lines (n = 1, 2, 3, ..., N), each of which provides additional information for one of the "classes" of slip patches and contains four real numbers:

```
Line (2+n): BFA(n) SDA(n) CS90(n) COH(n)
```

The meanings of these data are as follows:

```
BFA(n) = basic friction angle for class n in degrees.

SDA(n) = shear dilation angle for class n in degrees.

CS90(n) = 90% closure stress for class n in pascals.
```

COH(n) = cohesion for class n in pascals.

<u>2.3.8.3.</u> Describing individual slip patches – input file "infpdata.fil". This file specifies the remaining properties of the individual fracture slip patches, one at a time. First, data are provided for all of the "class 1" fracture patches, one per line. Then, a blank line serves to notify HeatEx that "class 1" input is complete. Next, all of the "class 2" patches are described,

followed by another blank line. The "class 3" data follows, and so on until all of the patches have been described.

Each "fracture patch" line contains eight real numbers:

with the following meanings:

CNE, CNN, CNA are the location in "world" coordinates (meters East, meters North and meters ASL respectively) of the geometric center of the circular fracture patch.

AZI and DIP provide the fracture patch orientation (azimuth angle α and dip angle δ , both in degrees). If a horizontal plane intersects the fracture patch, the line of intersection will be oriented α degrees east of true north. The dip angle δ is the downward angle between the fracture plane and the horizontal, using the right-handed convention. If one stands on the earth surface and faces in the azimuth direction, the fracture plane will tilt downward to one's right. If instead the fracture tips upward to the right, add 180 degrees to α .

RAD is the radius of the circular fracture patch, in meters. AP0 is the "zero-stress aperture"; λ_0 , the aperture that the fracture would exhibit if all stresses were zero, and is provided in meters. DAL is the "Darcian aperture limit" λ_D and is also provided in meters. The physical significance of λ_D is as follows. If the physical aperture of a fracture (λ) becomes sufficiently large, the Reynolds number of the fluid flow passing through the fracture will become large enough that a transition from laminar to turbulent flow will take place. A fundamental assumption in HeatEx (and in other reservoir simulators as well) is that Darcy's law (a linear relationship between fluid flow rate and local pressure gradient) applies to flow in fractures as well as on the intergranular level. But Darcy's Law implicitly assumes that laminar flow will always prevail. If turbulent flow begins, flow resistance will increase and Darcy's Law will overestimate the flow rate. The purpose of the λ_D term is to correct for this effect, at least approximately. In HeatEx, the "effective fracture aperture" λ_E (to be used for calculating permeability and fluid flow rate) is related to the actual physical fracture aperture λ by:

$$\lambda_E = (\lambda \lambda_D) / (\lambda + \lambda_D)$$

which has the desired asymptotic behavior: $\lambda_E \to \lambda$ for $\lambda << \lambda_D$ and $\lambda_E \to \lambda_D$ for $\lambda >> \lambda_D$.

2.3.9. Modeling Subsurface Electrical Disturbances

It has been recognized for many years that subsurface flows of fluids through underground rock formations can induce electric currents ("drag currents") through the mechanism of electrokinetic coupling, which can in turn give rise to nonuniform underground distributions of electrical potential through their interaction with the (generally fairly high) electrical resistivity of the earth, and that if the fluid flow is unsteady, the electrical potential thereby induced (the "electrokinetic self-potential" or EKP) will likewise be unsteady. The amplitudes of these electrical disturbances can easily reach tens or even hundred of millivolts, making their detection and characterization a fairly straightforward matter using subsurface electrodes and other properly designed instrumentation. The fluid flows induced in the earth by geothermal reservoir stimulation operations (hydrofracturing and similar activities) are highly transient and

entail large pressure disturbances, which means that they are presumably accompanied by substantial underground transient electrical signals.

Theoretical studies (*Pritchett and Ishido*, 2005, 2010) indicate that the detection and characterization of these electrical signals during the reservoir stimulation process can provide information concerning fracture location and characteristics that can supplement microseismic monitoring information and even provide additional useful insights that cannot be obtained in any other way. For typical EGS development scenarios, owing to their considerable depth, useful electrical signals will be confined to great depths (comparable to that of the reservoir itself), so that traditional earth-surface SP surveying is unlikely to be of much use. But subsurface electrodes might be placed deep within the reservoir using slim hole drilling and non-metallic casings (at least at reservoir depths) to avoid perturbing the electrical conductivity distribution. Other surveying possibilities also exist, such as monitoring downhole electrical potential changes on the casings of existing wells during stimulation and pressurization operations in nearby wells.

Accordingly, the HeatEx code was designed from the outset to be capable of simulating such subsurface electrical disturbances simultaneously with other more conventional monitoring techniques (such as pressure transient determinations, tracers, microseismicity, *etc.*). The general approach to modeling underground electrical transients arising from stimulation operations is similar to that used in a previous specialized simulator development effort focused on electrokinetic effects which was carried out for DOE several years ago (the **SPFRAC** simulator – see *Pritchett*, 2008).

To perform such calculations with HeatEx, it is first necessary that the user specify an "electrokinetic grid" which will be used to host the electrical potential calculations (see Section 2.3.4.2 above). This grid must be of sufficient spatial extent to encompass the entire region within which significant electrical signals are anticipated, since it will be assumed that the electrical disturbance at the outer boundary of this grid (and beyond) is negligible. It should also enclose most or all of the thermohydraulic grid (within which the hydrodynamic calculations take place), since various effects that are pertinent to the self-potential calculations (fluid flow, induced current, effects of temperature and salinity changes on electrical conductivity, and the like) are first calculated within the thermohydraulic grid and then interpolated to the electrokinetic grid blocks for use in electrical potential calculations.

Other input data that are likely to influence the electrokinetic calculations include the specifications of the well geometries (file *inwelgeo.fil*, Section 2.3.13.1 and file *inwelflo.fil*, Section 2.3.13.2). In addition to being in large part responsible for the subsurface flow rate changes that create changing "drag current", the mere presence of the wells can have major effects upon the distributions of subsurface electrical potential. Most wells have metallic casing pipe which is in contact with the surrounding formations, and the electrical conductivity of steel exceeds that of typical reservoir rocks by many orders of magnitude. As a result, these pipes can create "short circuits" that can substantially alter the electrokinetic potential distribution. At least two situations can be distinguished. If the pipe constitutes a continuous electrical conductor reaching upward to levels far above the reservoir (and perhaps all the way to the earth surface), the electrical potential on the pipe (which, owing to its enormous conductivity, will be uniform along its length) will likely be dominated by these distant regions

where, by presumption, the electrical disturbance is essentially zero. As a result, the presence of the pipe is likely to attenuate any induced electrokinetic signals nearby. On the other hand, if a relatively short section of the well casing is electrically isolated from the rest (by, for example, an open hole section or a casing section made of insulating material) and the isolated section is completely contained within the volume of the electrokinetic grid, then by conservation of charge the net electric current into or out of the pipe section must add up to zero. As a result, the potential on the isolated pipe section will be uniform but will vary with time, reflecting a "floating average" of the potentials in the formations with which it is in contact. Measurements of the time-history of the electrical potential upon such an isolated section can provide useful information as well.

In addition to the electrokinetic grid geometry and the description of conductive artifacts (well casings), three other input files are essential prerequisites for HeatEx to perform electrokinetic potential forecasts. First, one or more "libraries" of pertinent electrical property values must be created using input file *inelpram.fil*. Next, those "library" properties must be distributed through the volume of the thermohydraulic grid using input file *inelprds.fil*. Finally, input file *inecnbgr.fil* must be used to supply electrical properties for any parts of the electrokinetic grid that are not overlapped by the thermohydraulic grid.

<u>2.3.9.1.</u> Defining electrical parameter library – input file "inelpram.fil". This file consists of one or more "line pairs", each of which serves to specify one entry in the "electrical parameter library". The first line of each pair contains either five or six real numbers:

Line 1: TORTUO DLTAPH ECNSRF ECNRK0 ECNRKT (QMODEL) and the second line contains a one-word text string:

Line 2: ARCHIE OF BUDIANSKY OF CAPILLARY OF NOMIX OF PARALLEL OF SERIES

The first two entries in Line 1 (TORTUO = dimensionless flow path tortuosity = θ ; and DLTAPH = $\delta(pH)$, dimensionless parameters in *Ishido and Mizutani's* (1981) model for zetapotential) serve to help determine the drag current from the computed fluid flow rate based on their model. The remaining entries on Line 1 and the entry on Line 2 help to establish the electrical conductivity distribution. ECNSRF is rock "surface" conductivity σ_s and ECNRKO is "base" rock volumetric conductivity σ_{ro} (both to be provided in Siemens per meter). The volumetric dry rock conductivity is taken to be given by:

$$\sigma_r = \text{ECNRK0} \times \exp(\text{ECNRKT} \times T)$$

where T is local instantaneous rock temperature in degrees Celsius, ECNRKT has dimensions $(^{\circ}C)^{-1}$ and the total overall electrical conductivity of the system is given by:

$$\sigma = \sigma_s + \sigma_M(\sigma_r, \sigma_f)$$

where σ_M represents a "mixture" of the dry rock electrical conductivity (σ_r) and the fluid electrical conductivity (σ_f). The fluid electrical conductivity depends principally upon fluid temperature and salinity and is obtained from the equation-of-state, and the "mixture model" is specified by the text string on Line 2 and the optional parameter QMODEL from Line 1.

If Line 2 contains **NOMIX**, then $\sigma_M = \sigma_r$ (the fluid component conductivity is ignored).

If Line 2 contains **PARALLEL**, then the "parallel rule" is used to combine σ_r and σ_f .

$$\sigma_p = \varphi \sigma_f + (1 - \varphi) \sigma_r.$$

If Line 2 contains **SERIES**, then the "series rule" is used:

$$[1/\sigma_s] = [\varphi/\sigma_f] + [(1-\varphi)/\sigma_r].$$

If Line 2 contains **BUDIANSKY**, then Budiansky's Rule (*Budiansky*, 1970) is used to combine the solid and fluid electrical conductivities by solving:

$$[(3 \varphi \sigma_b) / (2 \sigma_b + \sigma_f)] + [(3 (1 - \varphi) \sigma_b) / (2 \sigma_b + \sigma_r)] = 1$$

for σ_b and then enforcing the restriction:

smaller of
$$[\sigma_p, \sigma_s] \leq \sigma_b \leq \text{larger of } [\sigma_p, \sigma_s].$$

If Line 2 contains **ARCHIE**, then Archie's Law is used to calculate electrical conductivity (QMODEL is dimensionless):

$$\sigma = \text{QMODEL } \varphi^2 \sigma_f$$
.

If Line 2 contains CAPILLARY, then the "capillary tube model" is used (QMODEL is dimensionless):

$$\sigma = \sigma_r + \text{QMODEL } \sigma_f$$
.

2.3.9.2. Spatial distribution of electrical properties – input file "inelprds.fil". Once the NLIB (> 0) electrical parameter library entries have been established using input file inelpram.fil, input file inelprds.fil is used to distribute them throughout the volume of the thermohydraulic grid. The first line in this file must contain a single integer:

where $1 \le \text{LIBDEF} \le \text{NLIB}$. This is the "default electrical parameter library entry"; all blocks in the thermohydraulic grid will be first assigned the electrical properties (above) associated with library entry LIBDEF. If this simple description suffices, then input file *inelprds.fil* will contain only this single line, and we may proceed to input file *inecnbgr.fil*, below.

Otherwise, though, following Line 1, file *inelprds.fil* must continue with a series (of indefinite length) of [Line A / Line B / Line C] triplets, to provide any required exceptions to the LIBDEF default assignment of electrical properties. Two possibilities exist for the contents of the triplets, and the two formulations may be intermixed in a single *inelprds.fil* file. The first locates the "exceptions" using the thermohydraulic grid block indexing system:

Line A: LIB (integer)
Line B: GRID (text string)
Line C: ILO IHI JLO JHI KLO KHI (6 integers)

This sequence will reset the electrical parameter library entries for all thermohydraulic grid blocks with index numbers (i, j, k) and ILO $\leq i \leq$ IHI, JLO $\leq j \leq$ JHI and KLO $\leq k \leq$ KHI to library entry number LIB. The alternative Line A/B/C sequence uses World coordinates (instead of Grid coordinates) to identify the subregion to be modified:

Line A: LIB (integer)
Line B: world (text string)
Line C: WE1 WE2 WN1 WN2 WA1 WA2 (6 real numbers)

This sequence will reset the library entry to LIB for all thermohydraulic grid blocks of which the centers lie between WE1 and WE2 meters East, between WN1 and WN2 meters North and between WA1 and WA2 meters ASL elevation in "World" coordinates.

2.3.9.3. Electrical conductivity beyond thermohydraulic grid – input file "inecnbgr.fil". Until this point, attention has centered on specifying the distribution of "drag current" and of "electrical conductivity" within the thermohydraulic grid volume, because that is the volume within which parameters are known (flow rate, temperature, salinity etc.) which are needed to determine these quantities. But the real objective is to calculate electrical potentials within the electrokinetic grid volume. For drag current, it suffices to assume that fluid flows (and therefore drag currents) outside the thermohydraulic grid volume may be safely neglected, so that in those portions of the electrokinetic grid which do not overlap the thermohydraulic grid, we may safely assume that drag current is zero. But this is not the case for electrical conductivity. It is probably safe to assume that the temporal changes in electrical conductivity outside the "overlap region" are negligible, but the electrical conductivity itself requires a definite value that (hopefully) merges relatively smoothly with the values obtained within the thermohydraulic grid volume obtained from the above "conductivity models".

It is the role of the *inecnbgr.fil* input file to supply electrical conductivity values throughout the volume of the electrokinetic grid. Within that portion of the grid that is overlain by the thermohydraulic grid, these values will be superseded by interpolated calculated time-varying thermohydraulic grid values, but in the regions (if any) that are not overlapped by the thermohydraulic grid, the values supplied by *inecnbgr.fil* will influence the solution.

The structure of this input file is fairly similar to the others. The first line contains a single real number:

```
Line 1: ECNDEF (real number)
```

ECNDEF is a default electrical conductivity value (S/m) that will initially be assigned to all of the blocks in the electrokinetic grid. If such a single constant value (which will be subsequently overridden in all regions that are overlain by the thermohydraulic grid) is sufficient, then *inecnbgr.fil* will simply consist of a single input line.

But if more complexity is needed, the first line may be followed with any desired number of line A-B-C triplets, of either of two forms. The first is:

Line A: ECN (real number)
Line B: GRID (text string)
Line C: ILOE IHIE JLOE JHIE KLOE KHIE (6 integers)

which will assign to all [i, j, k] blocks in the <u>electrokinetic</u> grid (Note: NOT the <u>thermohydraulic</u> grid!) with ILOE $\leq i \leq$ IHIE, JLOE $\leq j \leq$ JHIE and KLOE $\leq k \leq$ KHIE a conductivity value of ECN S/m. The second form is:

Line A: ECN (real number)
Line B: world (text string)
Line C: WE1 WE2 WN1 WN2 WA1 WA2 (6 real numbers)

This sequence will reset the conductivity to ECN S/m for all <u>electrokinetic</u> grid blocks for which the centers lie between WE1 and WE2 meters East, between WN1 and WN2 meters North and between WA1 and WA2 meters ASL in "World" coordinates.

Once again, the data on input file *inecnbgr.fil* have no effect except in those parts of the electrokinetic grid which are not overlapped by the thermohydraulic grid. If no such regions exist, *inecnbgr.fil* will have no effect. The simulator nonetheless requires that the file be present before EKP calculations will be performed.

2.3.10. Tracers

Provision has been made in HeatEx for the incorporation of dissolved "tracers" which move with the flow and serve to track different water masses. It is assumed that the presence of the tracers does not influence the properties of the fluid in any way, and so the presence or absence of tracer does not change the distributions of pressure, temperature and/or salinity that would be calculated otherwise. A total of up to three different tracer species may be present simultaneously. The tracers are followed using the HeatEx thermohydraulic grid, stepping the tracer distributions in time along with the mass and heat flow calculations. The tracers may act independently of each other, or their behavior may be coupled as parts of tracer "reaction systems".

<u>2.3.10.1.</u> Tracer chemistry – input file "intrchem.fil". Five different tracer "reaction system" possibilities exist, using the following models:

- 1. "conservative"
- 2. "radioactive"
- 3. "thermal degradation"
- 4. "equilibrium"
- 5. "absorption"

Not all can operate simultaneously. Only the "conservative" system involves just a single tracer species – the others all involve two. The "radioactive" and "thermal degradation" models both involve a primary material and a secondary material ("daughter" nuclides or "reaction products"). The "equilibrium" model describes the equilibrium populations of two interacting tracers, and the "absorption" model treats the (mobile) dissolved tracer material separately from the (immobile) fraction which has been absorbed on the solid rock. Owing to the limitation to three tracers altogether, only three "conservative" tracers can be treated simultaneously. Using any of the other four possibilities means that, at most, one additional "conservative" tracer may be accommodated. At some point in the future, if demand exists, it may be possible to relax the three-tracer limit in HeatEx.

The "intrchem.fil" input file specifies the number of tracers considered, the "reaction systems" that are considered to operate, and the parameter values that govern those reactions. The file structure will consist of (1) a "keyword" line, perhaps followed by (2) an associated "parameter" line, then perhaps followed by (3) another "keyword" line, and so on. The "keyword" lines contain case-insensitive character strings designating which of the above "reaction systems" is to be incorporated:

CONSERVATIVE
or
RADIOACTIVE
or
THERMAL DEGRADATION
or
EQUILIBRIUM
or
ABSORPTION

The "keyword" is followed immediately by the pertinent parameter values, with syntax that varies from case to case. For the single-tracer "conservative" case, there are no parameters; thus a simulation employing three independent conservative tracers might use a *intrchem.fil* input file reading simply:

conservative
conservative
def = conservative
def = conservative

The other cases, however, all require quantitative parameter values.

In the case of the "radioactive" reaction system, two tracers will be used – the first is the unstable radioactive tracer material itself, and the second represents the "daughter products" that are produced by radioactive decay. The subsequent "parameter" line must contain two real numbers in this case:

HALFLF RATMAS

which represent, respectively, the radioactive half-life (in seconds) of the primary tracer material, and the mass ratio of the daughter products (that is, [mass of daughters]/[initial mass]; frequently will be unity).

For the "thermal degradation" reaction system, two tracers are again involved – the original tracer material itself, and the products of the degradation reaction. The "parameter" line must contain three real numbers in this case:

TREFER HALFLF EACTIV

which represent, respectively, a "reference temperature" in degrees Celsius, the "half-life" (in seconds) of the degrading material at the "reference temperature", and the "activation energy" E_o for the reaction in Joules per mole. At the reference temperature, it will take HALFLF seconds for 50% of the tracer material present initially to degrade. At other temperatures, the half-life will vary in proportion to [$\exp(E_o / R_g T_k)$], where R_g is the universal gas constant (8.314 J/mole-degree) and T_k is absolute temperature in Kelvin ($T_k = T(\text{Celsius}) + 273.15$).

In the "equilibrium" case, the "parameter" line must contain seven real-number entries:

TREFER HALFLF EACTIV TEMPR1 TEMPR2 TR1FR1 TR1FR2 with the following significance. Two tracers are involved (tracer #1 and tracer #2), which are seeking a state of chemical equilibrium with each other. But the approach to equilibrium takes place at a finite rate. The half-life of the equilibrium reaction is HALFLF seconds at a reference temperature of TREFER degrees Celsius, and at other temperatures varies in proportion to [$\exp(E_o / R_g T_k)$], where R_g is the universal gas constant (8.314 J/mole-degree),

 T_k is absolute temperature in Kelvin ($T_k = T$ (Celsius) + 273.15) and $E_o = \text{EACTIV} = \text{activation}$ energy in Joules per mole. TEMPR1 and TEMPR2 are two datum temperatures in degrees Celsius (T_I and T_2); at $T = T_I$, the equilibrium mass fraction of tracer #1 of the total (tracer #1 + tracer #2) is equal to TR1FR1. At $T = T_2$, the same mass fraction is equal to TR1FR2. At intermediate temperatures, the equilibrium partition is interpolated.

Finally, the "absorption" model also entails a seven-entry "parameter" line:

TREFER HALFLF EACTIV TEMPR1 TEMPR2 AQUFR1 AQUFR2 In this case, an ordinarily-dissolved tracer material (tracer #1) has a tendency to become attached to the solid rock surfaces through which it flows (and thereby become renamed "tracer #2"). Tracer #1 flows with the fluid as usual, but tracer #2 is immobilized and cannot move again unless and until it re-dissolves and becomes mobile again (and changes back into tracer #1). Apart from the immobilization of tracer #2, the treatment is very similar to the "equilibrium" case described above. The half-life of the equilibrium reaction between dissolved and absorbed tracer is HALFLF seconds at temperature TREFER degrees Celsius, and varies in proportion to [$\exp(E_o / R_g T_k)$] at other temperatures. At temperature = TEMPR1 degrees Celsius, the equilibrium fraction of the tracer that remains dissolved (and is not absorbed on the rock) is AQUFR1, and the fraction is AQUFR2 at temperature TEMPR2, with interpolation being used at intermediate temperatures.

2.3.10.2. Initial tracer distribution – input file "inintrer.fil". The purpose of this file is to specify the initial thermohydraulic-grid spatial distributions of all of the "tracers" defined in file intrchem.fil (Section 2.3.10.1, above). The "VECTOR" procedure (Section 2.3.2) is used for this purpose – the "attributes" being distributed are the initial fluid-phase mass fractions of the various tracers. Each "attribute" line will contain between 1 and 3 non-negative real numbers ("tracer 1", then "tracer 2" if defined by intrchem.fil, then "tracer 3" if also defined by intrchem.fil). Note that, if no tracers are specified (that is, if file intrchem.fil is absent), the data supplied in file inintrcr.fil will be ignored, but if file intrchem.fil is present then file inintrcr.fil is required. More often than not, there will be no tracer present initially in the system – in this case, file inintrcr.fil degenerates to a single line containing from one to three zeroes.

2.3.11. Representing the Time-History

HeatEx finds the solution by integrating forward in a series of finite time-steps, each of which advances the solution by a time-interval Δt . In order to provide good temporal resolution at times when the system is likely to be changing rapidly, HeatEx first uses very small time-steps and then starts increasing the time-step size as the solution develops. At other times during the solution when rapid changes are likely (for example, when wells are started or shut in), the code may revert to small step sizes for a short time. This is all done internally and automatically. But the user ultimately dictates the maximum step size that HeatEx will use, and all steps taken will be either equal to the specified step size or equal to that step size divided by a power of two, as needed.

<u>2.3.11.1.</u> Specifying temporal discretization constraints – input file "intimscl.fil". The user must supply this file to designate the time-stepping scheme to be used. Examples may be

found in Sections 3.4.1.12, 3.4.4.12 and 3.4.6.20. The file must, at a minimum, contain five input lines. These are:

```
Line 1: MAXSTP (single integer)
Line 2: UNMXTM (text string)
Line 3: TIMMAX (single real number)
Line 4: UNSTPS (text string)
Line 5: STEPMX (single real number)
```

The first line contains an integer which provides an overall upper bound on the number of time-steps that will be attempted. The second line must contain one of the following strings: "seconds", "hours", "days" or "years", and the third line contains the maximum value of "computed time", or the time at which the calculation is to stop. This time-value is provided in the units specified by the second line. In this connection, HeatEx assumes that one hour = 3600 seconds, one day = 24 hours = 86,400 seconds and one year = 365 days = 8,760 hours = 31,536,000 seconds. The fourth line contains another text string, again either "seconds", "hours", "days" or "years", and the fifth line designates the maximum value of the time-step size that will be used (expressed in the units specified in the fourth line). All time-steps undertaken in the simulation will either be of STEPMX duration, or (STEPMX/2), or (STEPMX/4), or (STEPMX/8) etc.

In addition, the user may wish to apply further constraints on the time step size, such as was done in Illustrative Case 6 (Section 3.4.6.20), for example. Additional lines may be added after Line 5 (above), of the form:

N1 N2 N1 N2 N1 N2 etc.

Each such line contains two integers. These lines must be entered in order of increasing N1. Each such line means: "After t reaches (N1×STEPMX), constrain Δt to be (STEPMX / 2^{N2}) or less." N1 and N2 must both be non-negative.

<u>2.3.11.2.</u> Specifying output requirements – input file "inoutfrq.fil". Earlier in Section 2.3, seven simulator output files were introduced (rpdispts.fil, rpdistra.fil, rpfpaper.fil, rprkperm.fil, rprstart.fil, rpvoltge.fil and rpwelsum.fil) which may be optionally generated from time to time to create temporal "snapshots" of the state-of-the-system at the user's request. This is accomplished using input file "inoutfrq.fil". The file consists of six different groups of lines, each of which generates a particular time-sequence for output. The groups designate output generation as follows:

Group 1: rpdispts.fil and rpwelsum.fil
Group 2: rpdistra.fil
Group 3: rpfpaper.fil
Group 4: rprkperm.fil
Group 5: rpvoltge.fil
Group 6: rprstart.fil

and are to be entered in the above order. The structure of each group is the same, and is as follows. The first two lines of the group specify the "basic" frequency desired for output of the type in question. This can be specified in terms of *numbers of computational steps*, or in terms

of *elapsed time*. To specify the number of computational steps that are to be taken between output snapshots, the first two lines in the group should read:

Line 1: steps (character string)
Line 2: NSTEPS (integer)

which will specify that NSTEPS steps should intervene between successive snapshots. To instead specify the computed-time-interval between snapshots, use:

	Line 1:	seconds	(character string)
	Line 2:	SECNDS	(real number)
•			
I	Line 1:	hours	(character string)
I	Line 2:	HOURS	(real number)
•			
I	Line 1:	days	(character string)
I	Line 2:	DAYS	(real number)
<u>-</u>			
I	Line 1:	years	(character string)
I	Line 2:	YEARS	(real number)
: I : :	Line 1: Line 2: Line 1:	days DAYS years	(character strir (real number) (character strir

and the output will be created for snapshots every time-interval designated (SECNDS, HOURS, DAYS or YEARS as appropriate).

After the first two lines, if desired the data "group" may be terminated with a single line containing the single character string "end":

Line 3: end (character string)

Alternatively, "extra" output snapshots may be requested at irregular intervals using a "list" request:

Line 3: list (character string)

followed by another line designating an appropriate time unit (which need not be the same choice as in Line 1, above):

Line 4: seconds or hours or days or years (character string)

Line 4 is then followed by as many additional lines as desired, each designating "output times" in the units specified in Line 4. These must be entered in order of increasing time. Then, the Group is completed by entering the "end" line:

Last line: end (character string)

Care should be taken to assure that the "snapshot times" designated in the various "Groups" either choose an integer number of "steps", or a time-interval that is an integer multiple of STEPMX (see above), or at other times that are known in advance to be "even" computational times. HeatEx will not perform fractional computational steps to accommodate "snapshot" output requests. Any "snapshot times" that do not turn out to be at even computational times will simply be skipped.

2.3.12. Specialized Data Output Requirements

<u>2.3.12.1.</u> Subsurface sensor assemblies – input file "insnsors.fil". Provision has been made in HeatEx for the incorporation of hypothetical "sensor assemblies" at fixed subsurface locations. These sensors are idealized and occupy zero volume; their presence or absence does not influence the computed solution in any way. Each time step, conditions are interpolated from nearby principal grid block centers to the sensor location, and results are reported on special-purpose output files (*rpsnsr01.fil*, *rpsnsr02.fil*, etc.). The quantities reported are (1) electrokinetic self-potential if calculated by the simulation, (2) fluid pressure, (3) fluid temperature, (4) average rock temperature, (5) fluid salinity, and (6) tracer concentration for each tracer present.

Input file *insnsors.fil* establishes how many sensor assemblies are present and where they are located. If *insnsors.fil* is not found in the local directory, no sensor assemblies will be used. The file consists of a list (of arbitrary length) of lines, each referring to a particular sensor assembly and designating its location in "world" coordinates (meters East, meters North and meters ASL) using three real input numbers:

SAEAST	SANRTH	SAMASL
SAEAST	SANRTH	SAMASL
	•••	
SAEAST	SANRTH	SAMASL
	[end-of-file]	

2.3.12.2. Detailed output for "blocks of interest" – input file "inblintr.fil". This optional input file permits the designation of particular "grid blocks of interest" in the thermohydraulic computational grid for which detailed output records (named rpblock1.fil, rpblock2.fil, etc.) will be generated each computational time-step. These records will provide the instantaneous values of (1) fluid pressure, (2) fluid salinity, (3) tracer concentrations, (4) fluid enthalpy, (5) fluid temperature, (6) average rock temperature and (7) for each conductive-MINC assembly of concentric "shells" in the block, the temperature in each "shell".

Input file *inblintr.fil* simply consists of a sequence (of arbitrary length) of individual lines, each designating a particular thermohydraulic grid block as a "block of interest", and each containing three integers (the *i*, *j*, *k* indices for the grid block):

IBLOCK	JBLOCK	KBLOCK
IBLOCK	JBLOCK	KBLOCK
	•••	
IBLOCK	JBLOCK	KBLOCK
	[end-of-file]	

If the *inblintr.fil* input file is not found in the local directory, the *rpbloc**.fil* output files will not be created.

2.3.13. Incorporating Geothermal Wells

Geothermal wells are potentially important to the simulation calculations from at least two different standpoints: (1) they serve as conduits through which fluids may be withdrawn from

and injected into the subsurface reservoir, and (2) their metallic casings serve as subsurface electrical conductors which can influence the electrical signals that are observable from stimulation operations. Describing these wells entails two tasks - (1) establishing how many wells there are, their locations and their geometries, and (2) specifying their operational program - whether the well is producing, injecting or shut in, and how this status changes over time. Defining these two issues are the roles of input files *inwelgeo.fil* and *inwelflo.fil*, respectively.

<u>2.3.13.1.</u> Well geometries – input file "inwelgeo.fil". This file describes the geometries of the various wells that are present and pertinent. It consists of a series of "blocks" of data, each of which describes one of the wells. The "blocks" each consist of a series of lines which describe the well geometry, section by section, and also provide information concerning the well's hydraulic and electrical connections to the surrounding reservoir formations. The well specifications are all provided in the same file, and the descriptions (from wellhead to bottomhole) are simply provided for one well after the next:

Data block for well # 1
Data block for well # 2

Data block for last well end-of-file

The individual "well data blocks" consist of, first, four lines that provide basic essential data about the well, and then a series of four-line "clauses", each of which describes a portion ("section") of the well geometry. These "sections" are provided in order of increasing depth, from wellhead to bottomhole. The first four lines contain the following information:

Line 1:	wellhead		(character string)
Line 2:	WHEAST	WHNRTH	(two real numbers)
Line 3:	DATMEL		(real number)
Line 4:	WELSKN		(real number)

Line 1 advises HeatEx that this line marks the beginning of the description for a new well. Line 2 provides the geographic location of the wellhead (meters East and meters North; the vertical elevation of the wellhead above sea level is obtained from the topographic information provided in input file *intopogr.fil*). DATMEL, the "datum level elevation" for the well (provided in meters ASL) is the vertical elevation within the well where the "well pressure" will be reported, and should ordinarily be located at or near the vertical elevation of the well's principal feedpoint. WELSKN (dimensionless) is the so-called "skin factor" for the well (see e.g. *Matthews and Russell*, 1967).

Below the wellhead, it is assumed that the well geometry may be adequately approximated as a series of straight-line "sections", each of which is characterized by a four-line "clause". The contents of these four lines are:

Line A:	conductive or insulated	(character string)
Line B:	cemented or uncemented	(character string)
Line C:	DIAM	(real number)
Line D:	BEAST BNORTH BASL	(three real numbers)

BEAST, BNORTH and BASL represent the location (in "world" coordinates; meters East, meters North and meters ASL) of the "bottom" of the section – the "top" is either the "bottom" of the preceding section or the wellhead location. DIAM is the well diameter in meters, considered to be uniform in the section. If Line B contains "cemented", the well is cased and impermeable to the formation throughout the section length; if it contains "uncemented", the section communicates hydraulically with the formation (slotted or perforated liner, or open hole). If Line A contains "conductive", the section contains a conductive metallic liner (ordinary casing, slotted casing. etc.); if it contains "insulated", the casing/liner is either made of electrically insulating material (e.g. fiberglass), or the section is open-hole. HeatEx uses the "effective wellblock radius" approach (*Pritchett and Garg*, 1980) to automatically relate feedblock conditions (pressure, electrical potential) to those within the well.

Below Line D in the section clause, the next line will be either (1) another Line A describing a deeper well section, (2) a Line 1 ("wellhead") introducing the next well, or (3) the end of input file *inwelgeo.fil*, indicating that all well geometry data has been provided.

<u>2.3.13.2.</u> Well operations – input file "inwelflo.fil". In the same way that file inwelgeo.fil provides the geometrical description for all of the wells in a single input file, file inwelflo.fil provides the operating description – times of startup and shutin, flow rates, etc. – for all of the wells. The file consists of a series of "status instructions" separated by "time lines":

[WELL STATUS BLOCK]
time SECNDS
[WELL STATUS BLOCK]
time SECNDS
[WELL STATUS BLOCK]

time SECNDS
[WELL STATUS BLOCK]
[end of file]

Each "well status block" takes effect immediately after the time-variable t passes through the value provided in the preceding "time line", and describes any status changes that are to be implemented for any well at that time. Since the first "well status block" has no predecessor, the initial status of each well at t = 0 must be specified in the first block. Subsequently, wells need only be mentioned in "well status blocks" when their operating parameters change.

The "time lines" separating the "well status blocks" contain only (1) the four-character text string "time" (case insensitive), followed by (2) a single real number which represents the value of t (in seconds) at which status changes take place. The "well status blocks" have the following structure:

[WELL LINE]
[STATUS CLAUSE]
[WELL LINE]
[STATUS CLAUSE]
[WELL LINE]
[STATUS CLAUSE]
etc.

Each "well line" designates one of the wells defined in input file *inwelgeo.fil*, using a four-character text string ("well") followed by the appropriate integer, for example:

well 3

The "status clause" will take on one of three forms. If the well is to be shut in, the "status clause" will consist of just a single line containing the text string:

shut in

If the well is to start producing (withdrawing fluid from the reservoir), the "status clause" must consist of two lines, each containing a text string followed by a real number:

produce RATE
pressure PRES

The first of these lines designates the desired fluid withdrawal rate ("RATE"), in kilograms per second. The second establishes a lower bound on the well's flowing "datum level pressure" ("PRES"), in pascals. If necessary, the well's withdrawal rate will be reduced below RATE to maintain the datum level pressure at PRES.

If the well is to start injecting (pumping fluid into the reservoir), the "status clause" must consist of either four or five lines, each containing a text string followed by at least one real number:

inject RATE
pressure PRES
salinity SALT
enthalpy ENTH
tracers TR₁ TR₂ TR₃

Here, RATE (kilograms per second) is the desired upper bound on the rate of fluid injection into the reservoir. The well will inject at that rate unless and until doing so would cause the datum level pressure within the well to exceed PRES (to be provided in pascals). In that case, the flow rate will be reduced so that the datum pressure does not exceed PRES. The fluid being injected will be characterized by flowing enthalpy ENTH (J/kg) and salinity SALT (dimensionless mass fraction). If tracers have been specified as present in the problem by input file *intrchem.fil* (see Section 2.3.10.1, above), the "tracers" line must also be included in the "status clause" and specify the mass fractions of each tracer present in the injected fluid.

3. ILLUSTRATIVE CALCULATIONS

In this section, six illustrative calculations using HeatEx are presented in considerable detail. Cases 1, 2 and 3 are relatively simple one-dimensional calculations which exhibit some of the heat transfer mechanisms that can be described by the code. Cases 4 and 5 are two-dimensional problems which feature early transient effects followed by later stabilization of conditions surrounding flowing wells (Case 4 considers a production well, Case 5 considers an injection well). Finally, Case 6 is fully three-dimensional, and was run in part to demonstrate some of the more unusual features of the HeatEx code.

One of the purposes of these illustrative calculations is to provide examples of the use of the 30 various input file formats described in the preceding section. Their uses for the six sample cases are as follows (listed alphabetically):

TABLE 3.1. Utilization of Reserved-Name Input Files in Illustrative Cases

Input File Name	Case 1	Case 2	Case 3	Case 4	Case 5	Case 6
inaquifr.fil						used
inblintr.fil						used
incondrk.fil	used	used	used	used	used	used
inecnbgr.fil						used
inelpram.fil						used
inelprds.fil						used
infpdata.fil						used
infpprms.fil						used
ingravty.fil						
ingridek.fil						used
ingridte.fil						used
ingridth.fil	used	used	used	used	used	used
ininhydr.fil						used
ininpres.fil	used	used	used	used	used	
ininsalt.fil	used	used	used	used	used	
inintemp.fil	used	used	used	used	used	
inintrcr.fil	used	used	used			used
inmincnd.fil			used			used
inoutfrq.fil	used	used	used	used	used	used
inrgstrs.fil						used
inrkigpr.fil	used	used	used	used	used	used
inrkvolp.fil	used	used	used	used	used	used
insnsors.fil	used	used	used	used	used	
insorcen.fil				used	used	used
insorcms.fil	used	used	used	used	used	
intimscl.fil	used	used	used	used	used	used
intopogr.fil	used	used	used	used	used	used
intrchem.fil	used	used	used			used
inwelflo.fil				used	used	used
inwelgeo.fil				used	used	used

As the above table shows, most of the various HeatEx input file types occur in at least one illustrative case.

Subsection 3.1 describes the specifications provided to HeatEx for Cases 1, 2 and 3, presents computed results, and provides comparisons with approximate analytic solutions. Subsection 3.2 similarly describes Cases 4 and 5, and Subsection 3.3 describes Case 6. In subsection 3.4, the input files that were manually prepared for HeatEx for all six of these cases are presented in hardcopy form. These same files are also provided separately in electronic form along with the HeatEx source code and other pertinent materials as part of the software installation package.

3.1. ONE-DIMENSIONAL ILLUSTRATIVE CASES 1, 2 AND 3

Cases 1, 2 and 3 are nearly identical in terms of problem specifications, although they yield significantly different computed results. Therefore, the discussion of problem specifications will focus mainly on Case 1. Afterwards, computed results from all three cases will be presented and compared.

3.1.1. Cases 1 - 3 Problem Specifications

For Cases 1-3, we consider a one-dimensional problem geometry consisting of 100 cubical grid blocks (each of 1000 m³ volume and $10\times10\times10$ meters in size), forming a horizontal computing volume of 100,000 m³, extending one kilometer horizontally from west to east, 100 m² in cross-section and centered at 2000 meters below sea level vertical elevation. See description of this geometry in input file *ingridth.fil* displayed below in Section 3.4.1.2 of this report. The rock within this volume has uniform properties as follows (see Sections 3.4.1.8 and 3.4.1.9, input files *inrkigpr.fil* and *inrkvolp.fil*):

Grain density: 2800 kg/m³ Heat capacity: 1000 J/kg-°C

Porosity: 0.3
Pore compressibility: zero
Solute hydraulic dispersivity: zero
Heat hydraulic dispersivity: zero

Permeability: 10^{-12} m² (1000 millidarcies)

The system has a uniform time-invariant composite thermal conductivity which is equal to 3 W/m-°C (input file *incondrk.fil*. Section 3.4.1.1). The pore spaces contain pure water; initial conditions are likewise uniform along the entire 1000-meter length of the system (see Sections 3.4.1.3 – 3.4.1.6, input files *ininpres.fil*, *ininsalt.fil*, *inintemp.fil* and *inintrer.fil*):

Initial pressure: 10 MPa (approximately 99 atm.)

Initial salinity: zero
Initial temperature: 100°C
Initial tracer concentration: zero

Calculations are carried forward in time for 1200 days using a maximum time-step size of six hours (see file *intimscl.fil*, Section 3.4.1.2). A total of 4814 time-steps were required to complete the calculation. "Sensors" were placed every 100 meters between x = -400 m and x = +400 m (see file *insnsors.fil*, Section 3.4.1.10).

Starting at t = 0, at the western (upstream) end of the section at x = -500 m, a fluid mass source is imposed in the first grid block (i = 1, j = 1, k = 1) which injects 0.001 kg/m³-s of fluid (one kilogram per second total) into the block – the inflowing fluid is marked by a conservative passive tracer (see file *intrchem.fil*, Section 3.4.14) at a concentration of 0.000001 by mass (one part per million by mass, or "1 ppm"). The inflowing fluid contains no dissolved salt, and is injected at a specific enthalpy of 220 kJ/kg $(2.2 \times 10^5 \text{ J/kg})$. The temperature of pure water at this enthalpy is about 50°C, ranging from 50.50°C at 10 MPa pressure to 49.48°C at 15 MPa. Simultaneously, in the grid block at the opposite end of the test section (grid block i = 100, j = 1, k = 1), a mass sink is imposed which has the effect of maintaining the pressure within that block at its initial value (10 MPa) by withdrawing any excess fluid which flows into it. Both of these mass sources/sinks are specified by input file *insorcms.fil* (see Section 3.4.1.12).

The above description applies to Case 1. Case 2 is very similar, and differs from Case 1 only in that the hydraulic dispersion coefficients for dissolved materials (salt and tracers) and for advected hot water as specified in the Case 2 *inrkvolp.fil* input file (see Section 3.4.2.1 and compare with Section 3.4.1.9) are both equal to 8 meters (instead of to zero as in Case 1).

For Case 3, we revert to zero hydraulic dispersion as in Case 1, but relax the assumption of local thermal equilibrium between the fluid and the surrounding rock. Instead, a "conductive MINC" non-equilibrium heat exchange model is imposed which entails single representative MINC assemblies of 16 concentric conductive spherical "shells" of solid rock. Each of the 100 macroscopic grid blocks has its own associated 16-shell representative assembly. All of the representative assemblies are characterized by a "characteristic time" τ_{eq} of 10^8 seconds, which corresponds to a "50% cooling time" $\tau_{50\%}$ of 36 days and an "average fracture separation" (or spherical assembly diameter) of 20.7 meters for the Case 1-3 choices of rock density, thermal conductivity and heat capacity. This description is imposed for Case 3 using input file *inminend.fil* (Section 3.4.3.1).

3.1.2. Computed Results for Cases 1-3

HeatEx uses a second-order accurate upstream algorithm to represent convection effects for dissolved salt, tracers, and heat. This algorithm represents a significant improvement in accuracy over the more common "first order upwind" approach used in most other geothermal reservoir simulators. To illustrate, the Case 1 simulation was repeated twice, with one of these calculations using a temporary "patch" in the software to use the more conventional first-order scheme. For tracer migration, in the absence of any real diffusive effects, in principle a sharp tracer "front" should be transported with the local fluid velocity in the positive *x*-direction at a constant rate of 2.94 meters per day (thereby traversing the entire 1-km test section in slightly over 340 days). Figure 3.1 shows (in green) this discontinuous front's motion across the computing region in the analytic (incompressible) approximation. Also shown are results obtained using HeatEx (with the temporary first-order modification in blue and the normal second-order treatment in red). "Numerical dispersion" errors are seen to remain in all of the computed results, but are less pronounced using the HeatEx second order technique compared to the more conventional first-order upstream method.

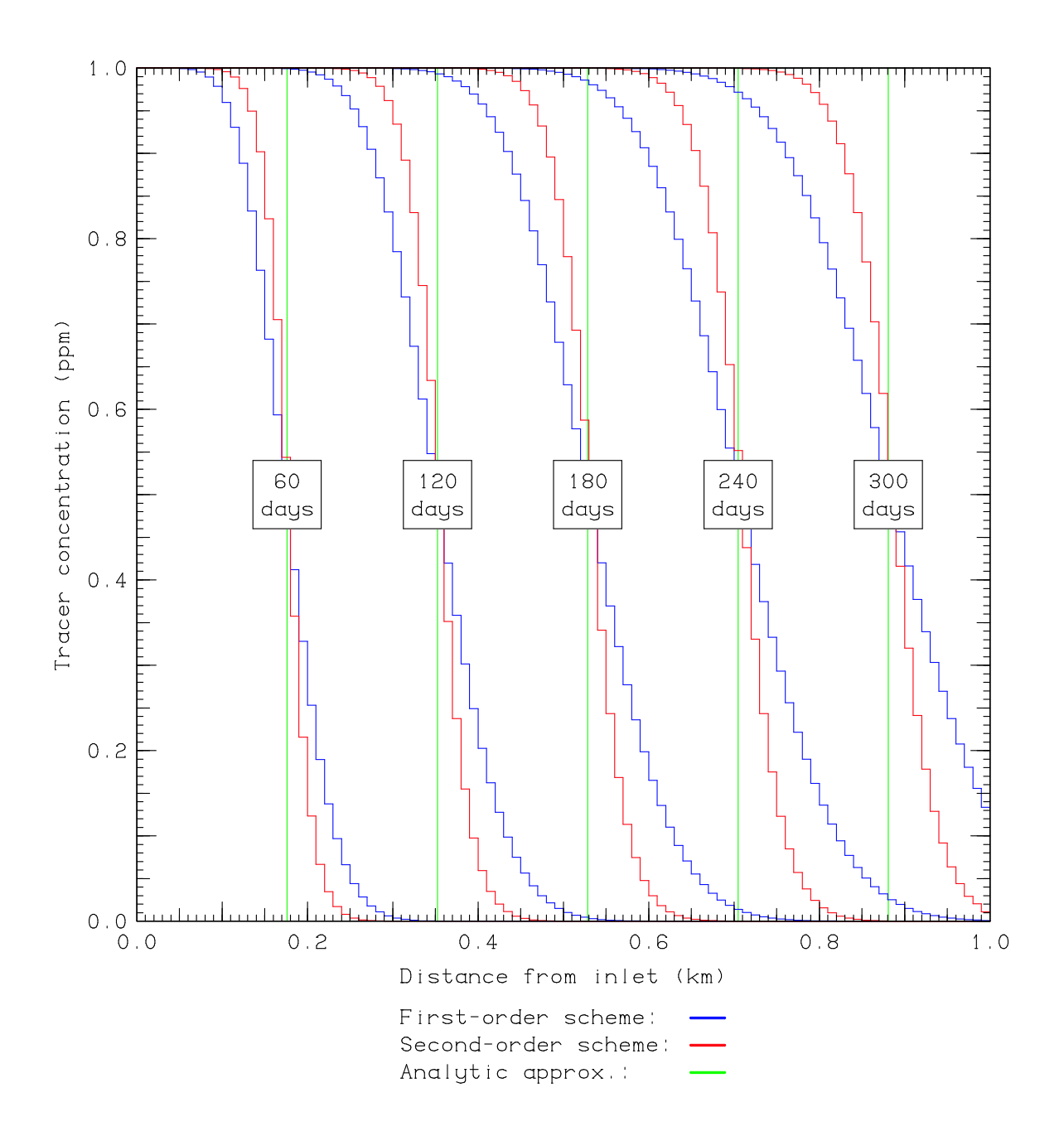


Figure 3.1. Numerical smearing of sharp tracer fronts using conventional *vs.* second-order treatment of convection effects.

Next, Figures 3.2, 3.3 and 3.4 illustrate synoptic "snapshots" at t = 500 days of the spatial distributions of fluid pressure (upper frames) and of temperature (lower frames) for Cases 1, 2 and 3 respectively as forecast by the HeatEx calculations. The distributions of pressure are very similar among all three cases, but the Case 1 pressure profile (Figure 3.2) exhibits a somewhat more pronounced "bend" near x = 0.55 km associated with the sharper temperature front in that case (and the resulting more abrupt change in fluid viscosity at the thermal front). In Case 2, hydraulic dispersion has spread the thermal front out to a width of around 0.3 km by this time (Figure 3.3). Results for Case 3, despite the deletion of hydraulic dispersion effects, exhibit the most widely distributed temperature variation of all (Figure 3.4); the temperature variation zone encompasses virtually the entire computing volume. Note that the "rock temperature" exceeds the "fluid temperature" as well, owing to the non-equilibrium MINC treatment of inter-phase heat transfer. The "rock temperature" value shown here actually represents the volumetric average of the values locally present in the various MINC concentric spherical shells. Temperatures in the outer shells (closer to the flowing fluid) have experienced greater amounts of cooling whereas the highest residual rock temperatures are to be found at the centers of the spherical assemblies.

Finally, Figure 3.5 compares Cases 1, 2 and 3 directly in terms of the time-histories of tracer concentration and of fluid temperature expected to be experienced at a "sensor assembly" located midway between the inlet and outlet of the 1-km test section. The tracer concentration histories (upper frame) are quite sharp and nearly indistinguishable as noted earlier for Cases 1 and 3 (neither of which incorporates hydraulic dispersion), but the Case 2 tracer front is significantly widened by dispersive effects, as expected. For temperature in Case 2 (lower frame), hydraulic dispersion broadens the relatively sharp thermal front of Case 1 (which is widened only by numerical effects combined with longitudinal heat conduction) into a significantly more gradual cooling trend, with an earlier arrival of cooled water. In the non-equilibrium MINC Case 3, of course, thermal breakthrough takes place much earlier, and temperature changes are starting to become noticeable shortly after the tracer front passes through the sensor location.

It is straightforward to combine the principles of fluid mass and total energy conservation with approximations of fluid incompressibility and the assumption of sharp material and thermal fronts to develop an algebraic approximation to the Case 1 results. This analytic treatment suggests that the tracer front should arrive at the 500-meter-downstream sensor at t = 169 days and that the thermal front should arrive 2.64 times later, at t = 446 days. These arrival times depend on inlet flow rate (1 kg/s), rock porosity (0.3), downstream distance (500 m), cross-section area (100 m²), initial fluid enthalpy (426.9 kJ/kg), inlet fluid enthalpy (220 kJ/kg), initial fluid temperature (100°C), inlet fluid temperature (50°C), rock heat capacity (1000 J/kg-°C), solid rock density (2800 kg/m³), and the densities of "cold" (50°C) and "hot" (100°C) water (992 and 963 kg/m³ respectively at 10 MPa pressure). These approximate analytical results are also compared with the computed tracer and heat recovery curves from the HeatEx results in Figure 3.5 (black dotted lines). Agreement of the times of front arrivals computed by HeatEx with the algebraic approximation is essentially exact.

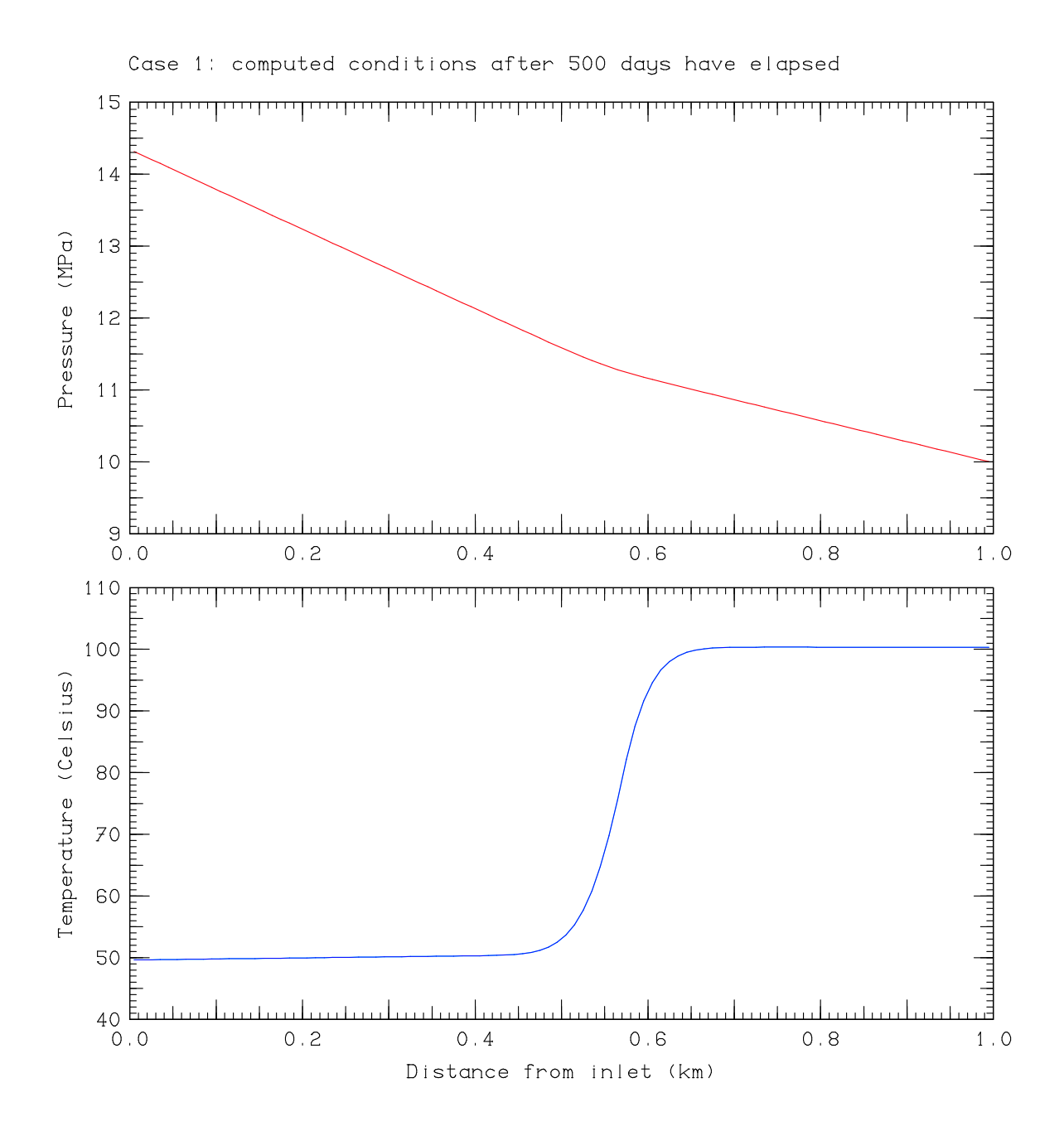


Figure 3.2. Distributions of fluid pressure and temperature at t = 500 days (Case 1).

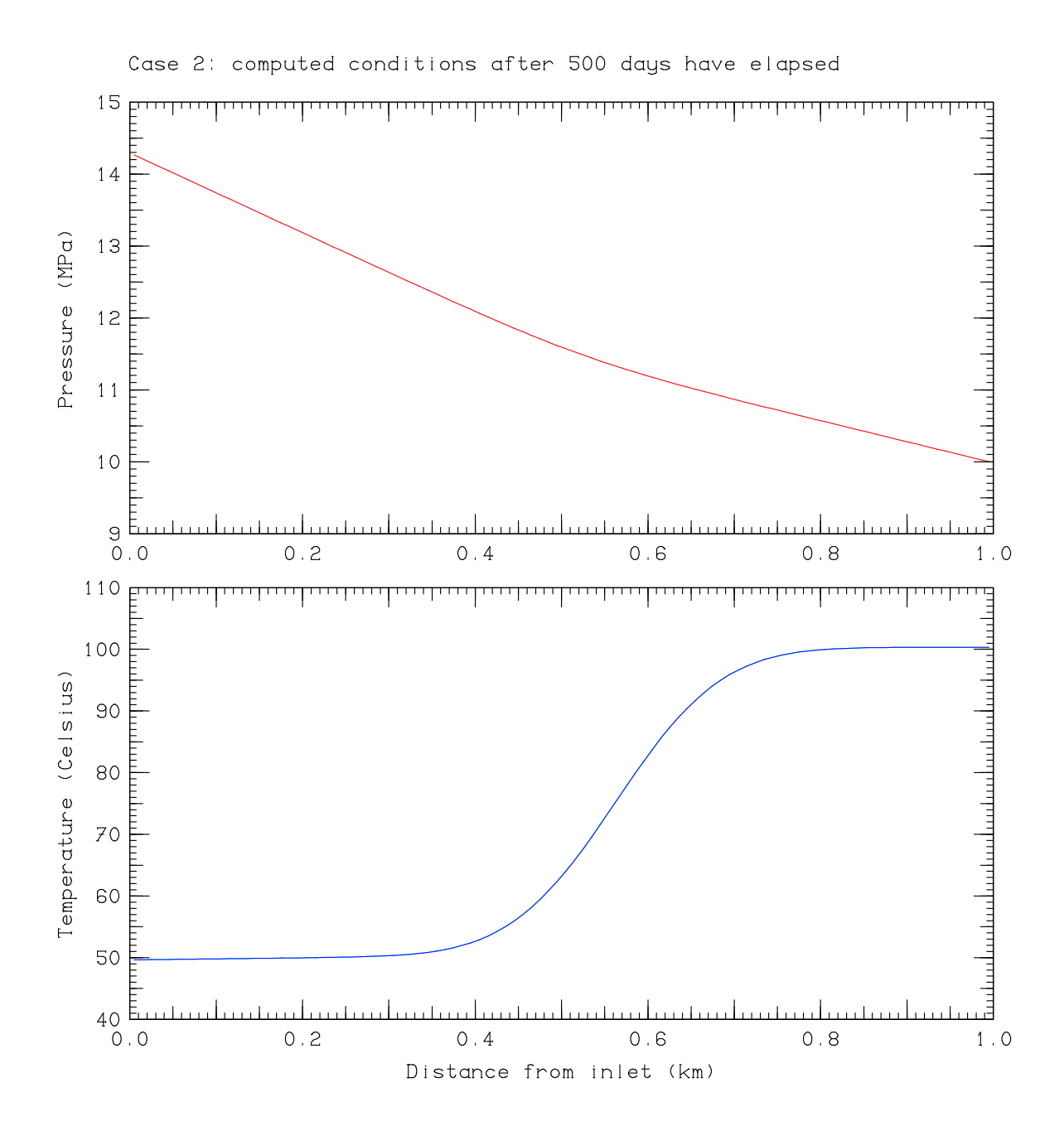


Figure 3.3. Distributions of fluid pressure and temperature at t = 500 days (Case 2).

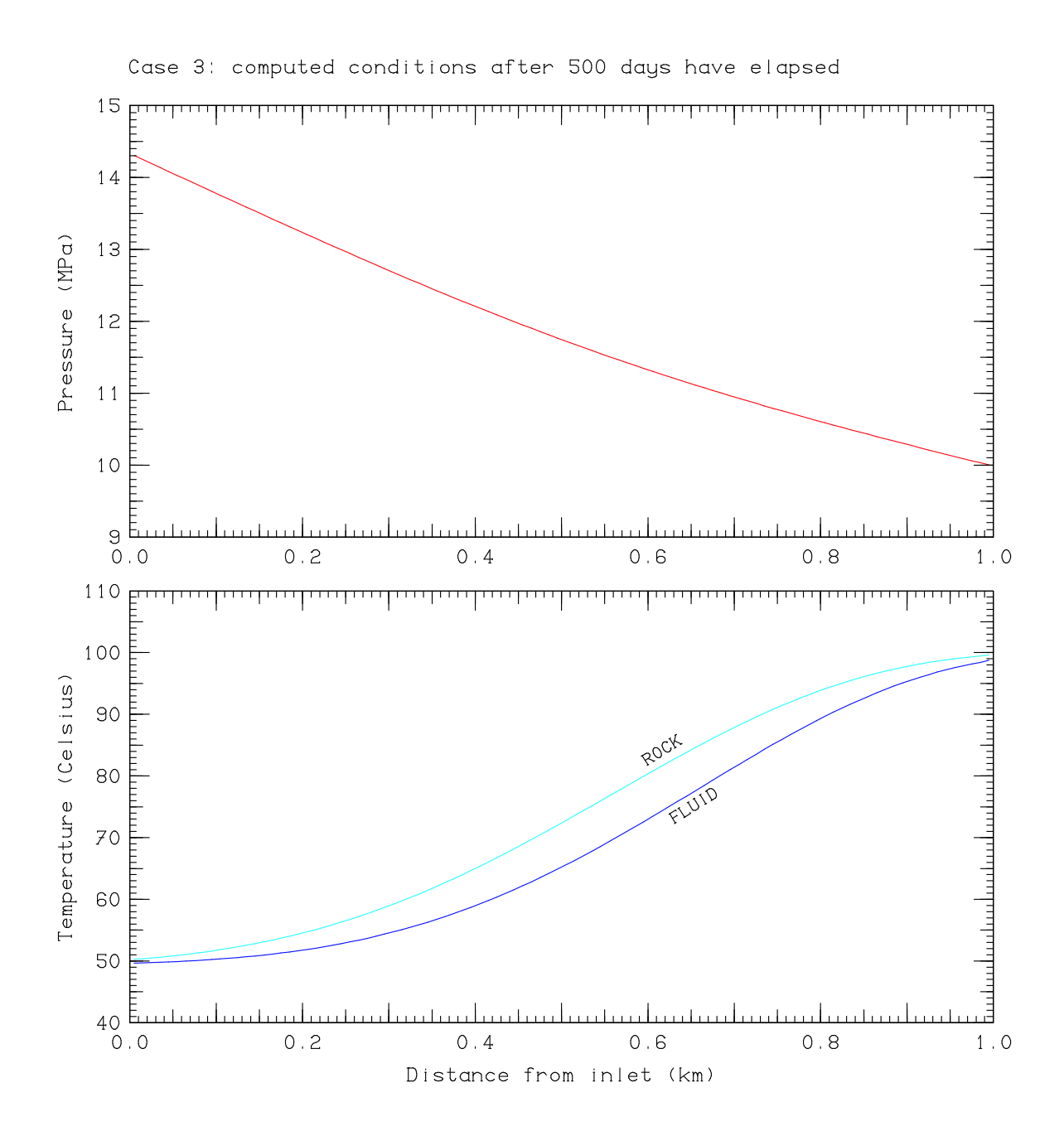


Figure 3.4. Distributions of fluid pressure and temperature at t = 500 days (Case 3).

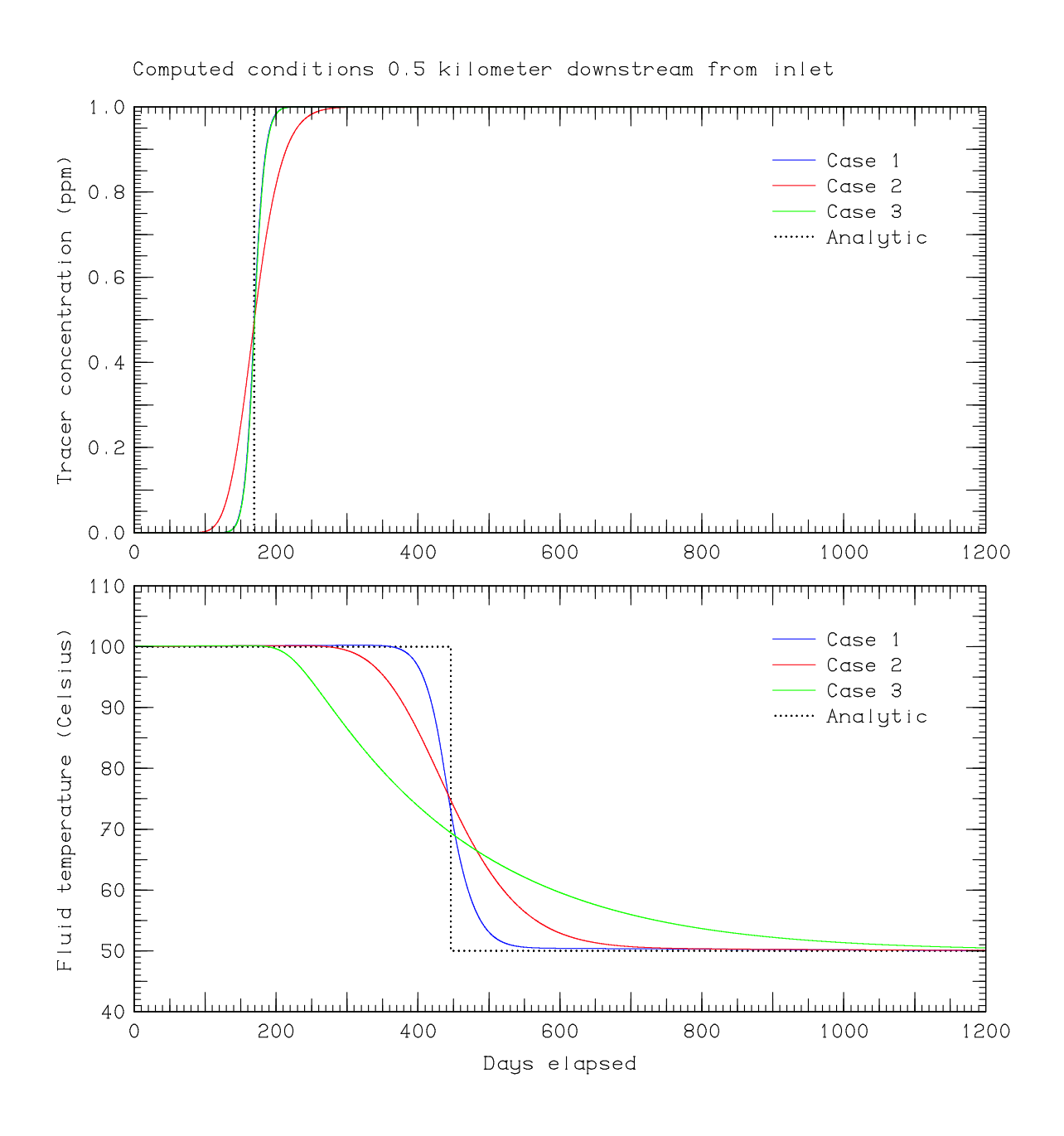


Figure 3.5. Time-histories of tracer content and fluid temperature 0.5 km downstream from inlet – Cases 1, 2 and 3.

3.2. TWO-DIMENSIONAL ILLUSTRATIVE CASES 4 AND 5

3.2.1. Problem Specifications

Consider next Cases 4 and 5. Most of the problem specification is identical for these two cases. The computing volume is essentially two dimensional – in both the *x*- and *y*-directions, the computational grid contains 51 grid blocks each representing 20 meters (1020 meters total in each direction), and the *x*-*y* plane is horizontal with the *x*-coordinate measuring distance Eastward and the *y*-coordinate measuring distance Northward (see Section 3.4.4.2, input file *ingridth.fil*). Also see Figure 3.6. A single layer of blocks is present, which is 100 meters thick in the vertical (*z*) direction and is centered at two kilometers below sea level elevation.

As Figure 3.6 shows, of the 2601 (51×51) blocks allocated for the computational grid, 548 of them (21%) are treated as "void" and do not participate in the calculations. The remaining region is approximately circular in shape, and a single vertical fully-penetrating well is considered to be located in the center of the computing volume. The outermost non-void grid blocks indicated by the yellow color in Figure 3.6 are used in the imposition of boundary conditions, and are located at a distance of 502.2 meters from the central well, on the average. We therefore may consider the study volume to be circular and of diameter 1004 meters.

Within this circular "reservoir", initial conditions are uniform: pressure is 20 MPa, temperature is 200°C and the dissolved NaCl fluid mass fraction ("salinity") is taken to be 0.036, about the same as ordinary seawater (see Sections 3.4.4.3 – 3.4.4.5; input files *ininpres.fil*, *ininsalt.fil* and *inintemp.fil*), Boundary conditions are imposed by assigning mass/energy sources/sinks to each of the 144 "boundary blocks" along the perimeter designated by the yellow color in Figure 3.6 (see Sections 3.4.4.10 and 3.4.4.11, input files *insorcen.fil* and *insorcms.fil*). The mass sources/sinks maintain the grid block pressures at their initial values (20 MPa) by adding or subtracting fluid mass as required. In case of mass addition, the salinity and enthalpy of the inflowing fluid are the same as the initial values (0.036 NaCl mass fraction and 837.36 kJ/kg respectively). The superimposed energy sinks provide any cooling required to maintain the temperature within the boundary block at or below the initial value (200°C).

Within the circular computing volume, rock properties are uniform (see Sections 3.4.4.1, 3.4.4.7 and 3.4.4.8; input files *incondrk.fil*, *inrkigpr.fil* and *inrkvolp.fil*), as follows:

Porosity: 0.10Pore compressibility: 10^{-8} / Pa

Permeability: $5 \times 10^{-14} \,\mathrm{m}^2$ (50 millidarcies)

Grain density: 2600 kg/m³
Heat capacity: 1000 J/kg-°C
Thermal conductivity: 2 W/m-°C

Dispersion coefficients: zero

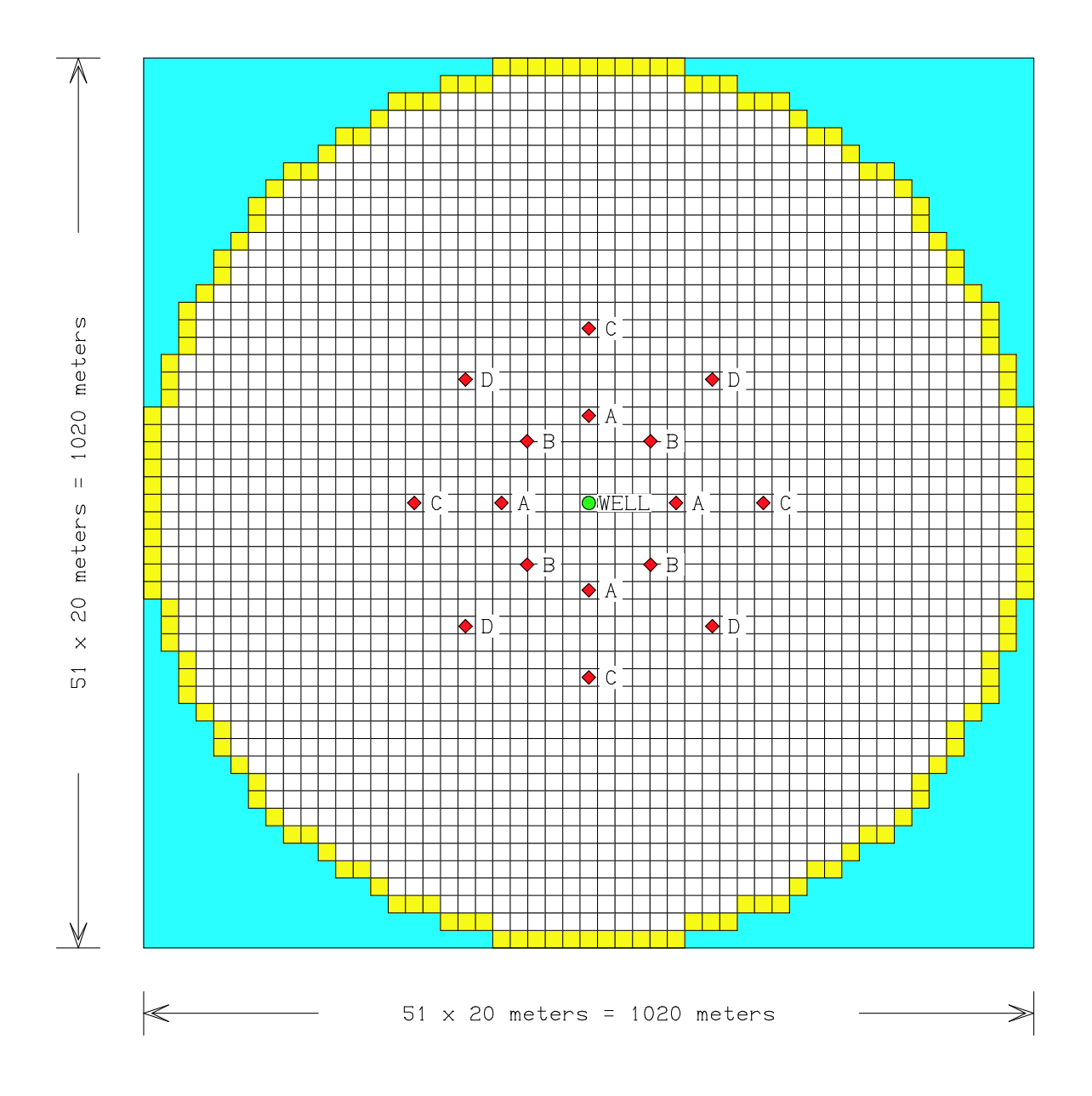


Figure 3.6. Horizontal problem geometry for two-dimensional Cases 4 and 5. *Cyan color:* void grid blocks. *Yellow color:* "boundary" blocks. *Green circle:* central well location. *Red diamonds:* locations of sensors ("A" and "B" sensors are 100 meters from well, "C" and "D" sensors are at 200 meter radius). Each grid block is 20 m × 20 m (horizontally) × 100 m (vertically) in size.

As noted above, a single vertical well is located in the center or the region, which is open to the formation for the entire 100-meter vertical height of the system. The hole diameter is 30 centimeters, and the "skin factor" is zero (see Section 3.4.4.15, input file *inwelgeo.fil*). In addition, the well is surrounded by two concentric rings of "sensor assemblies" at radii of 100 and 200 meters (see Section 3.4.4.9; input file *insensrs.fil*). Each "ring" has eight sensor positions spaced at 45° azimuth intervals around the central well as indicated in Figure 3.6.

The only distinction between the specifications for Cases 4 and 5 is in the designation of the flow rate history for the central well. In Case 4 (see Section 3.4.4.14) input file *inwelflo.fil* specifies that the well will start withdrawing fluid from the reservoir at a constant rate of 100 kg/s at t = 0, subject to a datum pressure lower limit of 5 MPa (which is never reached – the flow rate remains constant throughout). By contrast, the corresponding input file for Case 5 (Section 3.4.5.1) specifies that the well will begin *injecting* 100 kg/s at t = 0, and that the injected brine will have a higher salinity (0.048) than the *in-situ* reservoir fluid, as well as a lower enthalpy (420 kJ/kg) and temperature (about 95.8°C). Again, a limiting datum pressure value was assigned to the injection well (50 MPa), but this value was never reached.

3.2.2. Computed results for Case 4 – central production well

First, consider Case 4 in which the centrally-located well starts withdrawing 100 kg/s of fluid at t = 0 and continues indefinitely thereafter. Calculations continue forward in time until t = 1000 days (8.64×10^7 seconds). Within the production well, the pressure declines rapidly at first (from the initial value of 20 MPa) and then more and more slowly. For the first few days, the production well pressure declines in direct proportion to the logarithm of elapsed time, as indicated in Figure 3.7. This is in accordance with classical line-source pressure transient behavior (see, for example, *Matthews and Russell*, 1967, *pp.* 10-12). Theoretically, the slope of the straight-line trend is given by:

$$\partial P/\partial(\log_{10} t) = -2.303 R \mu/(4\pi \rho k h)$$

where P is pressure, t is time, R is (constant) production rate, μ is fluid viscosity, ρ is fluid density, k is formation permeability, and k is formation vertical thickness. Using

```
R = 100 \text{ kg/s},

\mu = 1.51 \times 10^{-4} \text{ Pa-s} (for 3.6% salinity brine at 20 MPa and 200°C),

\rho = 905 \text{ kg/m}^3 (for 3.6% salinity brine at 20 MPa and 200°C),

k = 5 \times 10^{-14} \text{ m}^2 = 50 \text{ millidarcies}, \text{ and}

h = 100 \text{ m}
```

we obtain $\partial P/\partial(\log_{10} t) = -0.61$ MPa per decade, as shown by the early-time dotted line of Figure 3.7.

At later times, however, the pressure-time curve flattens as the influence of the fixed boundary pressure begins to make itself felt. After t = 10 days or so, the flowing pressure in the production well becomes constant for all practical purposes (15.63 MPa), as Figure 3.7 indicates.

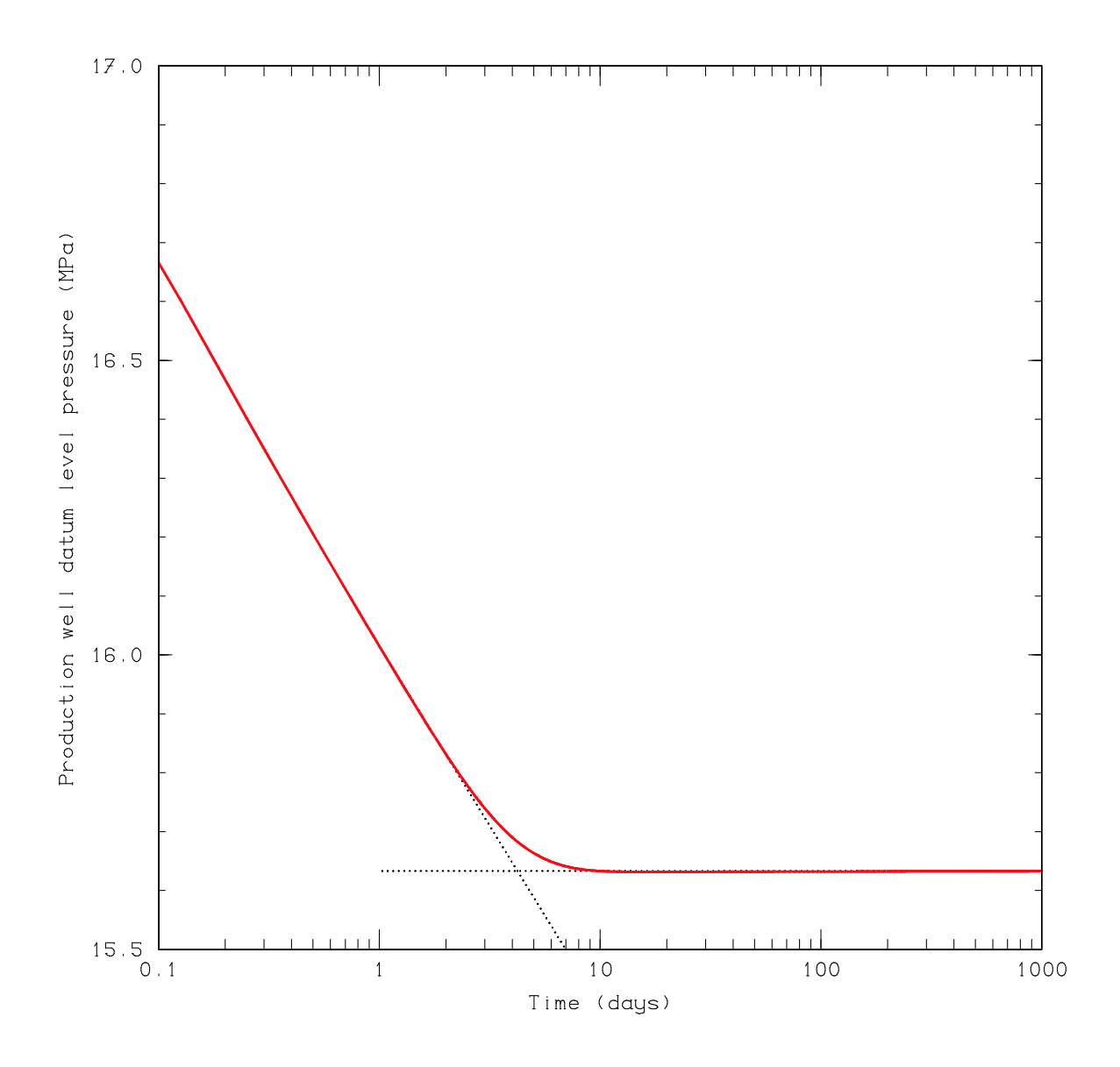


Figure 3.7. Case 4 – time-history of datum level pressure in central production well. **Red** curve: as computed by HeatEx. **Dotted lines**: early- and late-time asymptotic behavior (see text).

Figure 3.8 similarly shows the time-histories of pressure at the various "sensor locations" as calculated by HeatEx for Case 4. Pressures at 100 m radius ("A" and "B" sensors) are indicated in red/magenta, and those at 200 m radius ("C" and "D" sensors) are shown in blue/cyan. The results for the "A" and "B" histories (like those for "C" and "D") are indistinguishable on this graph. At early times (< 2 days or so), the results are consistent with the classical line-source solution (see *Matthews and Russell*, 1967), but after ~ 10 days, like the well pressure history, these "sensor" pressures become essentially constant. These late-time stabilized pressures increase with increasing radius:

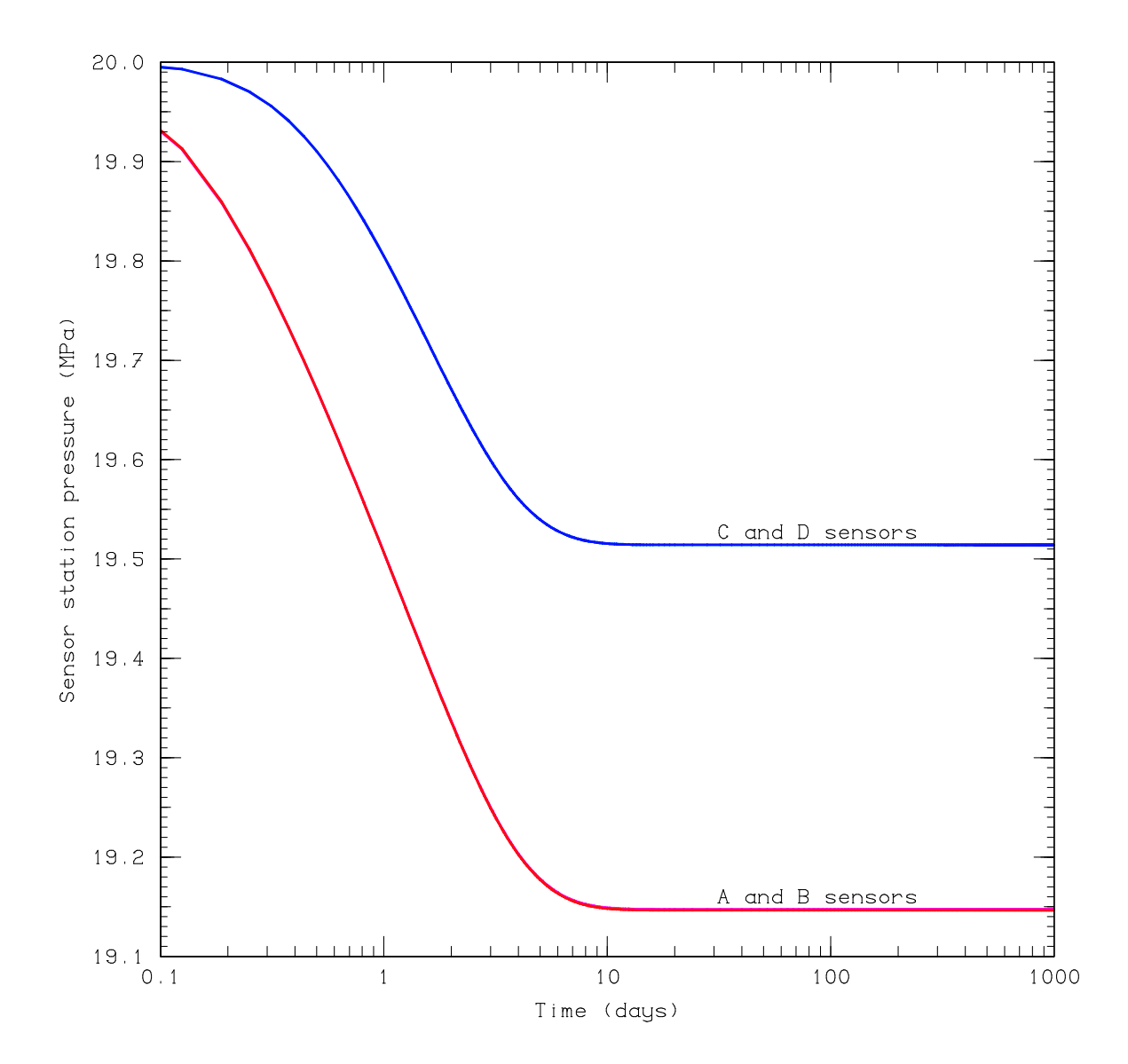


Figure 3.8. Case 4 – time-histories of pressure computed by HeatEx at sensor locations. *Red:* "A" sensors at 100 m distance from central production well. *Magenta:* "B" sensors at 100 m distance from well. *Blue:* "C" sensors at 200 m distance from well. *Cyan:* "D" sensors at 200 m distance from well.

```
r = 0.15 \text{ m} P = 15.63 \text{ MPa} (at the well)

r = 100 \text{ m} P = 19.15 \text{ MPa} ("A" and "B" sensors)

r = 200 \text{ m} P = 19.51 \text{ MPa} ("C" and "D" sensors)

r = 502 \text{ m} P = 20.00 \text{ MPa} (outer boundary)
```

The axisymmetric character of the stable late-time pressure distribution is preserved throughout the computational grid volume. For constant production rate from a central well with a fixed boundary pressure P_B at a fixed boundary radius r_B , it is straightforward to show (based on the

mass conservation principle, assumptions of uniform fluid salinity and temperature, the incompressible-fluid approximation, and Darcy's law) that the stable pressure as a function of radius will be given by:

$$P(r, t = \infty) = P_B - [2.303 R \mu \log_{10}(r_B/r)] / [2\pi \rho k h]$$

(notation and parameter values as above), as shown by the cyan (light blue-green color) straight line on Figure 3.9; that is, $P = [20 - 1.22 \log_{10}(r_B/r)]$ MPa. For comparison, for each non-void block in the computational grid, the computed pressure value for t = 1000 days is displayed using a red symbol at the radius value corresponding to the distance of the grid block center from the central production well. Agreement between computed and theoretical values is seen to be excellent.

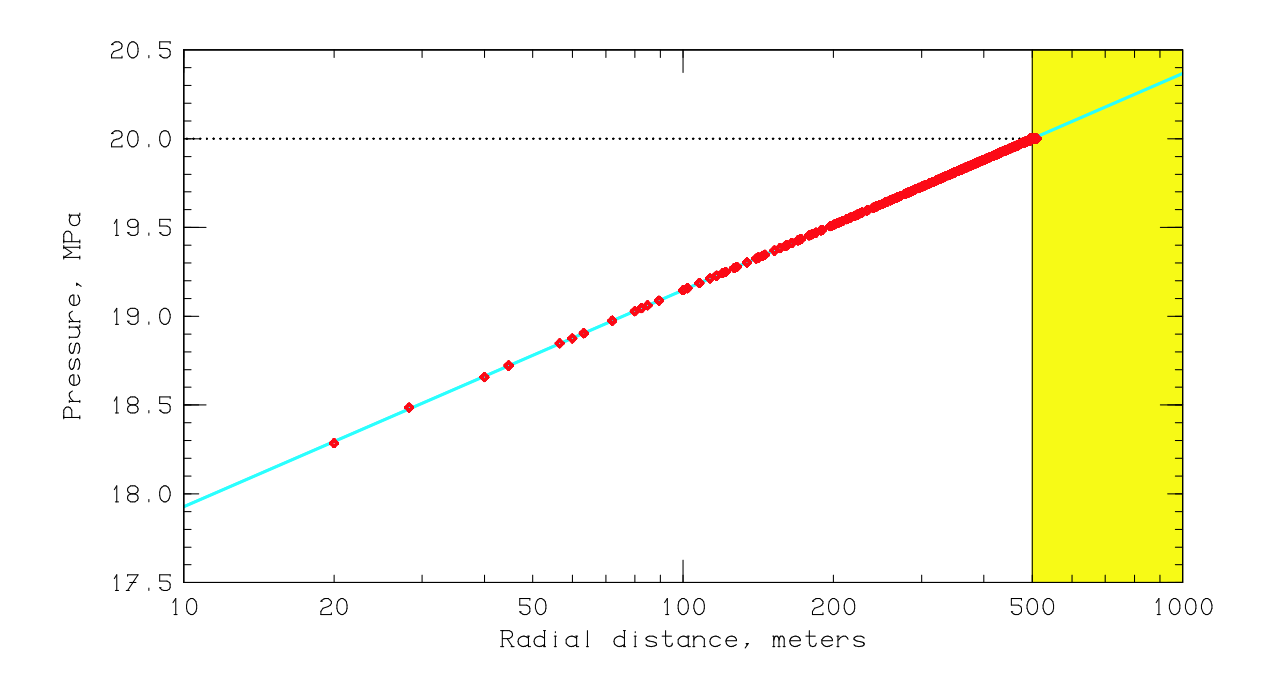


Figure 3.9. Case 4 – spatial distribution of pressure after 1000 days. *Cyan:* analytical (incompressible) approximation to steady-state pressure distribution as a function of distance from production well. *Red:* grid-block centered computed pressure values at t = 1000 days as function of the distance of the grid-block center from the production well. Horizontal grid resolution = 20 meters.

3.2.3. Computed results for Case 5 – central injection well

For Case 5, instead of *withdrawing* 100 kg/s from the deep circular reservoir, the central well *injects* 100 kg/s of "new" fluid. The injected brine is somewhat more saline than the *in-situ* fluid (4.8% NaCl by mass compared to 3.6%), and is also colder – the injected fluid enthalpy is 420 kJ/kg compared to the *in-situ* enthalpy value of 837 kJ/kg, which yields an injected fluid temperature which depends slightly on pressure:

P = 20 MPa	T = 100.5°C
P = 22 MPa	T = 100.1°C
P = 24 MPa	T = 99.8°C
P = 26 MPa	T = 99.4°C
P = 28 MPa	T = 99.0°C

as compared to an initial system temperature of 200°C. See input file *inwelflo.fil* for this case (Section 3.4.5.1 below).

Since the well is now injecting instead of producing, reservoir pressures increase with time. Figure 3.10 illustrates the computed datum pressure history in the injection well itself. At least three distinct regions are apparent, and, even at late times (t > 10 days), the borehole pressure does not reach a steady state but continues to rise slowly. Similarly, Figure 3.11 shows the computed pressure histories in the various "sensors" at 100 meters ("A" and "B") and 200 meters ("C" and "D") distance away. In Case 5, early transient pressure behavior gives way to a period of essentially constant pressure at about t = 10 days (similar to Case 4), but then later on, at a time which increases with increasing distance from the injection well (~200 days for the "A" and "B" sensors at 100 m separation and ~800 days for "C" and "D" at 200 m), the pressure starts increasing again.

This behavior may be understood by noting that the reservoir may be subdivided spatially into three migrating regions, as follows:

	Temperature	Salinity	Fluid density	Fluid viscosity
Region 1	200°C	3.6%	$904.6~\mathrm{kg/m^3}$	150.8 μPa-s
Region 2	200°C	4.8%	913.7 kg/m^3	154.7 μPa-s
Region 3	100°C	4.8%	999.2 kg/m^3	320.8 μPa-s

These density and viscosity values also depend slightly on pressure; here, 20 MPa pressure was assumed. Initially, the entire reservoir is in Region 1, but as time goes on Region 2 forms and expands radially outward from the injection well, followed by Region 3. Region 2 is separated from Region 1 by the "salinity front" whereas Region 3 is separated from region 2 by the "thermal front". The "salinity front" radius is approximately 17 $t^{1/2}$ meters in this case (t is time in days), and the "thermal front" radius is about 2.7 times smaller at the same time. As Figure 3.12 shows, the "salinity front" arrives at r = 100 m ("A", "B" sensors) at about 35 days and at 200 m ("C", "D") at about t = 140 days, whereas the thermal front (Figure 3.13) reaches t = 100 m at about 250 days and 200 m at around 1000 days (the end of the simulation).

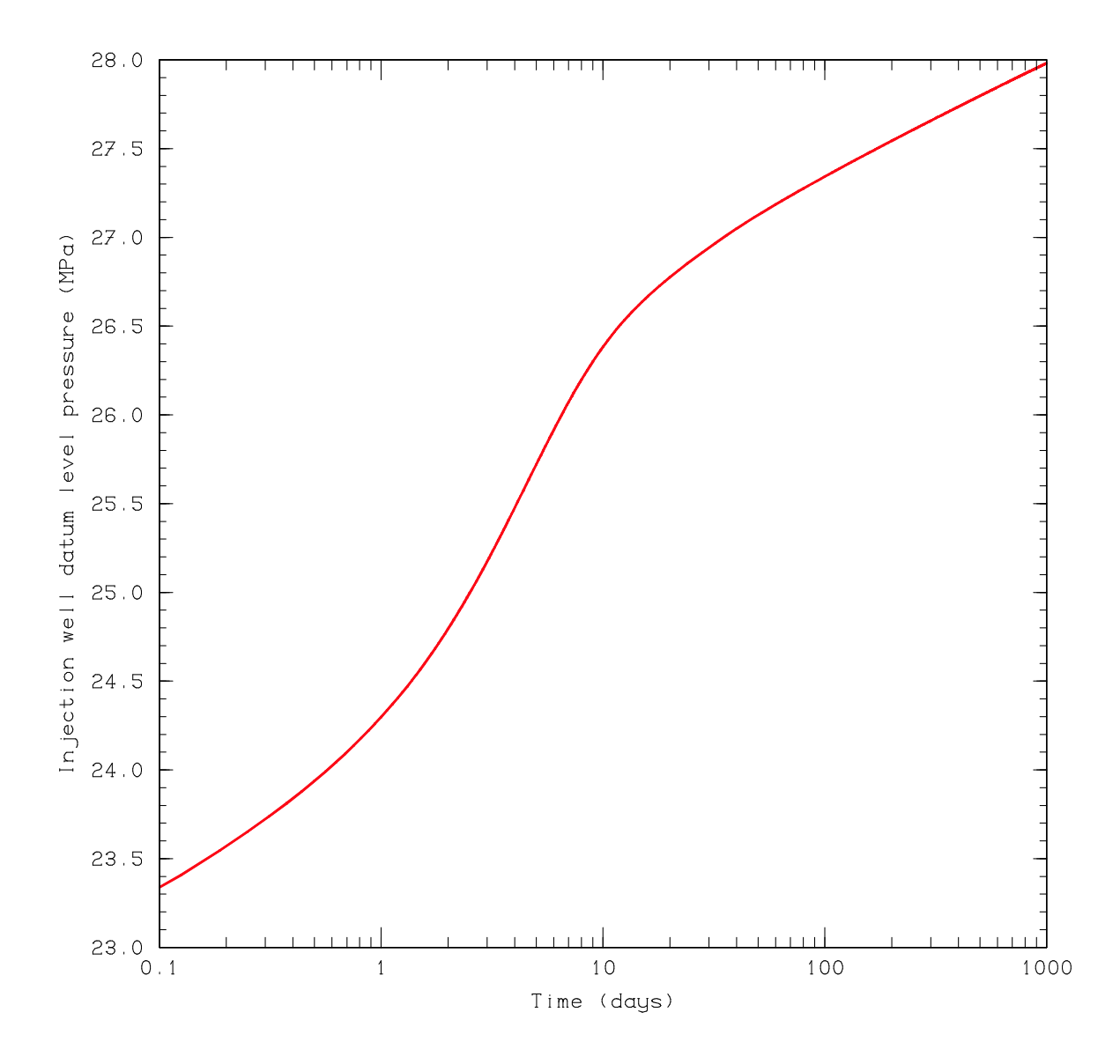


Figure 3.10. Case 5 – time-history of datum level pressure in central injection well as computed by HeatEx.

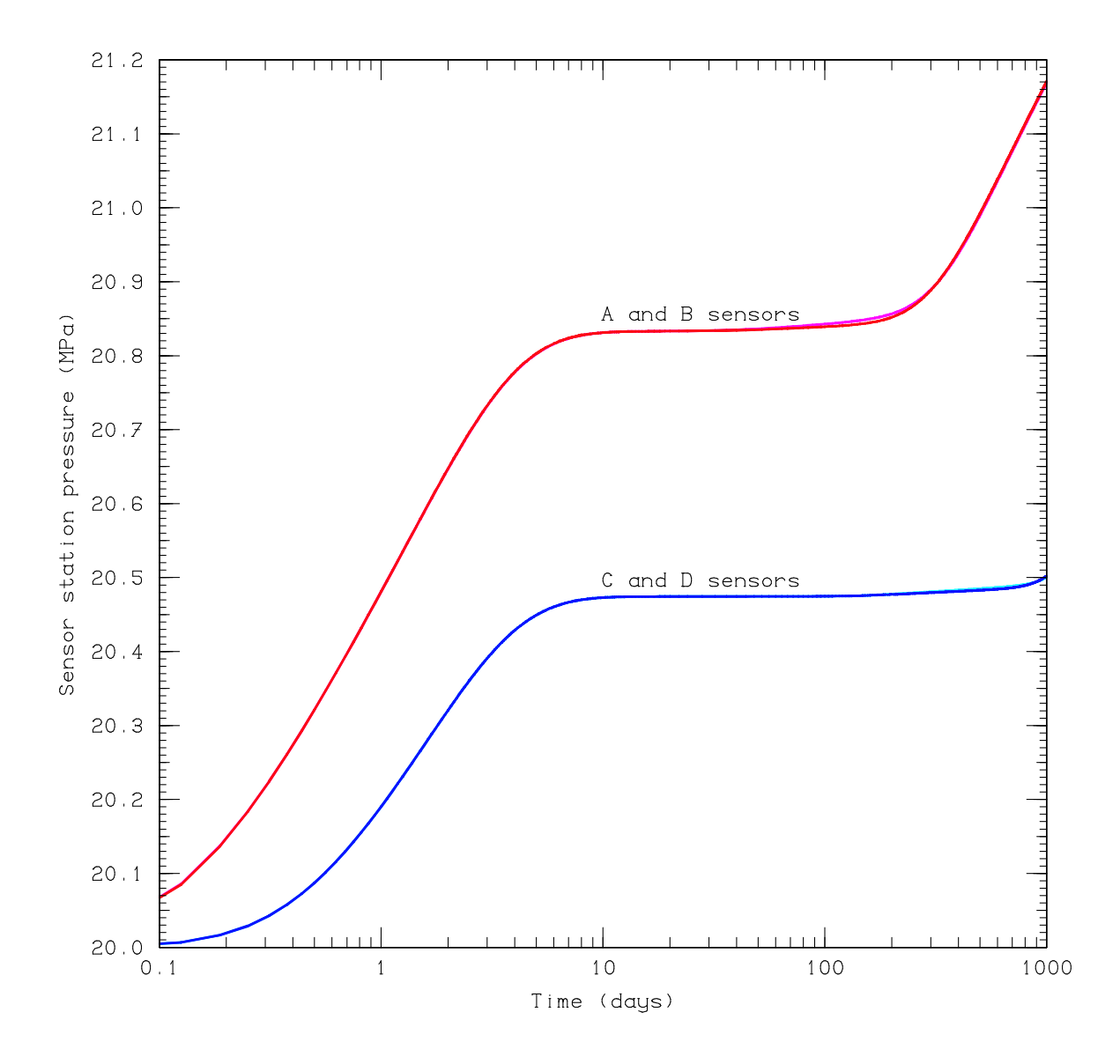


Figure 3.11. Case 5 – time-histories of pressure computed by HeatEx at sensor locations. *Red:* "A" sensors at 100 m distance from central injection well. *Magenta:* "B" sensors at 100 m distance from well. *Blue:* "C" sensors at 200 m distance from well. *Cyan:* "D" sensors at 200 m distance from well.

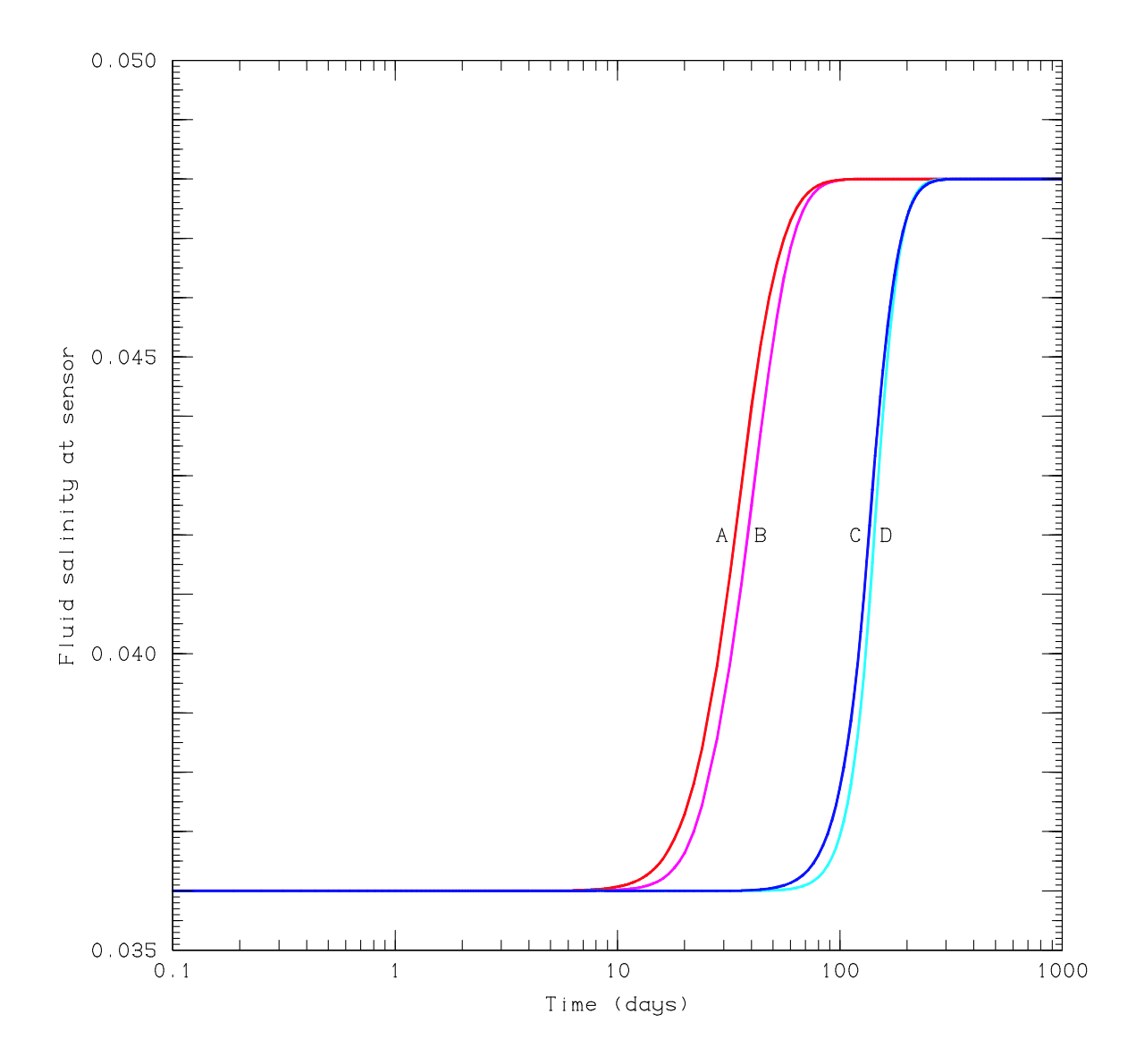


Figure 3.12. Case 5 – time-histories of salinity computed by HeatEx at sensor locations. Red: "A" sensors at 100 m distance from central injection well. Magenta: "B" sensors at 100 m distance from well. Blue: "C" sensors at 200 m distance from well. Cyan: "D" sensors at 200 m distance from well.

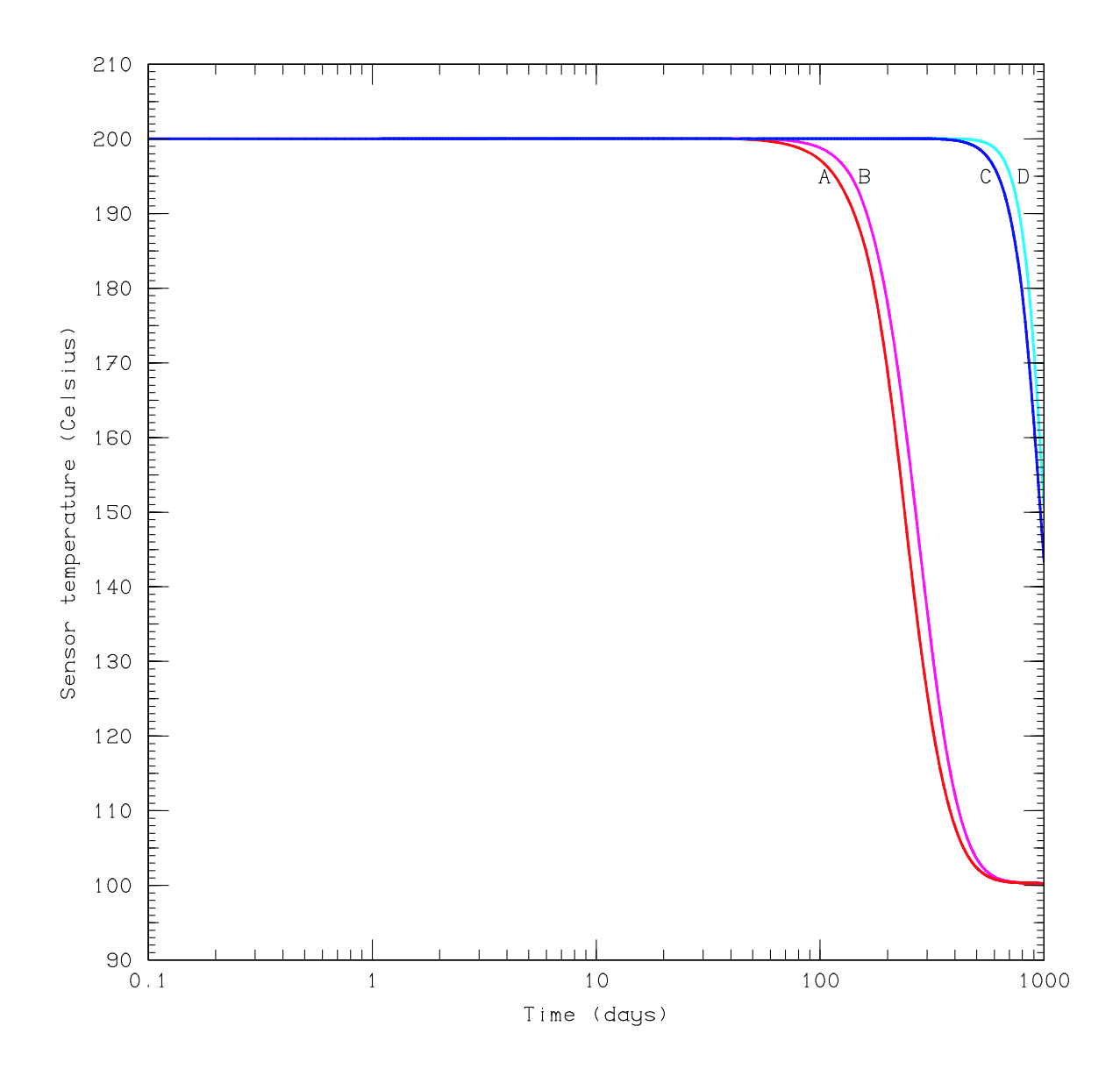


Figure 3.13. Case 5 – time-histories of temperature computed by HeatEx at sensor locations. Red: "A" sensors at 100 m distance from central injection well. Magenta: "B" sensors at 100 m distance from well. Blue: "C" sensors at 200 m distance from well. Cyan: "D" sensors at 200 m distance from well.

The "thermal front" passes through r = 100 m at t = 250 days, which is also when the sensor "A" and "B" pressure records begin to depart from the constant-pressure behavior which had prevailed previously since t = 10 days. The "C" and "D" pressure records similarly begin to increase again about four times later, at t = 1000 days (the end of the simulation) when the thermal front passes through r = 200 m. The "salinity front" has a much smaller effect, but the abrupt increase in viscosity from 155 to 321 Pa-s associated with the thermal front arrival causes a substantial increase in flow resistance at those times resulting in the rise in pressure.

This sequence of events can be better understood by consideration of Figures 3-14, 3-15, 3-16 and 3-17 which show, as functions of radial distance from the injection well, the pressure (in red), temperature (in blue) and salinity (green) for each grid block at t = 100, 200, 400 and 800 days, respectively. The approximate locations of the "salinity front" and the "thermal front" are indicated by the vertical cyan lines. An obvious correlation is present between the thermal front location and the point where the slope of the pressure vs. log (radius) curve changes abruptly. The salinity front has a similar but much weaker influence which can only be detected by careful examination of the computed results. The net effect is that, so long as the sensor lies beyond the thermal front, once early-time compressibility effects are over (after t = 10 days or so) the sensor pressure will remain essentially constant with time. But, after the thermal front passes over the sensor, the sensor pressure will begin to increase again.

Eventually, of course, a steady state will be reached after the thermal front reaches the outer boundary at r = 500 m, after t = 6500 days or so. Under steady conditions, salinity will be 4.8% and temperature will be 100°C everywhere. The asymptotic pressure will depend only on radial distance from the well according to:

$$P_{\infty}(r) = P(r, t = \infty) = P_B + [2.303 R \mu \log_{10}(r_B/r)] / [2\pi \rho k h]$$

Using $P_B = 20$ MPa, R = 100 kg/s, $\mu = 3.208 \times 10^{-8}$ Pa-s, $r_B = 500$ m, $\rho = 999.2$ kg/m³, $k = 5 \times 10^{-14}$ m² and h = 100 m, we obtain:

$$P_{\infty}(r) = [20 + 2.354 \log_{10} (500/r)] \text{ MPa}$$

where r is radius in meters, which takes on values as follows:

$$r = 0.15 \text{ m}$$
 (injection well) $P_{\infty} = 28.29 \text{ MPa}$
 $r = 100 \text{ m}$ ("A", "B" sensors) $P_{\infty} = 21.65 \text{ MPa}$
 $r = 200 \text{ m}$ ("C", "D" sensors) $P_{\infty} = 20.94 \text{ MPa}$

all of which exceed the 1000-day values at these same locations computed by the present simulation (27.98 MPa, 21.17 MPa and 20.50 MPa respectively). Note that, whereas in the production case (Case 4) a steady-state is attained after only about two weeks, complete stabilization of the injection case (Case 5) will take nearly eighteen years.

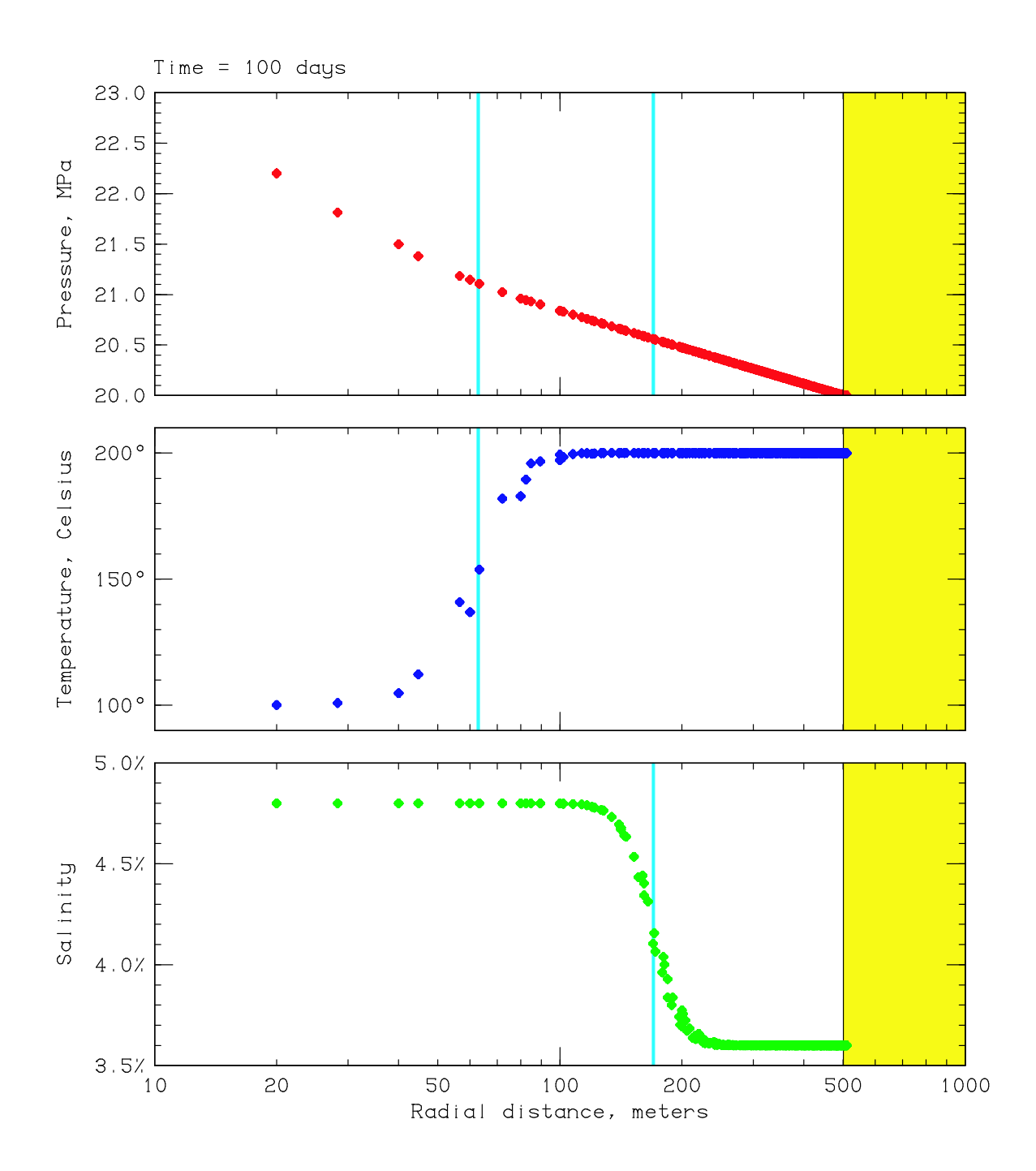


Figure 3.14. Case 5 – spatial distributions of pressure (upper), temperature (middle) and salinity (lower) after 100 days of injection. *Cyan:* approximate locations of thermal (left) and salinity (right) fronts at 100 days based on nondiffusive incompressible analytical approximation.. *Red, Blue, Green:* grid-block centered computed pressure, temperature and salinity values as function of the distance of the grid-block center from the injection well.

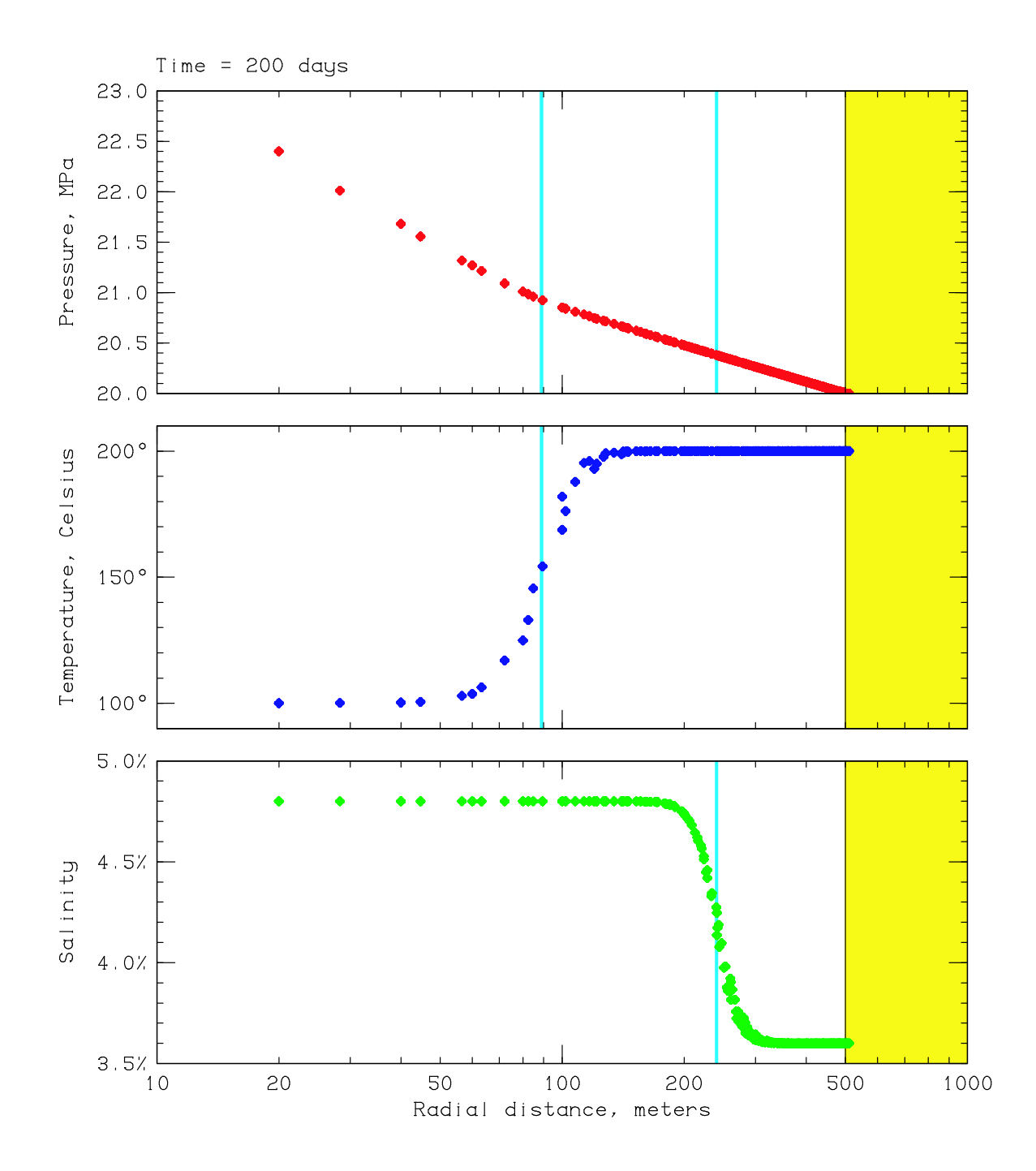


Figure 3.15. Case 5 – spatial distributions of pressure (upper), temperature (middle) and salinity (lower) after 200 days of injection. *Cyan:* approximate locations of thermal (left) and salinity (right) fronts at 200 days based on nondiffusive incompressible analytical approximation.. *Red, Blue, Green:* grid-block centered computed pressure, temperature and salinity values as function of the distance of the grid-block center from the injection well.

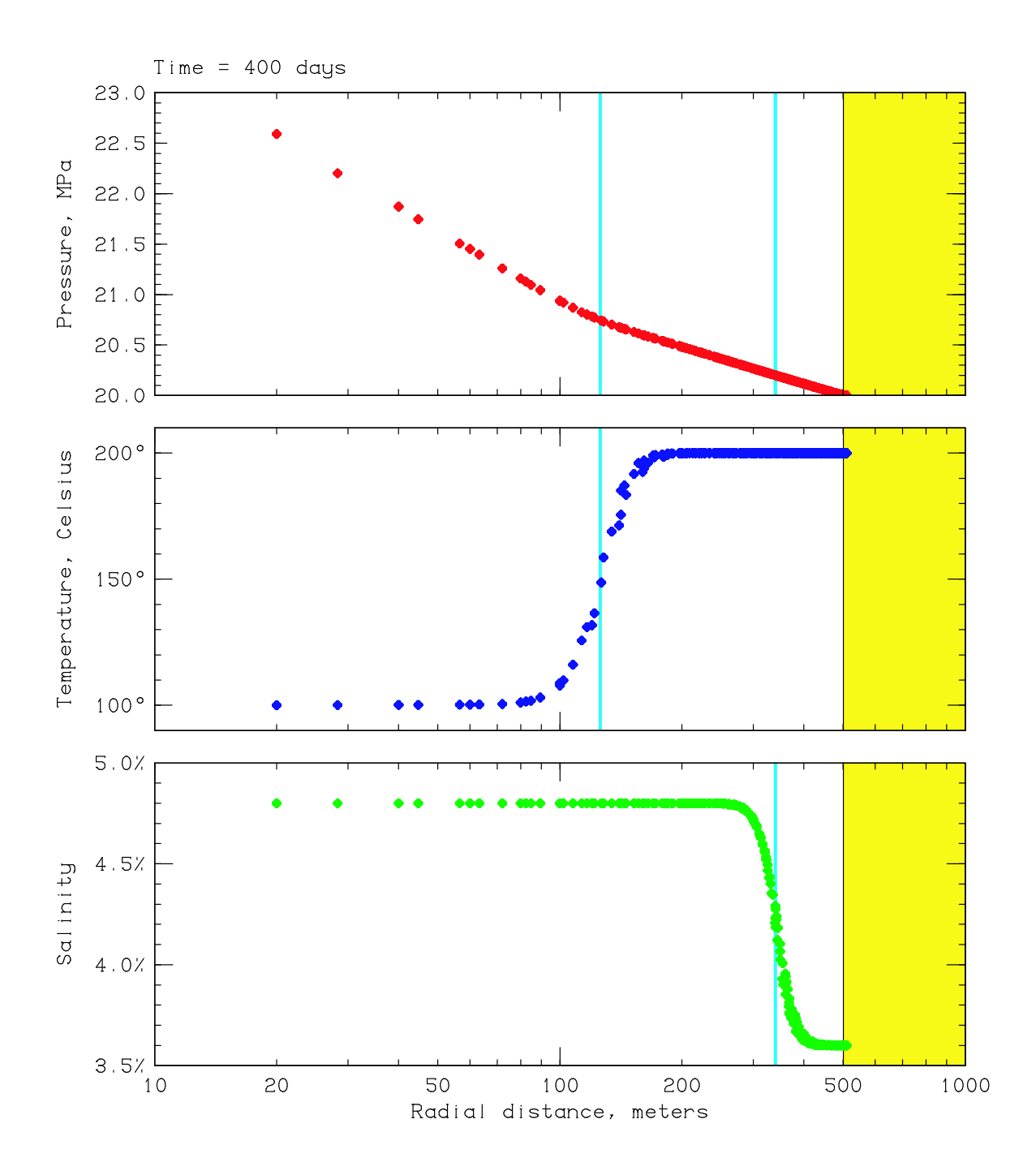


Figure 3.16. Case 5 – spatial distributions of pressure (upper), temperature (middle) and salinity (lower) after 400 days of injection. *Cyan:* approximate locations of thermal (left) and salinity (right) fronts at 400 days based on nondiffusive incompressible analytical approximation.. *Red, Blue, Green:* grid-block centered computed pressure, temperature and salinity values as function of the distance of the grid-block center from the injection well.

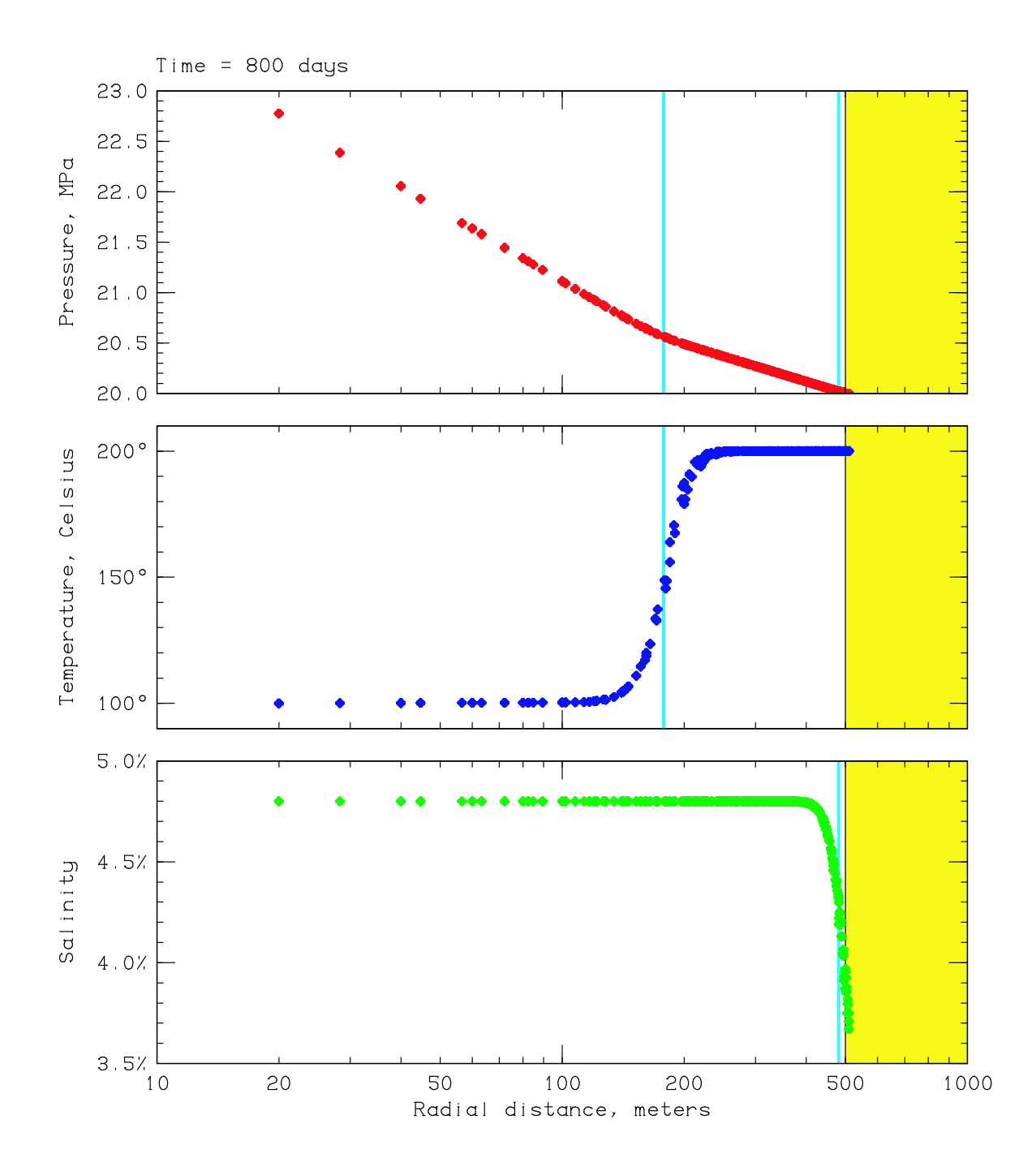


Figure 3.17. Case 5 – spatial distributions of pressure (upper), temperature (middle) and salinity (lower) after 800 days of injection. *Cyan:* approximate locations of thermal (left) and salinity (right) fronts at 800 days based on nondiffusive incompressible analytical approximation.. *Red, Blue, Green:* grid-block centered computed pressure, temperature and salinity values as function of the distance of the grid-block center from the injection well.

3.3. THREE-DIMENSIONAL ILLUSTRATIVE CASE 6

A fundamental purpose of the first five illustrative cases was to carry out calculations using HeatEx from which the results could be compared with (at least approximate) analytic solutions. As a result, it was not possible to exercise some of the more unusual HeatEx features which do not readily lend themselves to analytic approximation. Some of these features are:

- three-dimensional modeling with realistic topography,
- "aquifer" boundary conditions,
- electrokinetic effects,
- fracture slip patch dynamics, and
- spectral conductive MINC modeling of fluid/rock heat exchange.

A major purpose for Case 6 is to illustrate these and other unusual attributes of the HeatEx code.

Although no analytic approximations are available for direct verification of the Case 6 results, a deliberate effort was made to devise the problem in such a way that the solution should demonstrate various kinds of symmetries that proved useful for calculation verification. These observations will be made later, during the presentation of computed results.

3.3.1. Case 6 Problem Specifications

3.3.1.1. Problem geometry: For all five previous illustrative cases, the earth surface topography was taken to be a simple horizontal plane located at 500 meters above sea level elevation. For Case 6, to illustrate the specification procedure, a real digital "topographic map" is included as input file *intopogr.fil* (see Section 3.4.6.21). The map covers a 6×6 km area (36 km² total) and represents the earth surface with a 121×121 array of 14,641 discrete surface elevation values (50 meters horizontal spacing) which range between +497.95 and +1475.00 meters above sea level ("ASL") and average +801.22 m ASL; see Figure 3.18.

The actual area being represented is located in southern Japan in a region where the local earth coordinates range from 10,000 meters East to 16,000 meters East and from 13,000 meters North to 19,000 meters North according to the local land survey maps. Please note, however, that these topographic data are used only for illustrative purposes here, and no inferences should be drawn concerning actual subsurface conditions prevailing at this Japanese locale based upon the present sample calculation.

The thermohydraulic computational grid is centrally located within this area, and represents a 1 km³ cubical volume centered at an elevation of 2000 meters below sea level (-2000 m ASL), at 13,000 meters East and 16,000 meters North. The *x*-coordinate measures distance to the northeast and the *y*-coordinate measures distance northwest as shown – the *z*-coordinate measures distance upward (see Figure 3.18).

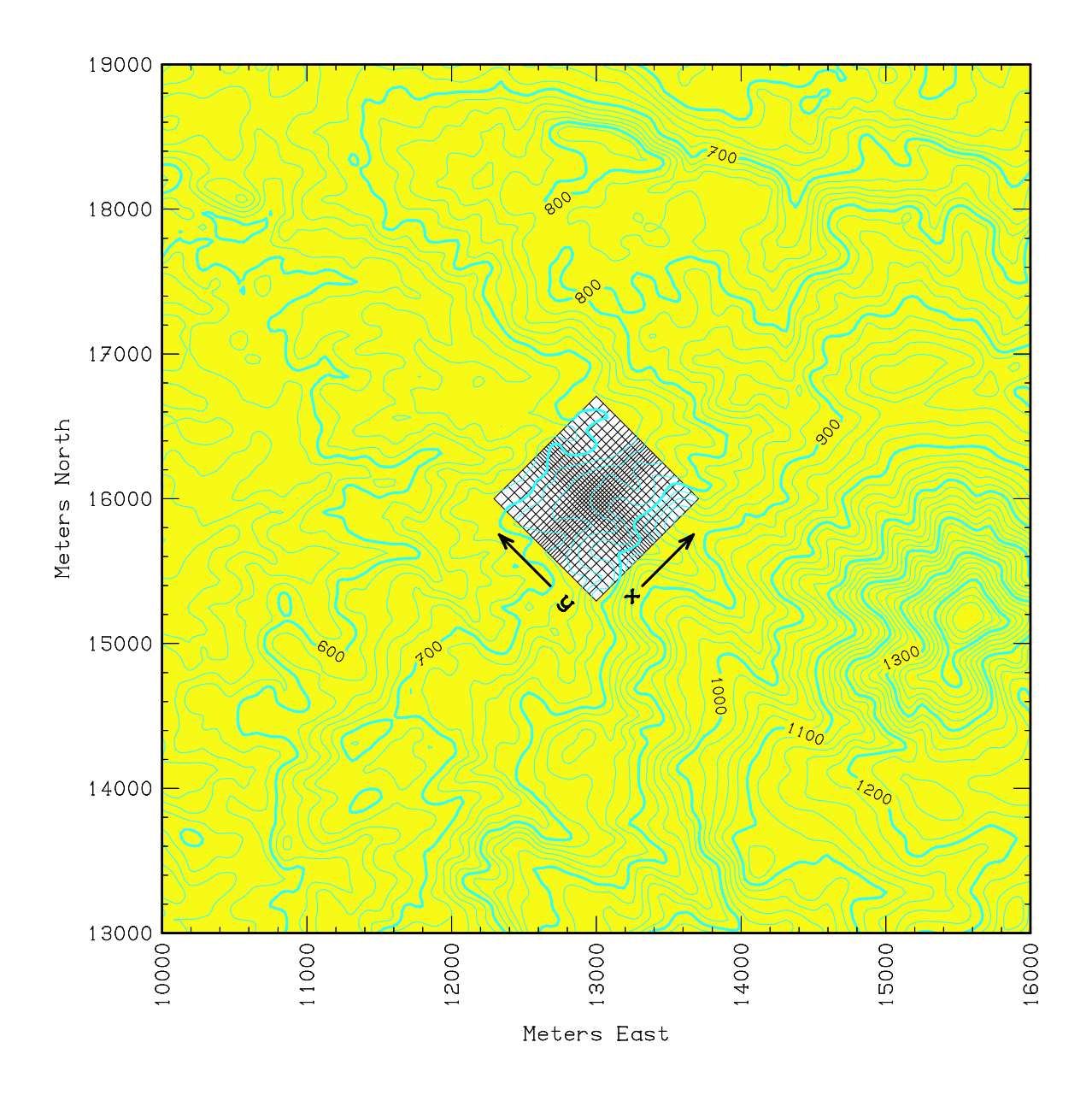


Figure 3.18. Case 6 – overall problem geometry. One-cubic-kilometer (1×1×1 km in spatial extent) computing volume is embedded in an outer 6×6 km region described by input files *ingridte.fil* (see Section 3.4.6.10) and *intopogr.fil* (see Section 3.4.6.21). The computing volume is centered at 13 kilometers East, 16 kilometers North, and –2 km ASL (two kilometers below sea level elevation), and is oriented such that the *x*-coordinate measures distance northeast as shown. The thermohydraulic and electrokinetic grids coincide (see input files *ingridek.fil* and *ingridth.fil*, Sections 3.4.6.9 and 3.4.6.11).

This grid geometry is specified by input file *ingridth.fil* (Section 3.4.5.11). The earth surface elevation in the one-km² area overlying the grid averages +765 m ASL, and ranges from +754 m ASL to +776 m ASL. The upper surface of the grid itself is located much deeper (at -1500 m ASL), and the lower surface is at -2500 m ASL. Electrokinetic calculations are also performed in Case 6, as discussed below – the electrokinetic grid is assumed to coincide with the thermohydraulic grid in this case (file *ingridek.fil*, Section 3.4.6.9). As shown in Figure 3.19, these grids each consist of 27×27×27 blocks (19,683 blocks altogether) – block dimensions range from 20 m near the center to 70 m at the periphery. The same arrangement of grid block spacing is used in all three coordinate directions. A much more spatially extensive grid using 30×30×36 200-meter cubical blocks is used to represent the regional stress field for use by the fracture dynamics model (see file *ingridte.fil*, Section 3.4.5.10) - this grid covers the entire 6 km × 6 km area of the Figure 3.18 topographic map, and extends vertically between –4100 m ASL and +2500 m ASL (*i.e.* to above the earth surface).

Figure 3.19 also shows the wellhead locations of nine wells arranged in a 120 m \times 120 m square pattern. All nine wells are considered to be vertically oriented, and the central well ("Well 5") is an injection well located at the center of the study area (13,000 m E, 16,000 m N). The other eight wells are all production wells, located as follows relative to Well 5 (of which the wellhead is located at the center of block i = 14, j = 14):

Well 1:	84.85 m South	(center of block $i = 11, j = 11$)
Well 2:	60.00 m Southeast	(center of block $i = 14, j = 11$)
Well 3:	84.85 m East	(center of block $i = 17, j = 11$)
Well 4:	60.00 m Southwest	(center of block $i = 11, j = 14$)
Well 6:	60.00 m Northeast	(center of block $i = 17, j = 14$)
Well 7:	84.85 m West	(center of block $i = 11, j = 17$)
Well 8:	60.00 m Northwest	(center of block $i = 14, j = 17$)
Well 9:	84.85 m North	(center of block $i = 17, j = 17$)

These well geometries are all specified by input file *inwelgeo.fil* (see Section 3.4.6.24). Except for horizontal location, the geometries of all eight production wells are the same. Figure 3.20 illustrates the deeper part of the well completions. At levels where the wells penetrate the computational grid, the well diameters are all 25 cm. All eight production wells are cased and cemented down to -1930 m ASL, so these portions of the wells are not in hydraulic communication with the formation. Below that level is a 60-meter section of slotted metallic liner, which permits hydraulic communication. A 20-meter open hole section with no metallic casing lies between -1990 m ASL and -2010 m ASL. Next is another 60-meter section of slotted liner, below which is solid cemented casing down to bottomhole at -2140 m ASL. Thus, all eight production wells are hydraulically connected to the reservoir over a vertical length of 140 meters centered at -2000 m ASL elevation, and represented by seven computational layers (k = 11-17).

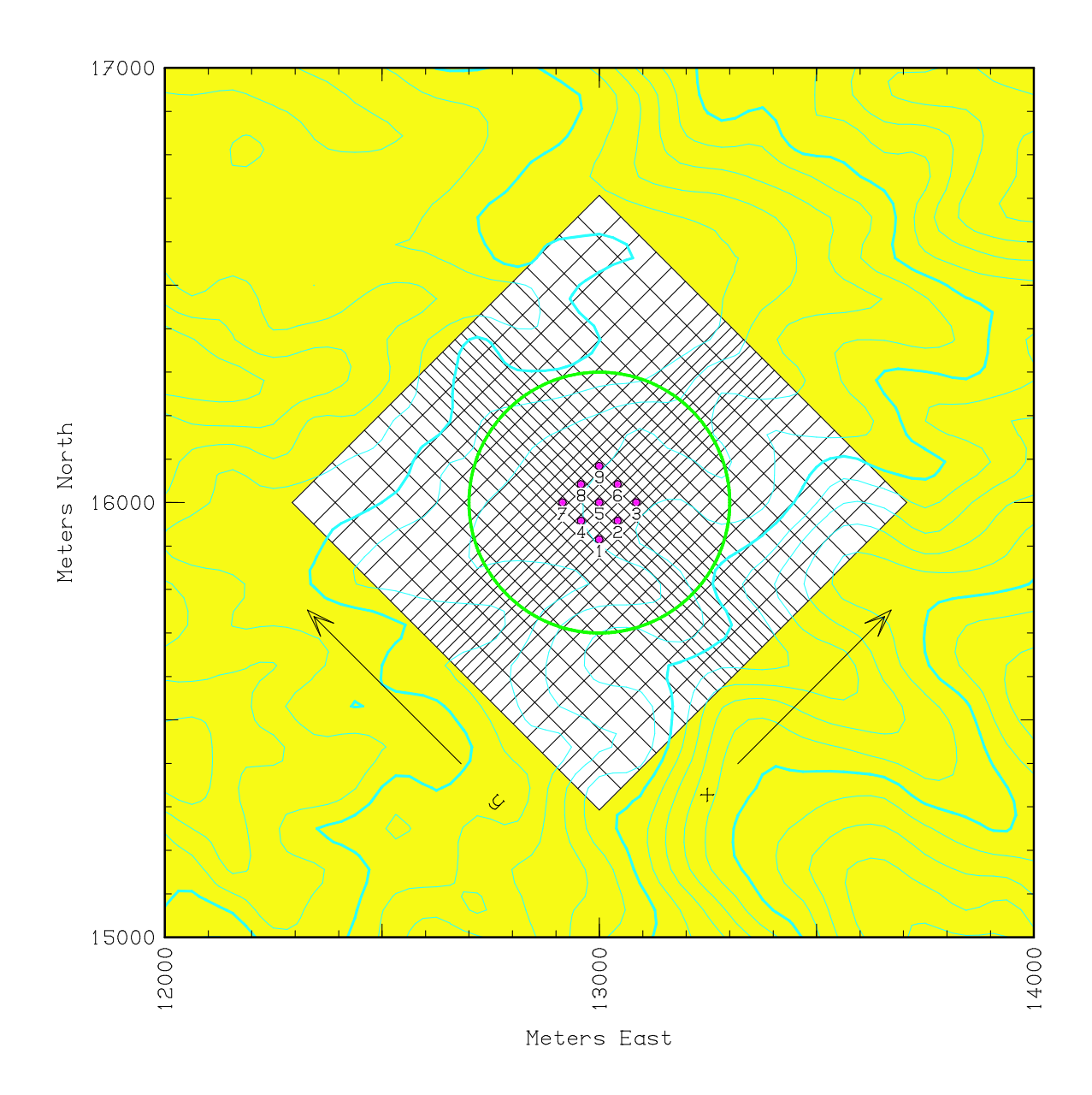


Figure 3.19. Case 6 – grid and wellfield geometry. The grid contains 27×27×27 blocks in the *x*-, *y*- and *z*-coordinate directions (total 19,683 blocks), with grid block dimensions ranging from 20 meters in the central region to 70 meters adjacent to the perimeter. Nine geothermal wells are located centrally as shown (using *red* color) – Wells 1-4 and 6-9 are production wells, and the central Well 5 is an injection well. Within the central spherical region indicated in *green* (diameter = 600 m), discrete "fracture slip patches" are located to represent the nonlinear fracture deformation and reservoir stimulation caused by pressurization and shearing.

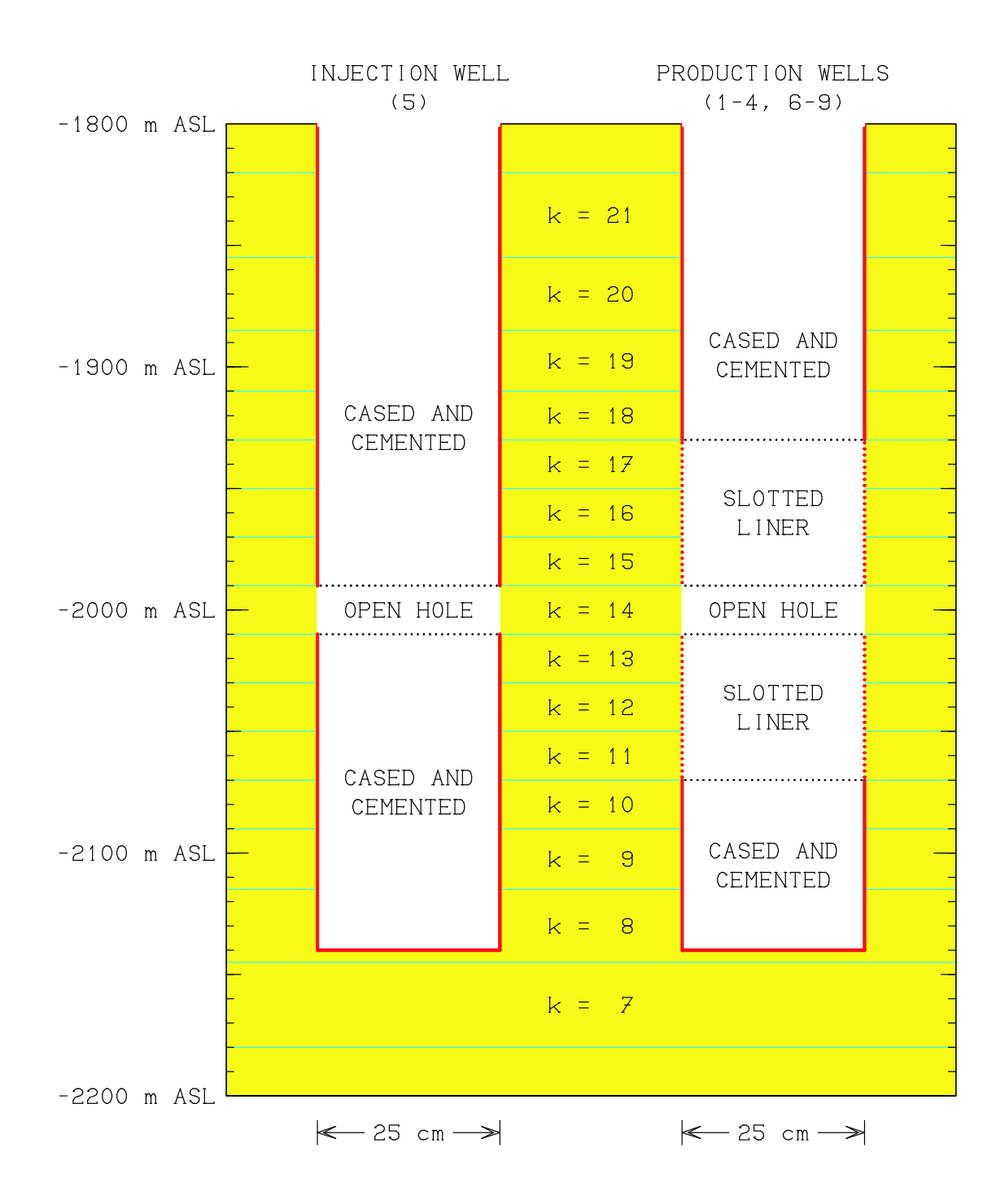


Figure 3.20. Case 6 – details of lower portion of well completions (also see input file *inwelgeo.fil*, Section 3.4.6.24). Completions are identical for all eight production wells. Note that the portions open to the formation are all centered at -2000 m ASL elevation, but while the open/slotted interval is 140 m high in the production wells (computational layers k = 11-17), it is only 20 m high (a single layer, k = 14) in the injection well.

The completion geometry for the central injection well (Well 5) is similar, except that there is no slotted liner. Communication with the formation is restricted to the 20-meter open hole section surrounding -2000 m ASL elevation (and to grid block i = 14, j = 14, k = 14), which is suitable to represent a packed-off interval for pressurization and stimulation operations. Also note that, in all nine wells, continuous electrically conductive metallic casing/liner is present everywhere except for the 20-meter open hole interval. As a result, in all wells the electrically conductive metallic casing is subdivided into two electrically independent portions, one above and one below this open hole interval. This fact will be important in interpretation of the electrokinetic effects, as will be seen below.

3.3.1.2. Temporal effects: The operational program for these wells is specified by input file *inwelflo.fil* (Section 3.4.6.23). Between t = 0 and t = 10 days (the "stimulation interval"), all eight production wells are shut in, but the central injection well (Well 5) injects pure water (no dissolved NaCl) into the reservoir at a rate of 100 kg/s, subject to an upper limit on flowing datum level pressure (at -2000 m ASL elevation within the well) of 50 MPa. The enthalpy of the water entering the formation is 420 kJ/kg, resulting in a downhole flowing injection temperature which ranges from 94.8°C (at the 30 MPa initial pressure) to 91.1°C (at the 50 MPa limiting pressure). During this 10-day injection interval, a conservative nonreactive tracer is injected along with the water at a concentration of one part per million by mass ("1 ppm"). Although the production wells are all shut-in in the sense that the net flow rate of fluid into or out of the well is zero, since the production wells are each hydraulically coupled to seven different computational grid blocks ("feedblocks"), fluid may simultaneously enter and leave the formation at different vertical elevations – only the total flow is zero.

Next, at t = 10 days (864,000 seconds), injection into Well 5 ceases and a thirty-day shut-in "soak" period begins during which the net flow into or out of each well is maintained at zero. The "soak" period ends at t = 40 days (3,456,000 seconds). At that time, the "production" period begins. Injection into Well 5 resumes, but this time at 100 kg/s flow rate subject to a smaller limiting pressure (40 MPa), and the injected fluid now consists of a 2% salinity NaCl brine (with no tracer). The injected fluid enthalpy remains 420 kJ/kg, which means that the injected fluid temperature now ranges from 96.4°C (at 30 MPa) to 94.6°C (at 40 MPa). Also at t = 40 days, all eight production wells ("odd" wells 1, 3, 7 and 9 located 84.85 m from the injection well, and "even" wells 2, 4, 6 and 8 located 60 m from the injector) begin to withdraw fluid from the reservoir. For all eight of these wells, the upper limit on production rate is 100 kg/s, but subject to a minimum flowing datum level pressure within the well (at -2000 m ASL elevation) of 20 MPa. Injection into Well 5 and production from the other eight wells continues indefinitely thereafter. The calculation is carried out to t = 400 days.

Temporal discretization for Case 6 is specified by input file *intimscl.fil* (Section 3.4.6.20), as follows. As noted above, the sequence of events may be subdivided into (1) a ten-day "stimulation" period during which only the injection well flows, followed by (2) a thirty-day "soak" period during which no wells flow, in turn followed by (3) a total of 360 days of the "production" period during which all wells are operating. During this entire period, the overall upper limit on the computational time-step size is 48 hours, but at early times, particularly during the earliest part of the "stimulation" phase, the time-step is constrained to even smaller values, as follows:

Time interval	Maximum Δt
0 to 2 days	90 minutes
2 to 12 days	6 hours
12 to 14 days	12 hours
14 to 16 days	1 day
16 to 400 days	2 days

Furthermore, as specified by input file *inoutfrq.fil* (Section 3.4.6.15).most types of intermittent "snapshot" program output are called for at ten day intervals, and also at additional times during the early parts of all of the three "phases" (stimulation phase, soak phase and production phase), as follows:

$t_o + 45 \min$	$t_o + 12$ hours
$t_o + 90 \min$	$t_o + 1 \text{ day}$
$t_o + 3$ hours	$t_o + 2 \text{ days}$
t_o + 6 hours	$t_o + 4 \text{ days}$

where $t_o = 0$, 10 days or 40 days.

3.3.1.3. Initial conditions and material properties: For Case 6, instead of using input files *ininpres.fil*, *inintemp.fil* and/or *ininsalt.fil*, the "hydrostatic" initialization option is used (file *ininhydr.fil* – Section 3.4.6.12) to assign initial distributions of pressure, temperature and brine salinity. The initial value of fluid pressure at the geometric center of the thermohydraulic grid (13,000 m East, 16,000 m North and –2000 m ASL) is specified to be equal to 30 MPa. Initially, brine salinity is uniform at 4% NaCl by mass everywhere within the grid, and a linear distribution of initial temperature with vertical elevation, equal to 200°C at –2000 m ASL and with a vertical gradient of –0.02°C per meter of elevation (210°C at –2500 m ASL and 190°C at –1500 m ASL), is also prescribed. Then, the hydrostatic distribution of initial fluid pressure is calculated automatically and assigned to each grid block. Initial conditions (pressure P, temperature T, and salinity S) in each vertical computational layer k are thereby assigned as listed in Table 3.2. A single conservative tracer is considered (file *intrchem.fil*, Section 3.4.6.22). For tracer content, initial concentrations are taken to be zero everywhere (Section 3.4.6.13, file *inintrcr.fil*).

Next, consider various scalar reservoir properties that are treated as uniform throughout the 1 km³ grid volume for Case 6. Specified by input files *incondrk.fil*, *inrkigpr.fil* and *inrkvolp.fil* (Sections 3.4.6.3, 3.4.6.17 and 3.4.6.18), these are:

Reservoir thermal conductivity:	3 W/m-°C
Intergranular rock permeability:	$10^{-15} \mathrm{m}^2 (1 \mathrm{millidarcy})$
Rock grain density:	2500 kg/m^3
Rock grain heat capacity:	1000 J/kg- °C
Initial rock porosity:	0.04
Pore compressibility:	10^{-8} Pa^{-1}
Hydraulic dispersion coefficients:	0

TABLE 3.2. Initial Thermodynamic State for Case 6

Vertical	l Location	Pressure	Temperature	Salinity
Layer $k = 1$	(-2465.0 m ASL)	P = 34.151 MPa	T = 209.30°C	S = 4%
Layer $k = 2$	(-2400.0 m ASL)	P = 33.573 MPa	T = 208.00°C	S = 4%
Layer $k = 3$	(-2342.5 m ASL)	P = 33.061 MPa	T = 206.85°C	S = 4%
Layer $k = 4$	(-2290.0 m ASL)	P = 32.593 MPa	T = 205.80°C	S = 4%
Layer $k = 5$	(-2242.5 m ASL)	P = 32.169 MPa	T = 204.85°C	S = 4%
Layer $k = 6$	(-2200.0 m ASL)	P = 31.789 MPa	T = 204.00°C	S = 4%
Layer $k = 7$	(-2162.5 m ASL)	P = 31.454 MPa	T = 203.25°C	S = 4%
Layer $k = 8$	(-2130.0 m ASL)	P = 31.164 MPa	T = 202.60°C	S = 4%
Layer $k = 9$	(-2102.5 m ASL)	P = 30.918 MPa	T = 202.05°C	S = 4%
Layer $k = 10$	(-2080.0 m ASL)	P = 30.716 MPa	T = 201.60°C	S = 4%
Layer $k = 11$	(-2060.0 m ASL)	P = 30.537 MPa	T = 201.20°C	S = 4%
Layer $k = 12$	(-2040.0 m ASL)	P = 30.358 MPa	T = 200.80°C	S = 4%
Layer $k = 13$	(-2020.0 m ASL)	P = 30.179 MPa	T = 200.40°C	S = 4%
Layer $k = 14$	(-2000.0 m ASL)	P = 30.000 MPa	T = 200.00°C	S = 4%
Layer $k = 15$	(-1980.0 m ASL)	P = 29.821 MPa	T = 199.60°C	S = 4%
Layer $k = 16$	(-1960.0 m ASL)	P = 29.641 MPa	T = 199.20°C	S = 4%
Layer $k = 17$	(-1940.0 m ASL	P = 29.463 MPa	T = 198.80°C	S = 4%
Layer $k = 18$	(-1920.0 m ASL)	P = 29.283 MPa	T = 198.40°C	S = 4%
Layer $k = 19$	(-1897.5 m ASL)	P = 29.089 MPa	T = 197.95°C	S = 4%
Layer $k = 20$	(-1870.0 m ASL)	P = 28.834 MPa	T = 197.40°C	S = 4%
Layer $k = 21$	(-1837.5 m ASL)	P = 28.542 MPa	T = 196.75°C	S = 4%
Layer $k = 22$	(-1800.0 m ASL)	P = 28.205 MPa	T = 196.00°C	S = 4%
Layer $k = 23$	(-1757.5 m ASL)	P = 27.823 MPa	T = 195.15°C	S = 4%
Layer $k = 24$	(-1710.0 m ASL)	P = 27.395 MPa	T = 194.20°C	S = 4%
Layer $k = 25$	(-1657.5 m ASL)	P = 26.923 MPa	T = 193.15°C	S = 4%
Layer $k = 26$	(-1600.0 m ASL)	P = 26.404 MPa	T = 192.00°C	S = 4%
Layer $k = 27$	(-1535.0 m ASL)	P = 25.818 MPa	T = 190.70°C	S = 4%

<u>3.3.1.4.</u> Boundary conditions: The external boundary conditions on fluid mass and heat flow applied to the periphery of the cubical computational grid are provided using input files *inaquifr.fil* and *insorcen.fil* (Sections 3.4.6.1 and 3.4.6.19). As noted above, the initial conditions on the distribution of temperature involve a vertical temperature gradient of 0.02°C per meter of depth and a reservoir thermal conductivity of 3 W/m-°C. Multiplying, this means that there is initially a steady upward conductive heat flux equal to 0.06 watts per square meter passing through the study volume.

To balance this heat flux, we must withdraw heat at that rate from the upper surface of the grid volume at -1500 m ASL and must add heat at the same rate to the lower surface at -2500 m ASL, resulting in a stable undisturbed conductive heat flow distribution. This is accomplished using file *insorcen.fil* and assigning a fixed volumetric heat source equal to 857.142 microwatts per cubic meter to the entire lowest (k = 1) layer of grid blocks, and a compensating heat sink of the same magnitude to the uppermost block layer at k = 27. Note that the vertical thicknesses of both of these layers is equal to 70 meters, and that $(70 \text{ m}) \times (857.142 \, \mu\text{W/m}^3) = 0.06 \, \text{W/m}^2$.

On the lower surface of the computational grid at -2500 m ASL, simple "impermeable" conditions (no vertical flow) are imposed, but the other five faces of the computational volume have "aquifer-type" conditions specified which permit fluid flow perpendicular to these boundaries, using input file *inaquifr.fil*. Affixed to the upper grid block surfaces at -1500 m ASL and extending upward 3000 m above that level are vertical "strips" subdivided into 16 vertical segments of unequal size which are used to calculate pressure changes at the grid surface based on linear pressure transient techniques, and an assumption that the pressure 3000 meters above the upper grid surface does not change with time (Dirichlet boundaries). In this overlying region, average values for (1) fluid temperature, (2) fluid pressure, (3) salinity, (4) rock bulk modulus, (5) rock shear modulus, (6) rock porosity and (7) rock permeability are taken to be 100°C, 10 MPa, 5000 ppm, 10 GPa, 4 GPa, 0.04 and one millidarcy respectively.

At the vertical outer grid boundaries (to the northeast, southeast, southwest and northwest), a similar treatment is used except that the perpendicular horizontal "strips" each contain 20 subdivisions and each extends eight kilometers horizontally outward from the grid boundary. In all four of these outer zones, the average values assumed for (1) fluid temperature, (2) fluid pressure, (3) salinity, (4) rock bulk modulus, (5) rock shear modulus, (6) rock porosity and (7) rock permeability are 200°C, 20 MPa, 4%, 10 GPa, 4 GPa, 0.04 and one millidarcy respectively. Within the "strips" (whether horizontal or vertical) the properties of the solid rock are taken to match those of the grid interior (permeability = one millidarcy and porosity = 4%). In all of these "aquifer boundary" strips (horizontal or vertical), the exterior grid block size adjacent to the interior grid is 70 meters, matching the outermost interior grid block size, to minimize numerical impedance mismatches between the aquifer boundary "strips" and the internal solution.

<u>3.3.1.5. Fluid/rock heat transfer:</u> As was done in Case 3 (see Section 3.1), the classical "porous medium" assumption of instantaneous local thermal equilibrium between the fluid and the rock was relaxed for Case 6 and, in fact, a more elaborate conductive MINC-type representation was employed for Case 6 than in Case 3. Using input file *inmincnd.fil* as shown in Section 3.4.6.14, a "library" of four different MINC sub-models was constructed.

Each entry in the library consists of a concentric-sphere assembly of "shells" (15 shells in each assembly), but represents a different "fracture spacing" and thus a different characteristic thermal relaxation time τ_{eq} . Thus, each library entry has a different "50% cooling time" $\tau_{50\%}$ and represents a different "average fracture separation" (or spherical assembly diameter) λ . The library entries are:

1. Characteristic $\tau_{eq} = 10^6$ seconds; $\tau_{50\%} = 8.6$ hours; $\lambda = 2$ meters.

2. Characteristic $\tau_{eq} = 10^7$ seconds; $\tau_{50\%} = 3.6$ days; $\lambda = 7$ meters.

3. Characteristic $\tau_{eq} = 10^8$ seconds; $\tau_{50\%} = 5.1$ weeks; $\lambda = 22$ meters.

4. Characteristic $\tau_{eq} = 10^9$ seconds; $\tau_{50\%} = 0.99$ years; $\lambda = 71$ meters.

Then, file *inmincnd.fil* specifies that each of the $27 \times 27 \times 27 = 19,683$ macroscopic grid blocks is subdivided into five subregions (each 20% of the grid block volume). One of these five subregions is treated as an ordinary porous medium, using instantaneous local thermal equilibration. Each of the other four subregions is described by one of the above four distributed MINC assemblies, which are characterized by 50% thermal equilibrium time-scales ranging from nine hours to one year. Thus, in all there is a grand total of $[27 \times 27 \times 27 \times (1+4 \times 15)] = 1,200,663$ individual independently-varying temperature values in the discretized representation of the Case 6 temperature distribution, each of which is a function of time.

3.3.1.6. Electrokinetic effects: As noted above, Case 6 involves the calculation of electrokinetic self-potential, and some of the pertinent problem specifications have already been discussed above in Section 3.3.1.1 with the introduction of the electrokinetic grid using file *ingridek.fil* (Section 3.4.6.9) and the specification of nine deep wells, each of which has two isolated sections of conductive metallic casing, by input file *inwelgeo.fil* (Section 3.4.6.24).

In addition, input file *inelpram.fil* (Section 3.4.6.5) specifies five other pertinent parameters which, for Case 6, are taken to be uniform throughout the computing volume. These are two parameters required by the Ishido-Mizutani (1981) mathematical representation for computing the flow-induced electrical drag current density:

average flow path tortuosity: 1.5 $\delta(pH)$ across the double layer: 4.0

and three parameters required to calculate the position- and time-dependent distribution of electrical conductivity:

surface electrical conductivity: 0.001 S/m dry rock electrical conductivity: 0.009 S/m rock/fluid conductivity mixing rule: Budiansky

The electrical conductivity of the liquid brine depends mainly on temperature and fluid salinity, and is calculated automatically as a function of position and time by HeatEx

internally. For Case 6, the net overall electrical conductivity of the 1 km³ study volume is initially about 0.0112 S/m and little change takes place throughout with time, except near the feedpoint of injection well 5 where the injection of (initially) pure water and (later) water of reduced salinity causes local electrical conductivity values to drop as low as 0.0094 S/m. As will be seen below, however, the substantial temporal changes in computed subsurface electrical potential exhibited by the Case 6 results arise mainly from temporal changes in the subsurface fluid flow pattern, as contrasted to changes in intrinsic electrical conductivity.

3.3.1.7. Fracture system dynamics: For Case 6, in addition to ordinary scalar intergranular rock permeability (equal to only one millidarcy for this case – see above), the dynamic fracture model is used to represent fractures acting as fluid conduits, with directional properties determined by fracture orientations and permeabilities which depend upon instantaneous fracture aperture. The result is a full six-component tensor representation for rock permeability, with individual tensor components being functions of position and time.

The first important parameter for the fracture dynamics representation in HeatEx is the spatial distribution of regional earth stress. This is specified using input file *inrgstrs.fil* (Section 3.4.6.16). In Case 6, a simple representation is employed, in which the six components of the stress field depend only upon vertical elevation relative to sea level. In terms of "earth" coordinates (E, N, A; *Eastward, Northward, Altitude*), these prescribed stresses are:

```
Normal stresses:  \begin{aligned} \varepsilon_{ee} &= \varepsilon_{nn} = 80 \text{ MPa} \times \eta \\ \varepsilon_{aa} &= 120 \text{ MPa} \times \eta \end{aligned}  Shear stresses:  \begin{aligned} \varepsilon_{en} &= \varepsilon_{na} = \varepsilon_{ea} = 0 \\ \text{where:} & \eta &= (3000 - A) \times 10^{-4} \text{ and } A = \text{elevation (m ASL)}. \end{aligned}
```

In other words, the regional stresses are assumed to be as follows at the upper surface, midplane, and lower surface of the thermohydraulic grid:

```
-1500 m ASL: \varepsilon_{ee} = \varepsilon_{nn} = 36 MPa, \varepsilon_{aa} = 54 MPa, \varepsilon_{en} = \varepsilon_{na} = \varepsilon_{ea} = 0
-2000 m ASL: \varepsilon_{ee} = \varepsilon_{nn} = 40 MPa, \varepsilon_{aa} = 60 MPa, \varepsilon_{en} = \varepsilon_{na} = \varepsilon_{ea} = 0
-2500 m ASL: \varepsilon_{ee} = \varepsilon_{nn} = 44 MPa, \varepsilon_{aa} = 66 MPa, \varepsilon_{en} = \varepsilon_{na} = \varepsilon_{ea} = 0
```

Properties of the fracture patches themselves are provided in input files *infpdata.fil* and *infpprms.fil* (Sections 3.4.6.7 and 3.4.6.8). For the present Case 6, many of the parameters specified for the fracture patch model are the same for all of the patches. These include:

Young's modulus:	60 GPa
Shear modulus:	24 GPa
Basic friction angle:	40°
Shear dilation angle:	3°
90% closure stress:	30 GPa
Cohesion:	0 Pa
Darcian aperture limit:	800 μ

Other parameters generally differ from one patch to the next, including (1) the location of the center of the patch, (2) the orientation (azimuth and dip angle) of the fracture patch plane, (3) the radius of the patch, and (4) the zero-stress fracture aperture value. Input files *infpdata.fil* and *infpprms.fil* designate three different "classes" of fracture patches in Case 6. Four "Class 1" patches, 24 "Class 2" patches and 1712 "Class 3" patches are described (1740 slip patches

altogether). The "Class 1" patches are the largest – all four of them are 60 meters in radius (120 m diameter) and are characterized by a zero-stress aperture of 3.18×10^{-4} meters (318 μ). "Class 2" patches are only one-half this size (radius = 30 m, zero-stress aperture = 159 μ) and the far more numerous "Class 3" patches are smaller by yet another factor of two (radius = 15 m, zero-stress aperture = 79.5 μ). Note that the actual initial apertures of these fractures will ordinarily be substantially smaller than the "zero-stress" values – for Case 6, the initial aperture values for the Class 1, Class 2 and Class 3 fractures are about 45 μ , 23 μ and 20 μ respectively (the value for any particular patch will depend on the local initial fluid pressure and regional stresses, and the fracture orientation relative to the stress field).

All of the four Class 1 fracture patches are co-located with their centers at 13,000 m East, 16,000 m North and -2000 m ASL (the geometric center of the grid, and also the location of the feedpoint for injection/stimulation Well 5). Thus, unlike the others, these four large fractures receive direct pressurization from the well. All four of them are also characterized by a dip angle of 45°. The azimuth angles (relative to true north) of patch numbers 1, 2, 3 and 4 are 45°, 135°, 225° and 315° respectively. Thus, these four patches form a symmetrical "cluster" at the geometrical center of the study volume.

The smaller Class 2 patches are also arranged in four-patch "clusters" with dip angle 45° and symmetrical azimuth angles of 0°, 90°, 180° and 270° relative to true north (note that the Class 2 patches are rotated 45° around the vertical axis relative to the Class 1 patches). There are six such Class 2 "clusters", for a total of 24 patches. The centers of these six "clusters" are equidistant from the Well 5 injection point (distance = 84.85 meters), and are located symmetrically surrounding the injection point as follows:

13000 m E	16000 m N	–1915.15 m ASL
12940 m E	15940 m N	-2000.00 m ASL
13060 m E	15940 m N	–2000.00 m ASL
12940 m E	16060 m N	–2000.00 m ASL
13060 m E	16060 m N	-2000.00 m ASL
13000 m E	16000 m N	-2084.85 m ASL

The 1712 still smaller Class 3 patches are arranged in 856 co-centered "pairs". All are oriented vertically, with one member of each pair having azimuth angle 45° and the other 135° relative to true north. The pair-center locations are arranged in a three-dimensional checkerboard pattern, with vertical elevations given by $(40 \times K - 2000)$ meters ASL where K is any integer (of either sign), and staggered horizontal spacing in each K-plane of 80 meters. All fracture patches specified (of any of the three classes) are centered at a point which lies within 300 meters of the injection point at 13,000 m E, 16,000 m N and -2000 m ASL. The resulting spatial distribution of fracture patches is illustrated in Figures 3.21 (top view) and 3.22 (side view) relative to the thermohydraulic grid block boundaries and the various production and injection well locations.

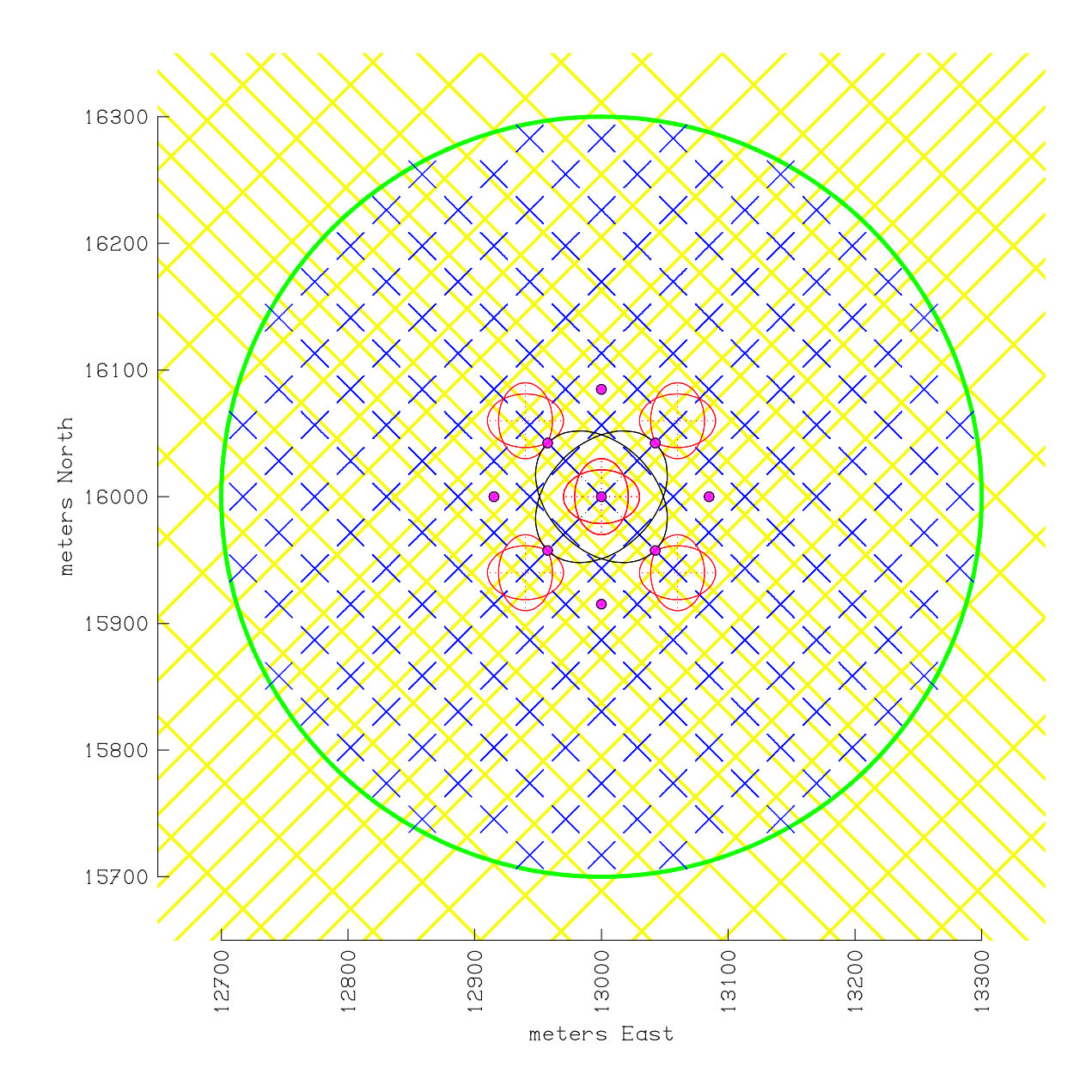


Figure 3.21. Case 6 – spatial distribution of fracture patches viewed from above. *Yellow:* computational grid block boundaries. *Green:* outer boundary of 600 m diameter spherical region containing fracture patches. *Magenta:* production and injection wells. *Black:* class 1 fracture patches (radius 60 m; azimuth 45°, 135°, 225° and 315°; dip 45°; four patches total). *Red:* class 2 fracture patches (radius 30 m; azimuth 0°, 90°, 180° and 270°; dip 45°; 24 patches total). *Cyan:* class 3 fracture patches (radius 15 m; azimuth 45° and 135°; vertical orientation; 1712 patches total). See input files *infpdata.fil* and *infpprms.fil* (Sections 3.4.6.7 and 3.4.6.8).

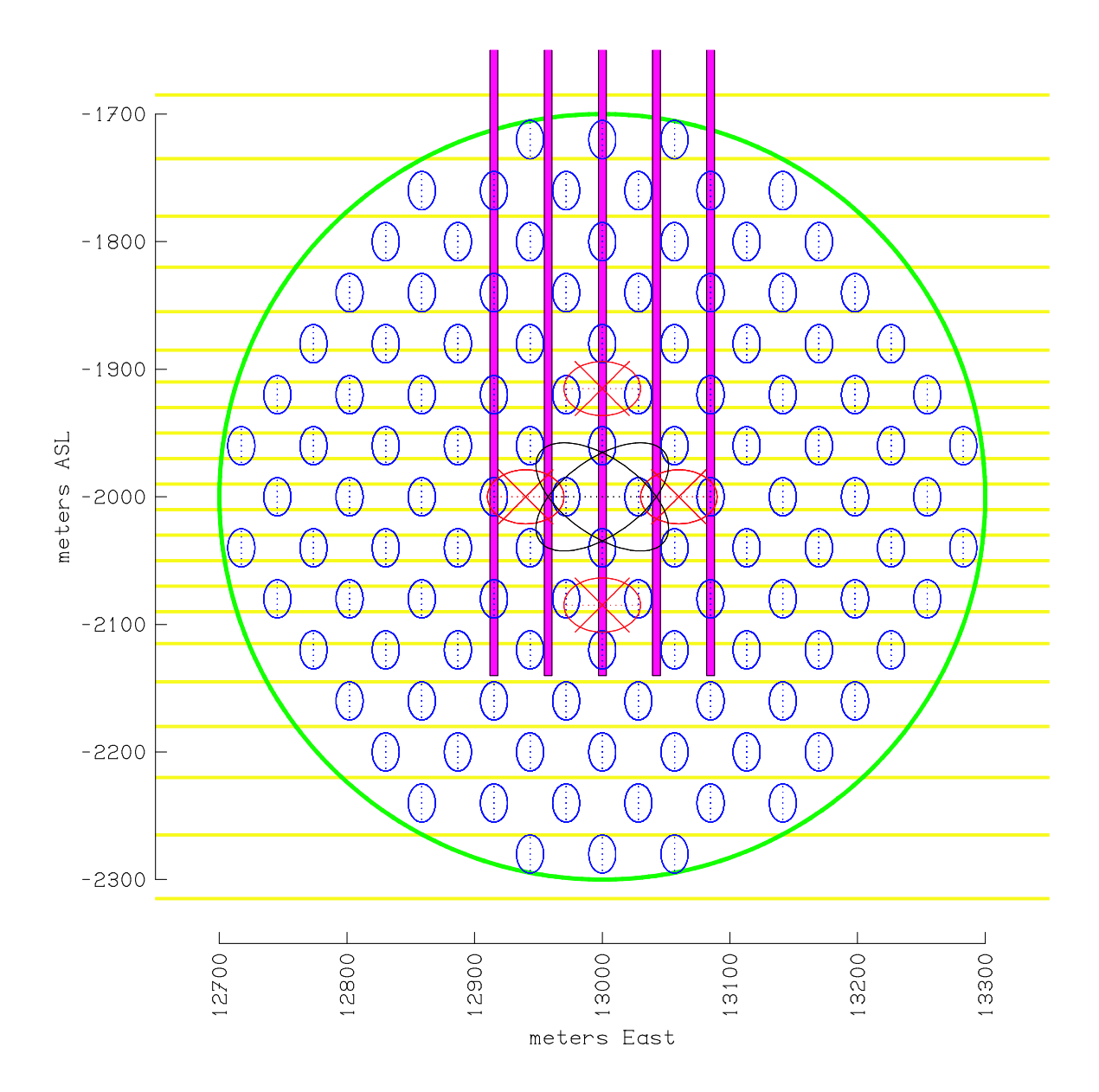


Figure 3.22. Case 6 – spatial distribution of fracture patches viewed from south. *Yellow:* computational layer boundaries. *Green:* outer boundary of 600 m diameter spherical region containing fracture patches. *Magenta:* production and injection wells. *Black:* class 1 fracture patches (radius 60 m; azimuth 45°, 135°, 225° and 315°; dip 45°; four patches total). *Red:* class 2 fracture patches (radius 30 m; azimuth 0°, 90°, 180° and 270°; dip 45°; 24 patches total). *Cyan:* class 3 fracture patches (radius 15 m; azimuth 45° and 135°; vertical orientation; 1712 patches total). See input files *infpdata.fil* and *infpprms.fil* (Sections 3.4.6.7 and 3.4.6.8).

3.3.2. Computed Results for Case 6

Case 6 was carried out to a point representing t = 400 days using a maximum time-step size of two days and a total of 399 computational time steps (average $\Delta t = \sim$ one day). Number of time-steps and computer-time requirements were as follows for the three main temporal phases of the calculation:

10-day "stimulation" phase: 69 steps 23.1% of computer time 30-day "soak" phase 135 steps 31.8% of computer time 360-day "production" phase: 195 steps 45.1% of computer time

Unsurprisingly, the "stimulation" part of the problem consumed a substantial part of the resources relative to the actual duration of the interval involved. At very early times, pressures near the injection well rise sharply and the four large "Class 1" fracture patches begin to deform significantly. Effective permeabilities (limited in much of the grid volume to the 1 millidarcy intergranular value and even centrally to less than three millidarcies because of the small initial fracture apertures) increase rapidly near the injection well. As a result, the disturbed region grows more and more rapidly and the region surrounding the injection well experiences substantially elevated pressures, causing further fracture deformation and permeability propagation along the fracture surfaces.

3.3.2.1. Evolution of the fracture system: Fracture deformation and aperture increase comes about by three mechanisms, as discussed elsewhere: "compliance" (elastic response to increase in pore pressure), "shearing", and "jacking". Aperture increases caused by pure compliance or pure jacking are generally reversible, but shearing deformation will produce irreversible and permanent increases in fracture aperture and induced permeability. Thus, for effective reservoir stimulation, shearing deformation is desirable. In Case 6, a substantial amount of shearing deformation is predicted by the calculation in the neighborhood of the injection well's feedpoint.

Figure 3.23 illustrates several salient features of the calculated behavior during the "stimulation" phase. Immediately upon the onset of high-pressure injection, the datum level pressure in the injection well (Well 5) rises to the limiting value (50 MPa) and the injection rate begins to increase above zero. The rise in pressure tends to inflate the four large Class 1 fractures intersected by the well, their fluid transmissivity rises, and the flow rate from the well into the reservoir increases. Within less than eight hours, the injection rate reaches the limiting value (100 kg/s, presumably arising from pump capacity) and the injection pressure drops somewhat, eventually stabilizing near 44 MPa.

As a consequence, the four large Class 1 fractures intersected by the injection well all experience shearing deformation prior to t = 3 hours. As the pressure disturbances propagate outward from the injection well and from the four large connected fractures, other fractures begin to be affected. By t = 8 hours, some of the closest Class 3 fracture patches have also experienced shearing deformation, and as time goes on more and more of them begin to shear as well. Because of their greater distance, none of the Class 2 fracture patches experience shearing deformation until t = 1.5 days, but within one day thereafter all 24 of them have failed in shear. Shearing failure continues to propagate outward among the Class 3 patch population,

with the final shear failure event taking place at t = 8.75 days. No further "first shear failure" events occur thereafter, even after 400 days. Shearing failure is confined to fracture patches whose centers are located within 90 meters of the injection point, but *all* patches so located eventually fail in shear.

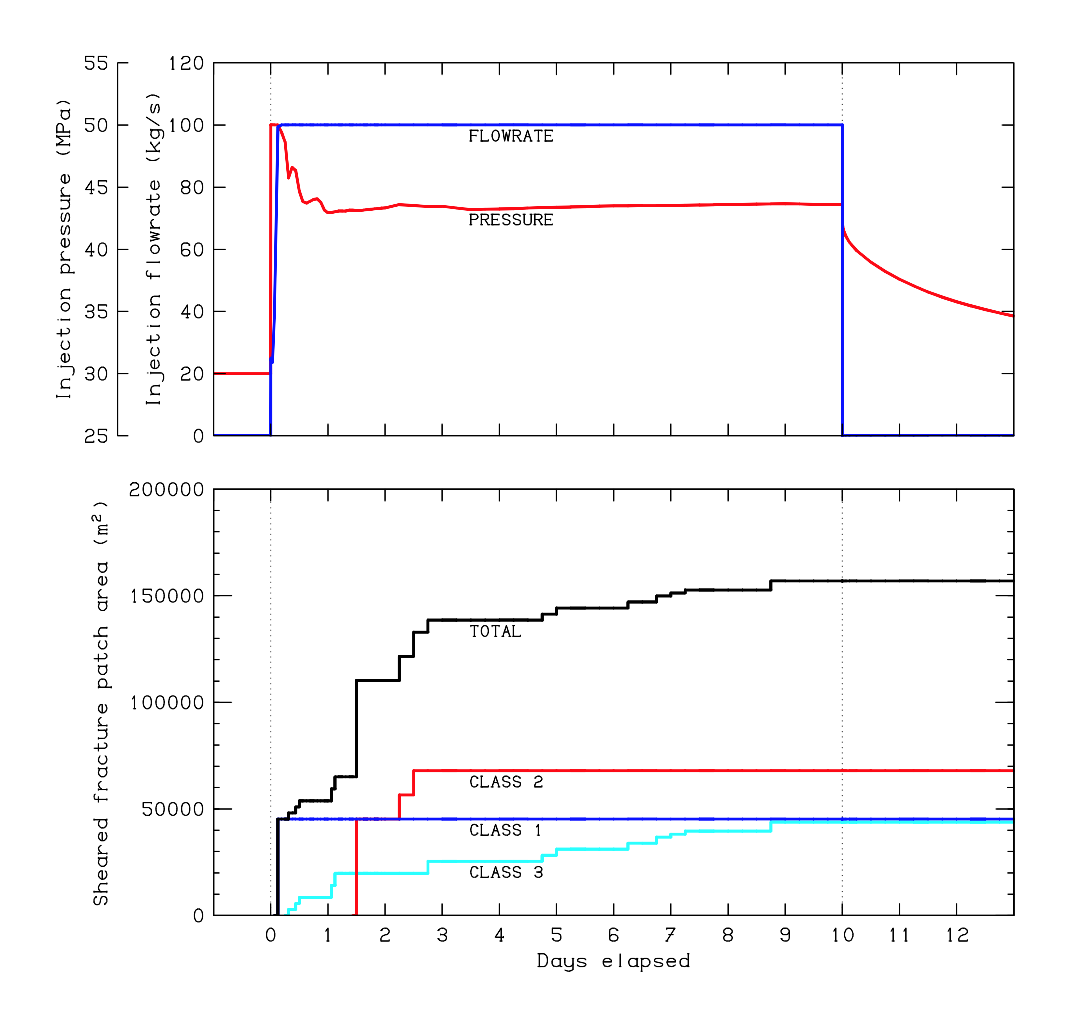


Figure 3.23. Case 6 – effectiveness of ten days of stimulation operations in causing irreversible fracture shearing deformation. *Upper:* injection well flow rate (maximum 100 kg/s) and datum level pressure (maximum 50 MPa). *Lower:* time-history of area of fracture patches that have experienced shearing deformation. *Notes:* although amounts of shearing deformation vary with time throughout, no new fracture surface area first experiences shearing onset after t = 8.75 days. All four class 1 patches shear within the first three hours. Class 2 patches first start shearing at 1.5 days and all 24 have sheared by 2.5 days. Some class 3 patches first shear in less than 8 hours, and 62 of them eventually shear by 8.75 days, representing 3.6% of the total. All of the patches that shear are centered within 90 meters of the injection point. No additional patches first experience shearing deformation after t = 8.75 days. Individual patch surface areas: Class 1, 11310 m²; Class 2, 2827 m²; Class 3, 707 m².

3.3.2.2. Well response: To understand the detailed computed results from Case 6, it is helpful to be aware of the degree of connectivity between the various production and injection wells and the major fracture structures presumed to be present in the subsurface. Obviously, the fact that injection well 5 is directly connected to all four of the large-diameter and large-aperture Class 1 fracture patches plays a major role in the early development of stimulated permeability. Furthermore, the same large Class 1 fractures also intersect the productive intervals of four of the production wells: fracture patch numbers 1 and 2 intersect production wells 2 and 8, and fracture patch numbers 3 and 4 intersect production wells 4 and 6 (as well as injection well 5, of course).

Therefore, the Class 1 fractures provide high-speed conduits connecting the injection well with these four production wells ("even" wells 2, 4, 6 and 8). Each of these same four production wells also intersects one of the Class 2 fracture patch clusters, as well as five individual Class 3 fracture patches, but none of these Class 2 or Class 3 fracture patches is connected directly to any other well. By contrast, none of the "odd" production wells (wells 1, 3, 7 or 9) directly intersects any of the fracture patches. As a result, it is to be expected that the performance of the "even" production wells (wells 2, 4, 6 and 8) will be significantly different from that of the "odd" wells (1, 3, 7 and 9).

It should also be noted, as a careful review of the problem specifications described in Section 3.3.1 reveals, that the Case 6 problem possesses fourfold symmetry. As a consequence, it is to be be expected that the predicted behavior of all four "even" production wells (wells 2, 4, 6 and 8) will be identical, and that the performance of the four "odd" production wells will also be the same (but presumably different from that of the "even" wells). Case 6 was deliberately designed with this fourfold symmetry, to provide a check on computational accuracy and consistency. As shown below, this expectation of the problem symmetry being reflected in the performance predictions is realized in the computed Case 6 results.

To begin with, consider the first 60 days of this forecast, which encompasses the "stimulation" phase (t = 0 to 10 days), the "soak" shut-in phase (t = 10 to 40 days) and the first part of the "production" phase ($t \ge 40$ days). Figure 3.24 (upper frame) shows the 60-day time-history of datum level pressure for all nine wells (that is, the pressure within the well at -2000 m ASL elevation). Calculated pressure within the injection well is shown in red; results for the "odd" production wells are shown in cyan, and those for the "even" wells in dark blue.

As noted previously (see Figure 3.23), the injection well sustains its limiting pressure value (50 MPa) briefly at the outset, but subsequently the 100 kg/s flow rate limit imposed by pumping capacity comes into play and the injection pressure drops back to a value which fluctuates slightly around 44 MPa until the end of the "stimulation" period at t = 10 days. Upon subsequent well shut-in, the downhole pressure in the injection well falls back toward the initial value in the reservoir at that level (30 MPa). Then, when operations begin again at t = 40 days, the injection well pressure immediately rises to its new (lower) limiting value of 40 MPa and remains at that value thereafter.

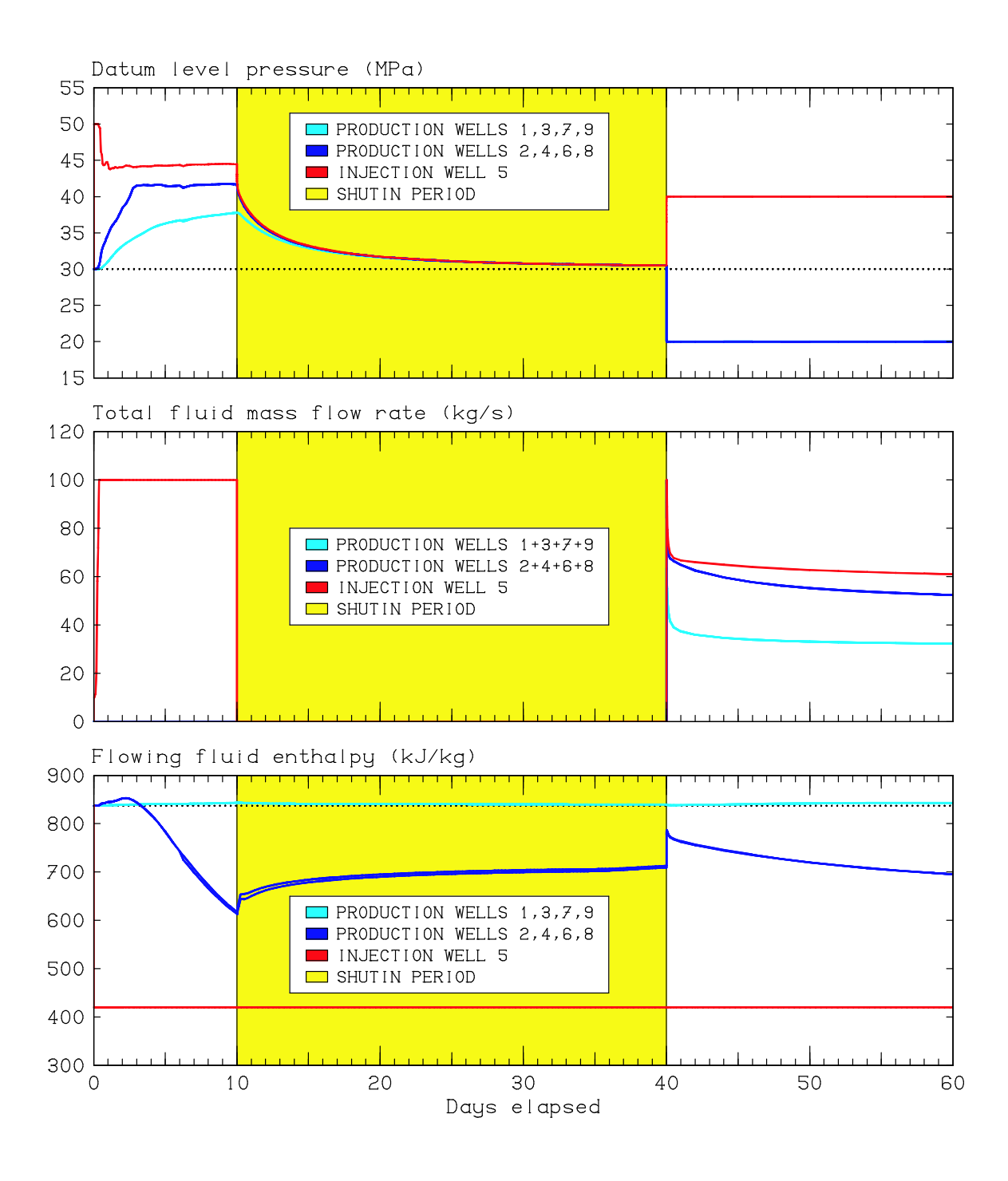


Figure 3.24. Case 6 – histories of well performance during first 60 days. *Upper:* datum level pressure. *Middle:* total mass flow rates of well groups. *Lower:* flowing enthalpies. *Yellow:* 30-day well shutin period. *Red:* injection well (#5). *Blue:* "even" production wells 2, 4, 6 and 8 (60 meters from injection well). *Cyan:* "odd" production wells 1, 3, 7 and 9 (85 meters from injection well).

The eight remaining pressure-time traces for the eight production wells in the upper frame of Figure 3.24 are seen to collapse into only two lines, with the "even" production wells (2, 4, 6, 8) in dark blue and the "odd" wells (1, 3, 7, 9) in cyan. During the "stimulation" phase, the shut-in "even" well pressures, with their enhanced fracture coupling to the injection well, exhibit a more rapid rise and within a few days stabilize at a pressure level that is then maintained only a few MPa lower than that in the injection well itself. The relatively decoupled "odd" wells also exhibit substantial pressure rise during the stimulation period, but less pronounced response than the "even" wells. After shutin at t = 10 days, within a few days all nine pressure traces collapse into a single time-history which asymptotically approaches the initial reservoir pressure at -2000 m ASL elevation. At t = 40 days the "production" phase begins, and all eight production wells start pumping and immediately attain their assigned limiting datum level pressure value (20 MPa), withdrawing fluid from the reservoir at the maximum possible rate subject to the pressure constraint.

The middle frame of Figure 3.24 displays the 60-day flow rate histories (injection or production rate as appropriate) for various groups of wells. The injection rate for Well 5 is shown in red; the total production rate of the four "even" production wells (2, 4, 6 and 8) is shown in blue, and the total for the "odd" producers (1, 3, 7 and 9) in cyan. In this graph, total production rates for these two groups are shown – the individual production rates for the various production wells in each group are each one-fourth of the total rate shown. Thus, at t =60 days for example, the total production for the four "even" wells is 52.37 kg/s, but the rate for each well individually is only 13.09 kg/s. The corresponding 60-day figures for the "odd" wells are 32.24 kg/s (total) and 8.06 kg/s (per well). The only well flowing prior to t = 40 days is injection well 5, which injects at a constant rate of 100 kg/s from t = -8 hours to t = 10 days, and is then shut in. When the "production" phase begins at t = 40 days, as noted above the injection well becomes pressure limited almost immediately. The injection rate remains at 100 kg/s for less than twelve minutes and then plunges to below 70 kg/s within six hours, reaches 66 kg/s two days later and is only 61 kg/s by t = 60 days. The various production wells first start operating at t = 40 days and become pressure-limited within three minutes, thereafter discharging at ever-decreasing rates as time goes on. It is, however, noteworthy that the total fluid production rate from all eight production wells combined significantly exceeds the injection rate into well 5. Thus, the excess pressurization remaining from the earlier "stimulation" phase is gradually being relieved over time

The lower frame in Figure 3.24 shows the time-histories of downhole flowing enthalpy in each of the nine wells. For injection well 5, this value is constant at 420 kJ/kg, as specified in the Case 6 problem prescription. The "odd" production well flowing enthalpy histories (wells 1, 3, 7 and 9) are all the same and only rise a tiny amount from the initial reservoir value at that elevation (837 kJ/kg) during the first 60 days. By contrast, the flowing enthalpies in the "even" production wells (2, 4, 6, 8) vary substantially over time. These wells are shut in up to t = 40 days, but during the early "stimulation" phase the pressure in these wells rises substantially at first, driving the enthalpy upward somewhat from the effects of compressive work. Then, cold water begins to flow into these wells from the horizons where the large Class 1 fracture patches intersect them. By t = 10 days this inflow amounts to 3.3 kg/s per well (with a corresponding outflow at horizons both above and below the fracture/well intersection level), and the enthalpy has dropped to 617 kJ/kg (a decline of 220 kJ/kg from the initial value, or a temperature drop of over 50°C). During the subsequent "soak" shut-in phase the enthalpy in

these wells recovers somewhat, and when production begins at t = 40 days, surrounding hotter fluid begins to be drawn in as well, but the flowing enthalpy histories for these wells for t > 40 days exhibit significant temporal decline. These "even" production wells are clearly suffering from "thermal short-circuiting" due to their fracture connections with the nearby injection well.

3.3.2.3. Diagnostic measurements. In a similar manner, Figure 3.25 depicts the computed Case 6 60-day time histories of a few quantities that often prove useful for diagnostic purposes in reservoir engineering analyses. The top frame shows the time-histories of downhole flowing salinity in all nine wells.

To review, the initial salinity throughout the reservoir is taken to be 4% by mass, and Well 5 injects 100 kg/s of pure water (zero salinity) for the first ten days (the "stimulation" phase). Next, the well is shut in for 30 days (the "soak" phase). Then, at t = 40 days, injection resumes but this time using injected water with 2% salinity by mass (half that of the original *in-situ* reservoir water), and the other eight wells begin to withdraw fluid from the reservoir ("production" phase) at the same time. The Well 5 salinity history is shown in red (zero prior to t = 40 days, 2% thereafter), the closely-coupled "even" production well histories (wells 2, 4, 6 and 8) are displayed in dark blue, and the "odd" production-well histories are cyan.

The influence of the injection well upon the "even" production wells is again very pronounced. Even with all production wells shut in during the "stimulation" phase, the fluid salinity within these wells has been reduced nearly to zero after only five days of injection by the inflow of fresh water through the Class 1 fractures and compensating outflow of saline brine. During the "soak" period, the salinity of the fluid in the "even" wells recovers only slightly, but then when injection of 2% salinity water begins at t = 40 days and production from these wells begins simultaneously, the well salinities swiftly rise to follow the injection well salinity trend.

The "odd" production wells exhibit much less direct influence from the injection well, although even in these wells the salinity declines from 4% to 3.73% by the end of the "stimulation" phase. After the "production" phase begins at t = 40 days, the "odd" production well salinities continue their decline in response to reduced-salinity fluid injection.

Similar influences are evident from the tracer records (middle frame of Figure 3.25). Tracer is initially absent from the system, and the only tracer introduced is at a one part-per-million concentration in the pure water injected into Well 5 during the ten-day "stimulation" phase. No additional tracer is added after t = 10 days. The Well 5 (injection) history is just 1 ppm for $t \le 40$ days and zero afterwards.

As these results show, the tracer contents in the closely-coupled "even" production wells follow the injection-well trend faithfully. There is a slight influence of injected tracer on the "odd" production wells also, but the response is much slower and the signal is less pronounced.

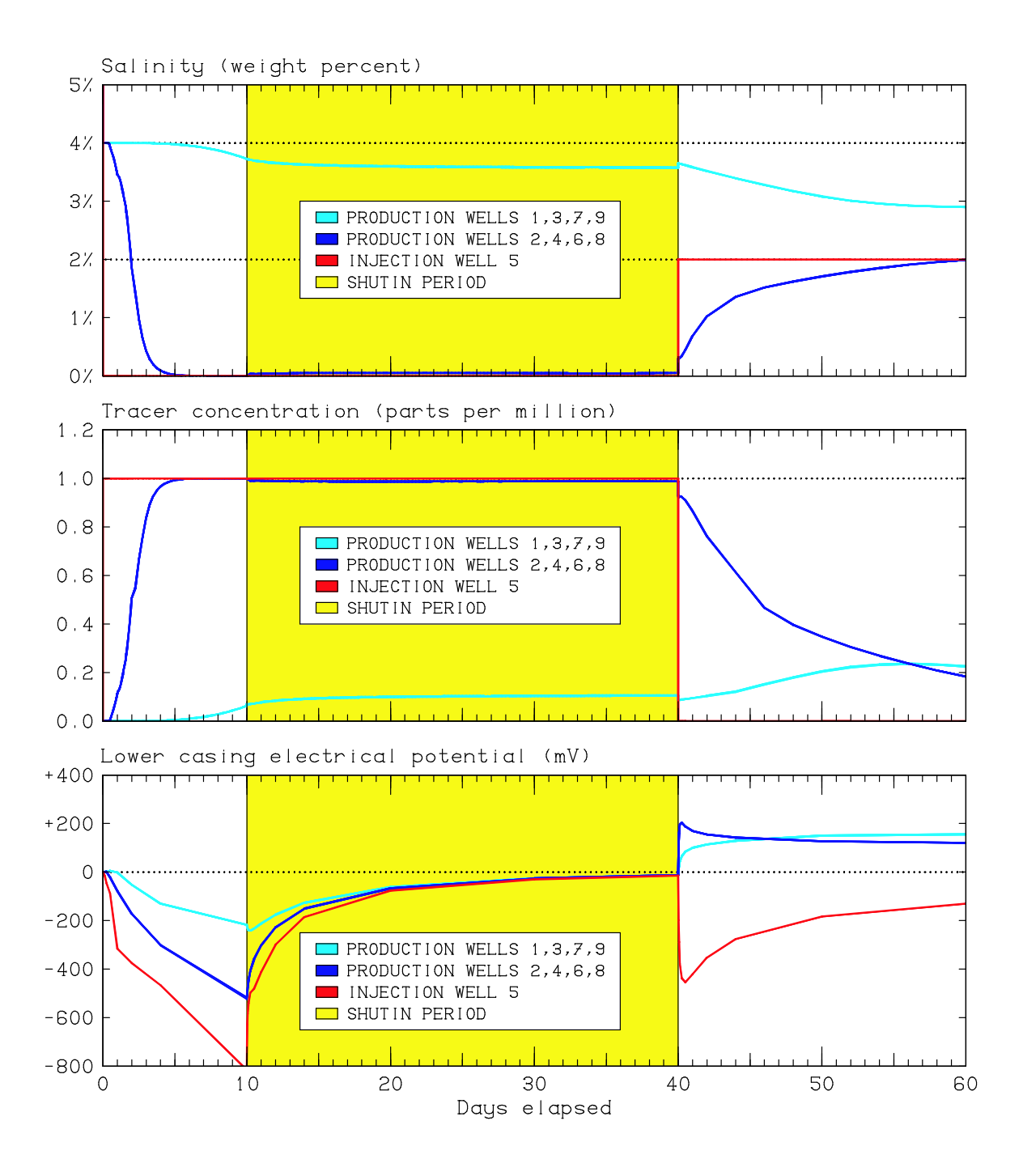


Figure 3.25. Case 6 – well diagnostic quantities during first 60 days. *Upper:* datum level salinities. *Middle:* tracer concentrations. *Lower:* induced electrokinetic potential on deep casing pipe. *Yellow:* 30-day well shutin period. *Red:* injection well (#5). *Blue:* "even" production wells 2, 4, 6 and 8 (60 meters from injection well). *Cyan:* "odd" production wells 1, 3, 7 and 9 (85 meters from injection well).

For a number of years, it has been recognized that downhole pressurization operations intended to stimulate rock fracturing have the potential to cause electrical transient signals ("SP" or "spontaneous potential") to propagate through the subsurface due to electrokinetic coupling which, if detected and characterized, could provide useful information about the characteristics of the permeability distribution thereby induced (*Pritchett and Ishido*, 2005; *Pritchett*, 2008; *Pritchett and Ishido*, 2010). In view of the promise of this possibility, HeatEx was designed to be capable of simulating effects of this general type, along with other useful diagnostic techniques such as pressure transient analysis, tracer studies, geochemical monitoring, wellhead production monitoring, and microseismic surveys.

Ordinarily, the approach proposed for this kind of survey is to drill special-purpose observation wells to host downhole electrodes for time-dependent subsurface SP determinations, using nonmetallic casing materials at and near the formation depths of interest to avoid interfering with the spatial distributions of electrical current and potential, and to perform continuous electrical potential measurements before, during, and after hydrofracturing operations in nearby injection wells. Another approach (considered for this Case 6 hypothetical study) is to use an electrically isolated portion of the well casing itself as an electrode for observation of the electrical transients induced by fracture pressurization.

As noted earlier (see Figure 3.20 and associated discussion), for the present illustrative Case 6 it has been assumed that the deepest 140 meters of each well casing (below the level of the principal feedzone of the injection well) is conductively continuous and electrically isolated from the upper part of the casing. If so, this deep portion of the casing could itself be used as an electrode for characterization of the electrical transient signals that are expected to arise from nearby high-pressure injection operations.

The lower portion of Figure 3.25 illustrates the electrical potential history expected to be measurable using these nine large "electrodes" for Case 6 during the first 60 days. As before, the signals obtainable from the "even" production wells (2, 4, 6, 8) are indistinguishable from each other, as are those from the "odd" wells (1, 3, 7 and 9) for reasons of symmetry. The signal obtained from the injection well itself is different from the others.

During the 10-day "stimulation" phase, negative potential signals of several hundred millivolts amplitude appear on all nine casing sections, which fall well into the amplitude range suitable for existing instrumentation capabilities. Unsurprisingly, the deep casing potential on the injection well itself has the largest magnitude and those on the shut-in "odd" production well casings are the weakest. These negative signals arise from the presence of a strong nearby fluid source (*i.e.* the injection well's feedpoint), which is of course closest to the injection well casing itself.

After shut-in at t = 10 days, the amplitudes of these signals all decay. Then after t = 40 days, the injection well is restarted, and furthermore all eight production wells begin to withdraw fluid from the reservoir. This time, the production well casings all exhibit SP signals of positive polarity; there is now a fluid sink nearby instead of just a source. The signal on the injection well's casing is again negative in polarity. Amplitudes are somewhat lower because of the cancellation effect between the local sources and sinks of fluid flow (and of electrokinetic drag current), but subsurface SP signals in the field may be routinely

characterized at levels down to 10 mV or less using modern measurement techniques, so these calculated forecasts indicate that this kind of measurement program should be practical under circumstances similar to those hypothesized here for Case 6.

3.3.2.4. Late-time observations: Finally, Figures 3.26 and 3.27 display similar information to that shown in Figures 3.24 and 3.25, but with the time-scale extended out to t = 400 days (the end of the Case 6 calculation). Generally speaking, the late-time signals are fairly featureless compared to the highly transient effects observed at early times. Figure 3.26 (upper frame) shows that all nine wells simply continue to operate at their limiting datum level pressure values (40 MPa for the injection well, 20 MPa for the surrounding production wells). As a result (Figure 3.26, middle frame), the flow rates continue to decline smoothly at late times. Computed well flow rate values are:

Elapsed Time	Well 5 Injection	Wells 2,4,6,8 Production	Wells 1,3,7,9 Production
50 days	62.76 kg/s	13.81 kg/s	8.28 kg/s
100 days	58.08 kg/s	12.23 kg/s	7.77 kg/s
150 days	56.55 kg/s	11.73 kg/s	7.57 kg/s
200 days	55.66 kg/s	11.37 kg/s	7.42 kg/s
250 days	55.08 kg/s	11.09 kg/s	7.25 kg/s
300 days	54.66 kg/s	10.87 kg/s	7.07 kg/s
350 days	54.35 kg/s	10.68 kg/s	6.89 kg/s
400 days	54.12 kg/s	10.52 kg/s	6.72 kg/s

One item of obvious practical importance and concern, however, is the long-term enthalpy trends seen in the production wells (Figure 3.26, lower frame). The "even" production wells continue to exhibit declining discharge enthalpy, and even the "odd" wells start to decline perceptibly after the first few months. Even the best-performing production wells experience a discharge enthalpy decline of about 60 kJ/kg by t = 400 days as compared to the initial values, and their discharge enthalpies are dropping at a rate of 0.3 kJ/kg per day by that time. This is equivalent to a cooling rate in excess of 2°C per month. And of course, the closely-coupled "even" production well discharge enthalpies have declined to only 538 kJ/kg (equivalent to brine temperature less than 125°C) by this time – already too low to be useful for significant electricity generation. We conclude that Case 6, while an interesting mathematical exercise, probably does not represent an electrical power production possibility of practical commercial interest.

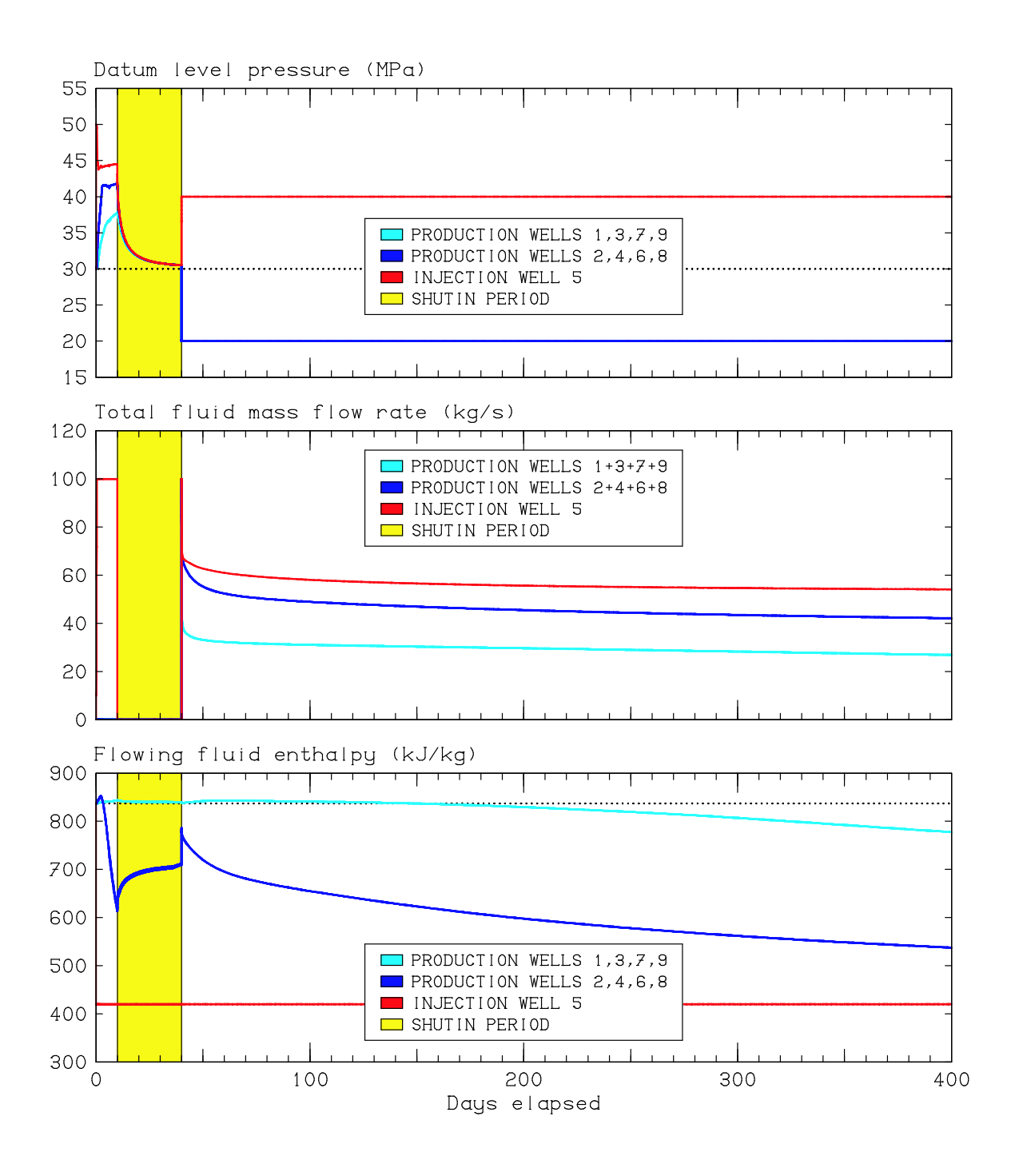


Figure 3.26. Case 6 – histories of well performance. *Upper:* datum level pressure. *Middle:* total mass flow rates of well groups. *Lower:* flowing enthalpies. *Yellow:* 30-day well shutin period. *Red:* injection well (#5). *Blue:* "even" production wells 2, 4, 6 and 8 (60 meters from injection well). *Cyan:* "odd" production wells 1, 3, 7 and 9 (85 meters from injection well).

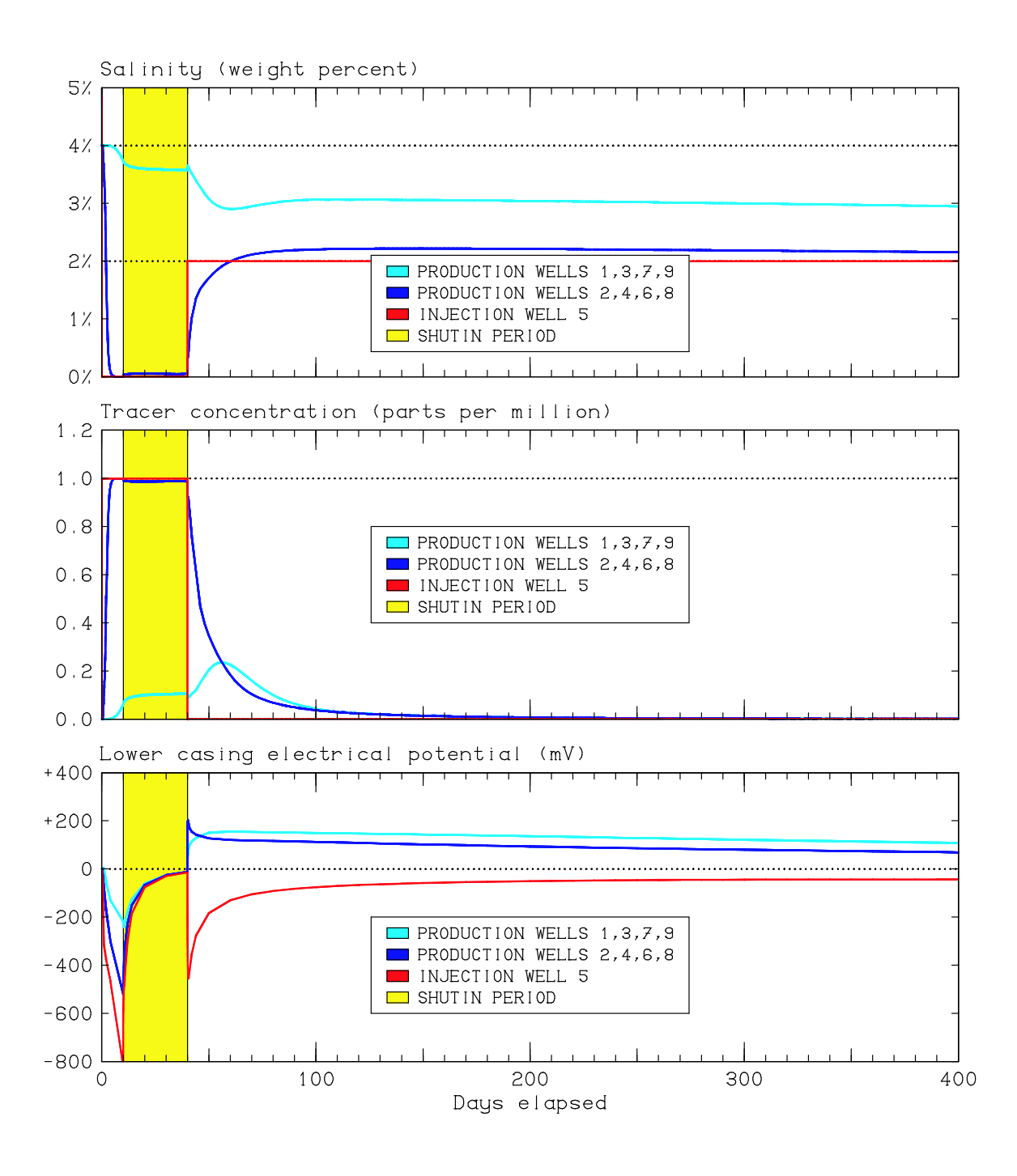


Figure 3.27. Case 6 – well diagnostic quantities. *Upper:* datum level salinities. *Middle:* tracer concentrations. *Lower:* induced electrokinetic potential on deep casing pipe. *Yellow:* 30-day well shutin period. *Red:* injection well (#5). *Blue:* "even" production wells 2, 4, 6 and 8 (60 meters from injection well). *Cyan:* "odd" production wells 1, 3, 7 and 9 (85 meters from injection well).

3.4. INPUT DATA SETS FOR ILLUSTRATIVE CASES

In this section, the input files used to obtain the numerical results discussed in the previous sections are provided in hardcopy form. Some of these files are quite large, and have consequently been abridged for purposes of this report. The complete files are available separately in electronic form.

3.4.1. Case 1 Input Data Files

To run illustrative Case 1, the HeatEx simulator must be provided with fourteen ASCII input data files:

```
incondrk.fil ininsalt.fil inoutfrq.fil insnsors.fil intopogr.fil ingridth.fil inintemp.fil inrkigpr.fil insorcms.fil intrchem.fil ininpres.fil inintrcr.fil inrkvolp.fil intimscl.fil
```

The contents of these files are as follows (in alphabetical order):

```
3.4.1.1. Case 1 input file "incondrk.fil":
```

```
# file incondrk.fil
3. 0
# end of file
```

3.4.1.2. Case 1 input file "ingridth.fil":

3.4.1.3. Case 1 input file "ininpres.fil":

```
# file ininpres.fil
100.e+05
# end of file
```

```
3.4.1.4. Case 1 input file "ininsaltn.fil":
# file ininsalt.fil
# end of file
3.4.1.5. Case 1 input file "inintemp.fil":
# file inintemp.fil
100
# end of file
3.4.1.6. Case 1 input file "inintrer.fil":
# file inintrcr.fil
0
# end of file
3.4.1.7. Case 1 input file "inoutfrq.fil":
# file inoutfrq.fil
# P, T, S snapshots and well summaries
days
100
end
# tracer snapshots
days
100
end
# permeability snapshots
end
# fracture patch apertures
end
# electrical snapshots
end
# restart dumps
end
# end of file
3.4.1.8. Case 1 input file "inrkigpr.fil":
# file inrkigpr.fil
1000.e-15
# end of file
```

```
3.4.1.9. Case 1 input file "inrkvolp.fil":
# file inrkvolp.fil
2800 1000 0.3 0 0 0
# end of file
3.4.1.10. Case 1 input file "insnsors.fil":
# file insnsors.fil
-400 0 -2000
-300 0 -2000
-200 0 -2000
-100 0 -2000
   0 0 -2000
+100 0 -2000
+200 0 -2000
+300 0 -2000
+400 0 -2000
# end of file
3.4.1.11. Case 1 input file "insorcms.fil":
# file insorcms.fil
1 1 1 1 1 1
1.0e-03 0
                        220.e+03 0 1.e-06
100 100 1 1 1 1
10. -1.e-06 0 0 0 0 0
# end of file
3.4.1.12. Case 1 input file "intimscl.fil":
# file intimscl.fil
 6000
           # max steps
           # units for max time
 days
           # max time
 1200
           # units for max step size
           # max step size
# end of file
3.4.1.13. Case 1 input file "intopogr.fil":
# file intopogr.fil
 2 2
-1000 +1000
-1000 +1000
 500 500
 500 500
# end of file
```

3.4.1.14. Case 1 input file "intrchem.fil":

```
# file intrchem.fil
conservative
# end of file
```

3.4.2. Case 2 Input Data Files

Case 2 also requires fourteen input files (the same list as for Case 1):

```
incondrk.fil ininsalt.fil inoutfrq.fil insnsors.fil intopogr.fil ingridth.fil inintemp.fil inrkigpr.fil insorcms.fil intrchem.fil ininpres.fil inintrcr.fil inrkvolp.fil intimscl.fil
```

and these files are identical to the corresponding files for Case 1, except for file "*inrkvolp.fil*". For Case 2, the last two numerical entries in this file (the "hydraulic dispersion coefficients" for dissolved materials and for heat) are both set to nonzero values (8 meters) whereas both were zero in Case 1. All other input specifications are identical to Case 1.

3.4.2.1. Case 2 input file "inrkvolp.fil":

```
# file inrkvolp.fil
2800 1000 0.3 0 8 8
# end of file
```

3.4.3. Case 3 Input Data Files

Case 3 requires fifteen input files. Fourteen of these are identical to those used for Case 1 (note - *not* Case 2):

```
incondrk.fil ininsalt.fil inoutfrq.fil insnsors.fil intopogr.fil ingridth.fil inintemp.fil inrkigpr.fil insorcms.fil intrchem.fil ininpres.fil inintrcr.fil inrkvolp.fil intimscl.fil
```

and in addition file "inmincnd.fil" must be included to specify the parameters for the non-equilibrium "conductive MINC" model for heat exchange between the fluid and the solid rock:

3.4.3.1. Case 3 input file "inmincnd.fil":

3.4.4. Case 4 Input Data Files

```
Two-dimensional Cases 4 and 5 both require fifteen ASCII input files:
    incondrk.fil
              ininsalt.fil
                       inrkigpr.fil
                                 insorcen.fil
                                          intopogr.fil
    ingridth.fil
              inintemp.fil
                       inrkvolp.fil
                                 insorcms.fil
                                          inwelflo.fil
    ininpres.fil
              inoutfrq.fil
                       insnsors.fil
                                 intimscl.fil
                                          inwelgeo.fil
For Case 4, the contents of these files are as follows (in alphabetical order):
3.4.4.1. Case 4 input file "incondrk.fil":
# file incondrk.fil
2. 0
# end of file
3.4.4.2. Case 4 input file "ingridth.fil":
# file ingridth.fil
20 20 20 20 20 20 20 20 20 20 20
    # blank line
20 20 20 20 20 20 20 20 20 20 20
    # blank line
100
    # blank line
510 510 50
           0 -2000
    0
0 0 0
 1 20
      1
         1
            1
              1
 1 17
       2
         2 1
              1
 1 14
      3
            1
              1
 1 13
      4
              1
         4
           1
 1 11
       5
         5
            1
              1
```

8 [64 similar lines skipped here]

1

1

```
45 51 44 44
                  1
              1
 44 51 45 45
                  1
              1
 42 51 46 46
                  1
 41 51 47 47
                  1
              1
 39 51 48 48
              1
 38 51 49 49
 35 51 50 50
 32 51 51 51
# end of file
```

6 6

7 7 1 1

8

1 10

7

1 8

1

```
3.4.4.3. Case 4 input file "ininpres.fil":
# file ininpres.fil
20.e+06
# end of file
3.4.4.4. Case 4 input file "ininsalt.fil":
# file ininsalt.fil
0.036
# end of file
3.4,4,5, Case 4 input file "inintemp.fil":
# file inintemp.fil
200
# end of file
3.4,4,6, Case 4 input file "inoutfrq.fil":
# file inoutfrq.fil
# P, T, S snapshots and well summaries
days
list
days
0.0625 0.125 0.25 0.5 1 2 8
end
# tracer snapshots
end
# permeability snapshots
end
# fracture patch apertures
end
# electrical snapshots
end
# restart dumps
# end of file
```

3.4.4.7. Case 4 input file "inrkigpr.fil":

```
# file inrkigpr.fil
50.e-15
# end of file
```

3.4.4.8. Case 4 input file "inrkvolp.fil":

```
# file inrkvolp.fil
2600 1000 0.1 1.e-08 0 0
# end of file
```

3.4,4,9, Case 4 input file "insensrs.fil":

```
# file insensrs.fil
        100
  0
              -2000
  70.7
         70.7 -2000
 100
          0
               -2000
  70.7 -70.7
              -2000
  0 -100
               -2000
 -70.7 -70.7
              -2000
-100
          0
               -2000
        70.7
 -70.7
              -2000
  0
        200
               -2000
 141.4 141.4 -2000
 200
          0
               -2000
 141.4 -141.4
              -2000
  0
      -200
               -2000
-141.4 -141.4
               -2000
-200
               -2000
          0
-141.4 141.4 -2000
# end of file
```

3.4.4.10. Case 4 input file "insorcen.fil":

```
# file insorcen.fil
21 21 1 1 1 1
                   -1.e+10
2.e+06
       -1.e+04
                            0.
22 22 1 1 1 1
                   -1.e+10
2.e+06
         -1.e+04
                            0.
23 23 1 1 1 1
2.e+06
         -1.e+04
                   -1.e+10
24 24 1
         1 1 1
2.e+06
         -1.e+04
                   -1.e+10
                            0.
25 25 1 1 1 1
2.e+06 -1.e+04
                   -1.e+10
                            0.
26 26 1 1 1 1
         -1.e+04
2.e+06
                   -1.e+10
                            0.
27 27 1 1 1 1
2.e+06
         -1.e+04
                   -1.e+10
                            0.
28 28 1 1 1 1
2.e+06
         -1.e+04
                   -1.e+10
                            0.
29 29 1 1 1 1
2.e+06
         -1.e+04
                   -1.e+10
                            0.
30 30 1 1 1 1
2.e+06 -1.e+04
                            0.
                   -1.e+10
31 31 1 1 1 1
2.e+06
         -1.e+04
                   -1.e+10
                            0.
18 18 2 2 1 1
2.e+06
       -1.e+04
                   -1.e+10
19 19 2 2 1 1
         -1.e+04
                   -1.e+10
                            0.
2.e+06
20 20 2 2 1 1
2.e+06
         -1.e+04
                   -1.e+10
32 32 2 2 1 1
2.e+06
         -1.e+04
                   -1.e+10
                            0.
[244 similar lines skipped here]
24 24 51 51
             1 1
2.e+06
       -1.e+04
                   -1.e+10
                            0.
25 25 51 51 1 1
2.e+06
         -1.e+04
                   -1.e+10
                            0.
26 26 51 51 1 1
2.e+06
         -1.e+04
                   -1.e+10
                            0.
27 27 51 51 1 1
2.e+06
        -1.e+04
                   -1.e+10
                            0.
28 28 51 51 1 1
2.e+06
         -1.e+04
                   -1.e+10
                            0.
29 29 51 51 1 1
2.e+06
         -1.e+04
                   -1.e+10
30 30 51 51 1 1
         -1.e+04
2.e+06
                   -1.e+10
                            0.
31 31 51 51 1 1
2.e+06
         -1.e+04
                   -1.e+10
# end of file
```

3.4.4.11. Case 4 input file "insorcms.fil":

```
# file insorcms.fil
21 21 1 1
             1
200. -1.e-05
             0
                0
                   837356.6 0.036
22 22 1 1
             1
               1
200. -1.e-05
                   837356.6 0.036
             0
                0
23 23 1 1
             1
               1
200. -1.e-05
             0 0
                   837356.6 0.036
24 24 1 1
             1
200. -1.e-05
                   837356.6 0.036
             0
                0
25 25 1
          1
             1 1
200. -1.e-05
                0
                   837356.6 0.036
             0
             1 1
26 26 1 1
200. -1.e-05
             0
                0
                   837356.6 0.036
27 27 1 1
             1
               1
200. -1.e-05
             0 0
                   837356.6 0.036
28 28 1 1
             1
                1
200. -1.e-05
                0
                  837356.6 0.036
             0
29 29 1 1
             1 1
200. -1.e-05
             0
                0
                   837356.6 0.036
30 30 1 1
             1 1
200. -1.e-05
                0
                  837356.6 0.036
             0
31 31 1 1
             1
200. -1.e-05
                   837356.6 0.036
            0
                0
18 18 2 2
                1
             1
200. -1.e-05
                   837356.6 0.036
             0 0
19 19 2 2
             1 1
200. -1.e-05
             0 0
                  837356.6 0.036
20 20 2 2
             1
               1
200. -1.e-05
            0 0
                   837356.6 0.036
32 32 2 2
             1
                1
200. -1.e-05
                   837356.6 0.036
             0
                0
[244 similar lines skipped here]
24 24 51 51
             1
               1
200. -1.e-05
               0
                   837356.6 0.036
             0
25 25 51 51
             1
                1
200. -1.e-05
            0 0
                   837356.6 0.036
26 26 51 51
             1 1
200. -1.e-05
             0
                0
                   837356.6 0.036
27 27 51 51
             1 1
200. -1.e-05
             0 0
                   837356.6 0.036
28 28 51 51
             1
200. -1.e-05
            0 0
                   837356.6 0.036
29 29 51 51
             1 1
200. -1.e-05
             0 0
                   837356.6 0.036
30 30 51 51
             1 1
200. -1.e-05
             0 0
                   837356.6 0.036
31 31 51 51
             1 1
200. -1.e-05 0 0 837356.6 0.036
# end of file
```

```
3.4.4.12. Case 4 input file "intimscl.fil":
# file intimscl.fil
4000
days
1000
days
0 6
1 5
2
  4
3 3
4 2
5 1
6 0
# end of file
3.4.4.13. Case 4 input file "intopogr.fil":
# file intopogr.fil
 2 2
-1000 +1000
-1000 +1000
 500 500
 500 500
# end of file
3.4.4.14. Case 4 input file "inwelflo.fil":
# file inwelflo.fil
well 1
produce 100.
pressure 5.e+06
# end of file
3.4.4.15. Case 4 input file "inwelgeo.fil":
# file inwelgeo.fil
 wellhead
 0.
     0.
                                  # wellhead
 -2000.
                                  # datum level elevation
                                  # skin factor
 0.
 conductive
                                      # electrical
 cemented
                                      # hydraulic
  .300
                                      # diameter
      0.
                      -1950.
                                  # uncased section begins
 insulated
                                      # electrical
 uncemented
                                      # hydraulic
  .300
                                      # diameter
 0 -
      0.
                      -2050.
                                  # bottomhole
# end of file
```

3.4.5. Case 5 Input Data Files

For Case 5, most of the problem specifications are the same as for Case 4, except that the central production well of Case 4 is instead a fluid injection well. Therefore, the Case 4 "inwelflo.fil" input file becomes, for Case 5:

3.4.5.1. Case 5 input file "inwelflo.fil":

file inwelflo.fil
well 1
inject 100.
pressure 5.e+07
salinity 0.048
enthalpy 420.e+03
end of file

3.4.6. Case 6 Input Data Files

Specification of the final and most complicated illustrative problem (three-dimensional Case 6) requires 24 ASCII input data files:

```
inelprds.fil
inaquifr.fil
                            ingridth.fil
                                           inrgstrs.fil
                                                          intopogr.fil
inblintr.fil
              infpdata.fil
                            ininhydr.fil
                                           inrkigpr.fil
                                                          intrchem.fil
              infpprms.fil inintrcr.fil
incondrk.fil
                                           inrkvolp.fil
                                                          inwelflo.fil
              ingridek.fil
inecnbgr.fil
                             inminend.fil insorcen.fil
                                                          inwelgeo.fil
inelpram.fil
             ingridte.fil
                             inoutfrg.fil
                                           intimscl.fil
```

The contents of these files are as follows (in alphabetical order):

3.4.6.1. Case 6 input file "inaquifr.fil":

```
# file inaquifr.fil
# Specification of "aquifer boundaries".
# Face at minimum value of "x"
all
dirichlet
20 8000 200.+05 200 0.04 100.+08 40.+08 0.04 1.-15
# Face at maximum value of "x"
all
dirichlet
20 8000 200.+05 200 0.04 100.+08 40.+08 0.04 1.-15
# Face at minimum value of "y"
all
dirichlet
20 8000 200.+05 200 0.04 100.+08 40.+08 0.04 1.-15
# Face at maximum value of "y"
all
dirichlet
20 8000 200.+05 200 0.04 100.+08 40.+08 0.04 1.-15
# Face at minimum value of "z"
none
# Face at maximum value of "z"
all
dirichlet
16 3000 100.+05 100 .005 100.+08 40.+08 0.04 1.-15
# end of file
```

```
3.4.6.2. Case 6 input file "inblintr.fil":
# file inblintr.fil
11 14 14
```

17 14 14

14 11 14

14 17 14

14 14 14

end of file

3.4.6.3. Case 6 input file "incondrk.fil":

```
# file incondrk.fil
```

3. 0

end of file

3.4.6.4. Case 6 input file "inecnbgr.fil":

```
# file inecnbgr.fil
```

.01

end of file

3.4.6.5. Case 6 input file "inelpram.fil":

file inelpram.fil

1.5 4. .001 .009 0.

budiansky

end of file

3.4.6.6, Case 6 input file "inelprds.fil":

file inelprds.fil

1

end of file

3.4.6.7. Case 6 input file "infpdata.fil":

```
# file infpdata.fil
                           Azi-
#
                                            Zero- Turbulent
#
    Patch center location
                           muth Dip r0
                                           stress effective
#
    East
           North
                      ASL
                           (dg)(dg)(m)
                                         aperture
                                                   ap limit
Begin Class 1 fracture patches
13000.00 16000.00 -2000.00
                             45
                                 45
                                     60
                                          318.0-06
                                                    800.-06
13000.00 16000.00 -2000.00
                                 45
                            225
                                     60
                                          318.0-06
                                                    800.-06
13000.00 16000.00 -2000.00
                                 45
                                     60
                                                    800.-06
                            135
                                          318.0-06
13000.00 16000.00 -2000.00
                            315
                                 45
                                     60
                                          318.0-06
                                                    800.-06
          # blank line
Begin Class 2 fracture patches
13000.00 16000.00 -1915.15
                                 45
                                                    800.-06
                              0
                                     30
                                          159.0-06
13000.00 16000.00 -1915.15
                             90
                                 45
                                     30
                                                    800.-06
                                          159.0-06
13000.00 16000.00 -1915.15
                            180
                                 45
                                     30
                                          159.0-06
                                                    800.-06
13000.00 16000.00 -1915.15
                            270
                                 45
                                     30
                                          159.0-06
                                                    800.-06
12940.00 15940.00 -2000.00
                                 45
                                     30
                                          159.0-06
                                                    800.-06
                              0
12940.00 15940.00 -2000.00
                             90
                                 45
                                     30
                                          159.0-06
                                                    800.-06
12940.00 15940.00 -2000.00
                            180
                                 45
                                     30
                                          159.0-06
                                                    800.-06
12940.00 15940.00 -2000.00
                            270
                                 45
                                     30
                                          159.0-06
                                                    800.-06
13060.00 15940.00 -2000.00
                              0
                                 45
                                     30
                                          159.0-06
                                                    800.-06
13060.00 15940.00 -2000.00
                             90
                                 45
                                     30
                                                    800.-06
                                          159.0-06
13060.00 15940.00 -2000.00
                            180
                                 45
                                     30
                                          159.0-06
                                                    800.-06
                                                    800.-06
13060.00 15940.00 -2000.00
                            270
                                 45
                                     30
                                          159.0-06
12940.00 16060.00 -2000.00
                              0
                                 45
                                     30
                                          159.0-06
                                                    800.-06
                             90
12940.00 16060.00 -2000.00
                                 45
                                     30
                                                    800.-06
                                          159.0-06
12940.00 16060.00 -2000.00
                            180
                                 45
                                     30
                                          159.0-06
                                                    800.-06
12940.00 16060.00 -2000.00
                            270
                                 45
                                     30
                                          159.0-06
                                                    800.-06
13060.00 16060.00 -2000.00
                                          159.0-06
                                 45
                                     30
                                                    800.-06
                              0
                                                    800.-06
13060.00 16060.00 -2000.00
                             90
                                 45
                                     30
                                          159.0-06
13060.00 16060.00 -2000.00
                            180
                                 45
                                     30
                                          159.0-06
                                                    800.-06
13060.00 16060.00 -2000.00
                            270
                                 45
                                     30
                                          159.0-06
                                                    800.-06
13000.00 16000.00 -2084.85
                                 45
                              0
                                     30
                                          159.0-06
                                                    800.-06
13000.00 16000.00 -2084.85
                             90
                                 45
                                     30
                                          159.0-06
                                                    800.-06
                                                    800.-06
13000.00 16000.00 -2084.85
                                 45
                                     30
                            180
                                          159.0-06
13000.00 16000.00 -2084.85
                            270
                                 45
                                     30
                                          159.0-06
                                                    800.-06
         # blank line
Begin Class 3 fracture patches
13000.00 16000.00 -2040.00
                             45
                                 90
                                     15
                                           79.5-06
                                                    800.-06
13000.00 16000.00 -2040.00
                                 90
                                     15
                                           79.5-06
                                                    800.-06
                            135
13028.28 15971.72 -2000.00
                                     15
                                                    800.-06
                             45
                                 90
                                           79.5-06
13028.28 15971.72 -2000.00
                            135
                                 90
                                     15
                                           79.5-06
                                                    800.-06
12971.72 15971.72 -2000.00
                                     15
                                           79.5-06
                                                    800.-06
                             45
                                 90
12971.72 15971.72 -2000.00
                            135
                                 90
                                     15
                                           79.5-06
                                                    800.-06
13028.28 16028.28 -2000.00
                             45
                                 90
                                     15
                                           79.5-06
                                                    800.-06
                                     15
13028.28 16028.28 -2000.00
                                 90
                                           79.5-06
                                                    800.-06
                            135
12971.72 16028.28 -2000.00
                                                    800.-06
                             45
                                 90
                                     15
                                           79.5-06
12971.72 16028.28 -2000.00
                            135
                                 90
                                     15
                                           79.5-06
                                                    800.-06
```

```
13000.00 16000.00 -1960.00
                                         15
                                                79.5-06
                                                         800.-06
                                45
                                     90
13000.00 16000.00 -1960.00
                               135
                                         15
                                               79.5-06
                                                         800.-06
                                     90
13000.00 15943.43 -2040.00
                                45
                                     90
                                         15
                                                79.5-06
                                                         800.-06
13000.00 15943.43 -2040.00
                                         15
                                                79.5-06
                                                         800.-06
                               135
                                     90
13056.57 16000.00 -2040.00
                                45
                                     90
                                         15
                                               79.5-06
                                                         800.-06
13056.57 16000.00 -2040.00
                               135
                                     90
                                         15
                                               79.5-06
                                                         800.-06
12943.43 16000.00 -2040.00
                                45
                                     90
                                         15
                                                79.5-06
                                                         800.-06
12943.43 16000.00 -2040.00
                               135
                                     90
                                         15
                                               79.5-06
                                                         800.-06
13000.00 16056.57 -2040.00
                                         15
                                                         800.-06
                                45
                                     90
                                                79.5-06
13000.00 16056.57 -2040.00
                               135
                                     90
                                         15
                                                79.5-06
                                                         800.-06
13000.00 15943.43 -1960.00
                                45
                                     90
                                         15
                                               79.5-06
                                                         800.-06
13000.00 15943.43 -1960.00
                               135
                                     90
                                         15
                                               79.5-06
                                                         800.-06
13056.57 16000.00 -1960.00
                                45
                                     90
                                         15
                                               79.5-06
                                                         800.-06
13056.57 16000.00 -1960.00
                                         15
                                                79.5-06
                               135
                                     90
                                                         800.-06
[1654 similar lines skipped here]
13197.99 16141.42 -1840.00
                                45
                                     90
                                         15
                                               79.5-06
                                                         800.-06
13197.99 16141.42 -1840.00
                               135
                                     90
                                         15
                                                79.5-06
                                                         800.-06
12802.01 15858.58 -1840.00
                                45
                                     90
                                         15
                                               79.5-06
                                                         800.-06
12802.01 15858.58 -1840.00
                               135
                                     90
                                         15
                                               79.5-06
                                                         800.-06
13141.42 16197.99 -1840.00
                                     90
                                         15
                                               79.5-06
                                                         800.-06
                                45
13141.42 16197.99 -1840.00
                               135
                                     90
                                         15
                                               79.5-06
                                                         800.-06
12802.01 16141.42 -1840.00
                                45
                                     90
                                         15
                                                79.5-06
                                                         800.-06
12802.01 16141.42 -1840.00
                                         15
                                                79.5-06
                                                         800.-06
                               135
                                     90
12858.58 16197.99 -1840.00
                                45
                                     90
                                         15
                                               79.5-06
                                                         800.-06
12858.58 16197.99 -1840.00
                                     90
                                         15
                                               79.5-06
                                                         800.-06
                               135
13084.85 15858.58 -1760.00
                                         15
                                                79.5-06
                                                         800.-06
                                45
                                     90
13084.85 15858.58 -1760.00
                                         15
                                                         800.-06
                               135
                                     90
                                               79.5-06
13141.42 15915.15 -1760.00
                                45
                                     90
                                         15
                                                79.5-06
                                                         800.-06
                                                79.5-06
13141.42 15915.15 -1760.00
                               135
                                     90
                                         15
                                                         800.-06
12915.15 15858.58 -1760.00
                                45
                                     90
                                         15
                                               79.5-06
                                                         800.-06
12915.15 15858.58 -1760.00
                               135
                                     90
                                         15
                                               79.5-06
                                                         800.-06
13141.42 16084.85 -1760.00
                                     90
                                         15
                                               79.5-06
                                                         800.-06
                                45
13141.42 16084.85 -1760.00
                               135
                                     90
                                         15
                                                79.5-06
                                                         800.-06
12858.58 15915.15 -1760.00
                                45
                                     90
                                         15
                                                79.5-06
                                                         800.-06
12858.58 15915.15 -1760.00
                               135
                                     90
                                         15
                                                79.5-06
                                                         800.-06
13084.85 16141.42 -1760.00
                                45
                                     90
                                         15
                                               79.5-06
                                                         800.-06
13084.85 16141.42 -1760.00
                               135
                                     90
                                         15
                                               79.5-06
                                                         800.-06
12858.58 16084.85 -1760.00
                                     90
                                         15
                                               79.5-06
                                                         800.-06
                                45
12858.58 16084.85 -1760.00
                                                         800.-06
                               135
                                     90
                                         15
                                                79.5-06
12915.15 16141.42 -1760.00
                                45
                                     90
                                         15
                                                79.5-06
                                                         800.-06
12915.15 16141.42 -1760.00
                                         15
                                                         800.-06
                               135
                                     90
                                               79.5-06
13056.57 15943.43 -1720.00
                                     90
                                         15
                                               79.5-06
                                                         800.-06
                                45
13056.57 15943.43 -1720.00
                               135
                                     90
                                         15
                                               79.5-06
                                                         800.-06
12943.43 15943.43 -1720.00
                                45
                                     90
                                         15
                                                79.5-06
                                                         800.-06
12943.43 15943.43 -1720.00
                                         15
                                                79.5-06
                                                         800.-06
                               135
                                     90
13056.57 16056.57 -1720.00
                                                         800.-06
                                45
                                     90
                                         15
                                               79.5-06
13056.57 16056.57 -1720.00
                               135
                                     90
                                         15
                                               79.5-06
                                                         800.-06
12943.43 16056.57 -1720.00
                                45
                                     90
                                         15
                                               79.5-06
                                                         800.-06
12943.43 16056.57 -1720.00
                               135
                                     90
                                         15
                                               79.5-06
                                                         800.-06
# end of file
```

```
3.4.6.8. Case 6 input file "infpprms.fil":
```

```
# file infpprms.fil
6.0e+10
         # Youngs modulus, pa
             # shear modulus, pa
 2.4e+10
# basic friction angle, shear dilation angle,
     90% closure stress, cohesion
# Class 1:
40. 3. 30.e+06
                    0.
# Class 2:
40. 3. 30.e+06
# Class 3:
40. 3. 30.e+06
                    0.
# end of file
3.4.6.9. Case 6 input file "ingridek.fil":
# file ingridek.fil
70 60 55 50 45 40 35 30 25
20 20 20 20 20 20 20 20 20
```

25 30 35 40 45 50 55 60 70 # blank line

70 60 55 50 45 40 35 30 25 20 20 20 20 20 20 20 20 20

25 30 35 40 45 50 55 60 70

blank line

70 60 55 50 45 40 35 30 25

20 20 20 20 20 20 20 20 20

25 30 35 40 45 50 55 60 70

blank line

500 500 500

13000 16000 -2000

45 0 0

end of file

```
3.4.6.10. Case 6 input file "ingridte.fil":
```

```
# file ingridte.fil
# blank line
# blank line
# blank line
3000 3000 2100
13000 16000 -2000
0 0 0
# end of file
```

3.4.6.11. Case 6 input file "ingridth.fil":

```
# file ingridth.fil
70 60 55 50 45 40 35 30 25
20 20 20 20 20 20 20 20 20
25 30 35 40 45 50 55 60 70
     # blank line
70 60 55 50 45 40 35 30 25
20 20 20 20 20 20 20 20 20
25 30 35 40 45 50 55 60 70
     # blank line
70 60 55 50 45 40 35 30 25
20 20 20 20 20 20 20 20 20
25 30 35 40 45 50 55 60 70
     # blank line
500 500 500
13000 16000 -2000
45 0 0
# end of file
```

3.4.6.12. Case 6 input file "ininhydr.fil":

```
# file ininhydr.fil
13000 16000 -2000 300.e+05
-2500 210 0.04
-1500 190 0.04
# end of file
```

```
3.4.6.13 Case 6 input file "inintrer.fil":
# file inintrcr.fil
# end of file
3.4.6.14. Case 6 input file "inminend.fil":
# file inmincnd.fil
15
1.e+06
1.e+07
1.e + 08
1.e+09
     # blank line
1. 1. 1. 1. 1.
# end of file
3.4.6.15. Case 6 input file "inoutfrq.fil":
# file inoutfrq.fil
# P, T, S snapshots and well summaries
days
10
list
days
 0.03125 0.0625 0.125 0.25 0.5 1 2 4
10.03125 10.0625 10.125 10.25 10.5 11 12 14
40.03125 40.0625 40.125 40.25 40.5 41 42 44
end
# tracer snapshots
days
10
list
days
 0.03125 0.0625 0.125 0.25 0.5 1 2 4
10.03125 10.0625 10.125 10.25 10.5 11 12 14
40.03125 40.0625 40.125 40.25 40.5 41 42 44
end
# permeability snapshots
days
10
list
days
0.03125 0.0625 0.125 0.25 0.5 1 2 4
10.03125 10.0625 10.125 10.25 10.5 11 12 14
40.03125 40.0625 40.125 40.25 40.5 41 42 44
end
# fracture patch apertures
```

```
steps
1
end
# electrical snapshots
10
list
days
0.03125 0.0625 0.125 0.25 0.5 1 2 4
10.03125 10.0625 10.125 10.25 10.5 11 12 14
40.03125 40.0625 40.125 40.25 40.5 41 42 44
end
# restart dumps
steps
5
end
# end of file
3.4.6.16. Case 6 input file "inrgstrs.fil":
# file inrgstrs.fil
  9000 17000
               12000 20000
                               -7000 +3000
  80.e+06 80.e+06 120.e+06
                                    0
                                         0
  80.e+06 80.e+06 120.e+06
                               0
                                    0
                                         0
  80.e+06 80.e+06 120.e+06
                               0
                                    0
                                         0
  80.e+06
           80.e+06 120.e+06
                               0
                                    0
                                         0
```

0 (# end of file

```
3.4,6,17. Case 6 input file "inrkigpr.fil":
# file inrkigpr.fil
1.e-15
# end of file
3.4.6.18. Case 6 input file "inrkvolp.fil":
# file inrkvolp.fil
2500.
         1000. 0.04
                                    0.
                                            0.
                           1.e-08
# end of file
3.4.6.19. Case 6 input file "insorcen.fil":
# file insorcen.fil
  1 27 1 27 1
 +857.142e-06 0. 0.
  1 27 1 27 27 27
 -857.142e-06 0. 0. 0.
# end of file
3.4.6.20. Case 6 input file "intimscl.fil":
# file intimscl.fil
# Maximum steps
500
# Maximum calculated time
days
400
# Maximum stepsize
hours
48
# Timestep variations
   0 5
   1
      3
      2
   7
      1
   8
      0
# end of file
```

3.4.6.21. Case 6 input file "intopogr.fil":

- # file intopogr.fil
- # Size of topographic data array
 121 121
- # Locations of topographic data points in meters East 10000. 10100. 10150. 10200. 10050. 10250. 10300. 10350. 10400. 10450. 10500. 10550. 10600. 10650. 10700. 10750. 10800. 10850. 10900. 10950. 11000. 11050. 11100. 11150. 11200. 11250. 11300. 11350. 11400. 11450. 11500. 11550. 11650. 11700. 11750. 11800. 11850. 11900. 11950. 11600. 12000. 12050. 12100. 12150. 12200. 12250. 12300. 12350. 12550. 12600. 12650. 12400. 12450. 12500. 12700. 12750. 12950. 13000. 13050. 12800. 12850. 12900. 13100. 13150. 13200. 13250. 13300. 13350. 13400. 13450. 13500. 13550. 13600. 13650. 13700. 13750. 13800. 13850. 13900. 13950. 14000. 14050. 14100. 14150. 14200. 14250. 14300. 14350. 14400. 14450. 14500. 14550. 14600. 14650. 14700. 14750. 14900. 14950. 15000. 14800. 14850. 15050. 15100. 15150. 15250. 15350. 15400. 15200. 15300. 15450. 15500. 15550. 15600. 15650. 15700. 15750. 15800. 15850. 15900. 15950. 16000.
- # Locations of topographic data points in meters North 13000. 13050. 13100. 13150. 13200. 13250. 13300. 13350. 13450. 13400. 13500. 13550. 13600. 13650. 13700. 13750. 13800. 13850. 13900. 13950. 14000. 14050. 14100. 14150. 14400. 14200. 14250. 14300. 14350. 14450. 14500. 14550. 14600. 14650. 14700. 14750. 14800. 14850. 14900. 14950. 15150. 15200. 15000. 15050. 15100. 15250. 15300. 15350. 15400. 15450. 15500. 15550. 15600. 15650. 15700. 15750. 15850. 15900. 15950. 16000. 16050. 16100. 15800. 16150. 16250. 16350. 16400. 16450. 16500. 16200. 16300. 16550. 16600. 16650. 16700. 16750. 16800. 16850. 16900. 16950. 17000. 17050. 17100. 17150. 17200. 17250. 17300. 17350. 17400. 17450. 17500. 17550. 17600. 17650. 17700. 17750. 17800. 17850. 17900. 17950. 18000. 18050. 18100. 18150. 18200. 18250. 18300. 18350. 18400. 18450. 18500. 18550. 18650. 18750. 18800. 18600. 18700. 18850. 18900. 18950. 19000.

```
# Topographic data values (meters above sea level)
# 13000 m N to 19000 m N at 10000 m E
                            560.93
                                                               525.00
  540.71
           551.17
                   559.50
                                     558.12
                                             543.71
                                                      525.30
  524.42
           533.09
                   548.42
                            550.00
                                     552.59
                                             560.82
                                                      572.87
                                                               585.21
  588.17
          580.33
                   564.99
                            547.38
                                     535.76
                                             525.20
                                                      527.46
                                                               543.63
  544.95
           528.20
                   528.18
                            548.08
                                     556.98
                                             547.44
                                                      541.82
                                                               540.37
                            557.60
                                                      549.32
  543.61
           549.07
                   556.61
                                     552.52
                                             546.50
                                                               547.93
  540.08
          524.74
                   512.85
                            502.98
                                     500.00
                                             501.26
                                                      497.95
                                                               503.11
  512.78
                   525.20
                                             521.27
                                                      517.43
           519.29
                            524.83
                                     526.30
                                                               523.84
  527.10
          527.03
                   528.18
                            543.55
                                     527.23
                                             525.32
                                                      518.05
                                                               535.06
  550.07
          560.84
                   564.16
                            564.86
                                     567.63
                                             572.33
                                                      586.43
                                                               585.88
  586.84
           563.41
                   546.38
                            548.91
                                     558.29
                                             571.28
                                                      580.03
                                                               589.84
  588.66
           586.58
                   585.93
                            592.12
                                     594.04
                                             585.69
                                                      572.07
                                                               555.98
                   550.47
                                     572.05
                                             590.70
                                                      611.77
  550.60
           556.73
                            556.57
                                                               625.00
  623.22
          607.19
                   601.33
                            605.76
                                     620.77
                                             628.67
                                                      593.96
                                                               577.39
                   591.76
                                     642.22
  583.57
          582.26
                            618.26
                                             661.29
                                                      674.27
                                                               678.79
  679.89
          679.66
                   671.13
                            663.43
                                     653.92
                                             641.88
                                                      633.30
                                                               650.43
  662.74
# 13000 m N to 19000 m N at 10050 m E
  538.22
           550.42
                   557.26
                            558.70
                                     549.63
                                             532.37
                                                      524.44
                                                               524.31
  529.27
           541.64
                   551.82
                            559.34
                                     570.14
                                             579.26
                                                      588.18
                                                               591.48
                   562.59
                            542.12
                                                      526.41
  588.58
          577.26
                                     531.58
                                             525.21
                                                               531.40
  545.15
           546.76
                   550.05
                            559.38
                                     554.79
                                             548.47
                                                      544.17
                                                               545.20
  545.61
           551.94
                   555.93
                            558.26
                                     562.00
                                             558.84
                                                      551.14
                                                               540.96
  533.46
           526.65
                   514.06
                            503.06
                                     500.00
                                             500.00
                                                      500.00
                                                               500.64
  506.17
          520.13
                   525.00
                            525.00
                                     525.82
                                             522.44
                                                      518.74
                                                               525.54
                   532.09
                            547.69
                                     538.15
                                             527.98
                                                      530.59
  530.56
          528.17
                                                               539.50
  546.35
           547.03
                   554.67
                            560.15
                                     568.42
                                             574.35
                                                      585.04
                                                               587.03
  576.78
          556.98
                   545.48
                            553.96
                                     567.61
                                             574.08
                                                      577.16
                                                               587.97
  593.79
          593.57
                   594.30
                            593.78
                                     594.83
                                             581.74
                                                      576.45
                                                               553.68
  550.59
           550.00
                   550.00
                            552.97
                                     571.28
                                             578.68
                                                      594.48
                                                               607.72
  606.37
           605.69
                   601.65
                            600.65
                                     630.12
                                             622.21
                                                      578.31
                                                               581.33
  588.00
           583.87
                   588.38
                            617.48
                                     642.05
                                             661.57
                                                      675.04
                                                               679.29
  680.00
           679.65
                   673.29
                            666.05
                                     656.76
                                             645.02
                                                      633.82
                                                               640.13
  646.29
# etc.
  544.94
          552.45
                   560.73
                            554.05
                                     539.12
                                             527.00
                                                      526.84
                                                               535.26
  545.25
           551.85
                   563.15
                            570.10
                                     580.60
                                             590.03
                                                      599.32
                                                               594.91
  581.21
          568.24
                   553.98
                                     528.36
                                             525.29
                                                      525.03
                                                               526.75
                            533.98
                            567.54
  549.06
           559.43
                   562.20
                                     559.78
                                             551.53
                                                      557.81
                                                               561.80
  563.65
           563.83
                   556.78
                            553.65
                                     556.99
                                             553.55
                                                      549.78
                                                               540.10
  522.09
           517.17
                   510.21
                            501.10
                                     500.00
                                             501.39
                                                      500.93
                                                               500.36
                   524.76
  501.19
          520.77
                            525.00
                                     524.52
                                             524.62
                                                      522.04
                                                               524.56
                   530.11
                                     544.85
                                                      543.20
  529.72
          529.74
                            545.11
                                             541.63
                                                               544.94
                                                               580.47
  546.70
           549.79
                   556.41
                            563.73
                                     568.80
                                             572.96
                                                      582.16
  567.14
           552.55
                   545.64
                            553.07
                                     565.77
                                             575.00
                                                      580.24
                                                               586.41
  587.20
           584.00
                   580.78
                            581.96
                                     584.40
                                             587.18
                                                      574.60
                                                               551.65
                                     572.94
  550.00
          550.00
                   557.61
                            567.99
                                             575.00
                                                      576.80
                                                               589.90
  604.31
          603.98
                   599.88
                            612.02
                                     634.20
                                             626.68
                                                      602.61
                                                               600.56
  599.44
           591.66
                   588.64
                                     641.98
                                             659.93
                                                      671.97
                            619.85
                                                               678.83
  680.00
          680.74
                   675.81
                            669.31
                                     660.42
                                             649.84
                                                      632.76
                                                               636.73
  634.96
```

```
559.86
        559.73
                 559.15
                         551.44
                                  540.30
                                          534.69
                                                   541.84
                                                            560.69
572.84
        578.54
                 575.35
                         580.27
                                  589.86
                                           603.79
                                                   606.68
                                                            592.43
                 551.03
                                  530.29
                                                   525.10
                                                            537.29
576.06
        557.22
                         544.72
                                           525.00
549.91
                 570.47
                         576.67
                                  566.72
                                           564.18
                                                   570.08
                                                            575.75
        561.36
579.67
        577.21
                 564.61
                         550.73
                                  545.99
                                          539.10
                                                   533.12
                                                            523.79
516.93
        515.71
                 511.14
                         508.10
                                  508.21
                                           512.94
                                                   508.46
                                                            501.44
                         522.06
                                  523.60
                                           524.44
499.15
        506.88
                 517.51
                                                   524.01
                                                            524.83
527.50
        528.77
                 529.77
                         540.54
                                  550.85
                                          554.43
                                                   554.45
                                                            551.90
        560.14
547.80
                 569.23
                         569.65
                                  574.75
                                           585.90
                                                   588.74
                                                            580.64
                 549.22
                                                   577.28
567.54
        554.46
                         568.13
                                  568.89
                                           574.30
                                                            582.61
583.49
        580.20
                 580.38
                         576.48
                                  576.13
                                          577.67
                                                   569.56
                                                            558.01
                         577.36
548.95
        553.77
                 567.14
                                  575.00
                                           575.00
                                                   582.07
                                                            596.60
603.92
        604.02
                 592.13
                         629.44
                                  632.37
                                           602.80
                                                   605.84
                                                            607.87
618.22
        601.13
                 602.46
                         625.28
                                  643.78
                                                   665.78
                                           655.42
                                                            672.15
679.15
        680.06
                 677.85
                         672.95
                                  665.94
                                          648.60
                                                   636.63
                                                            638.39
636.72
```

[1840 similar lines skipped here]

1227.97 1246.55 1255.94 1256.64 1255.50 1254.39 1250.37 1241.04 1231.71 1226.38 1220.76 1214.05 1206.38 1200.98 1204.82 1213.40 1221.35 1224.23 1214.69 1210.00 1210.00 1210.19 1210.03 1214.38 1215.84 1221.16 1224.93 1227.36 1229.78 1223.79 1211.29 1202.77 1204.66 1180.22 1206.97 1211.86 1243.07 1262.38 1258.96 1260.64 1280.34 1312.13 1342.18 1359.06 1354.51 1332.22 1296.68 1262.33 1231.98 1212.49 1210.22 1217.53 1215.39 1194.21 1165.08 1138.35 1115.34 1094.10 1078.05 1064.77 1052.40 1040.97 1028.60 1015.75 979.55 967.45 955.26 943.79 1001.39 990.89 936.18 930.47 915.25 895.62 896.05 895.00 906.78 923.82 943.17 933.02 918.60 900.81 888.11 877.43 862.26 848.86 837.90 821.49 809.90 800.88 797.94 798.22 797.49 798.39 802.26 797.67 753.33 732.72 724.16 785.96 772.84 719.06 716.75 712.53 706.69 697.26 696.96 680.28 671.22 666.52 662.47 657.93 654.70 651.89 648.62 644.95 637.95 635.42 635.17 629.55 628.40 1211.78 1229.36 1227.60 1227.61 1233.30 1247.66 1246.65 1240.56 1235.16 1232.88 1227.90 1219.93 1211.26 1203.99 1202.92 1211.38 1218.97 1224.65 1217.22 1210.00 1210.00 1210.00 1210.01 1210.01 1209.34 1210.67 1214.21 1219.01 1219.84 1206.18 1201.04 1189.96 1199.20 1200.00 1207.49 1210.29 1235.20 1242.35 1243.22 1247.49 1263.21 1292.73 1324.45 1332.08 1330.18 1321.77 1298.29 1260.63 1220.26 1196.52 1196.77 1194.71 1188.01 1173.39 1148.36 1120.84 1097.43 1080.93 1065.50 1051.20 1041.23 1031.36 1019.88 1007.99 963.71 951.84 938.78 996.61 985.86 975.31 932.81 927.88 904.91 894.57 898.73 899.62 897.14 917.91 923.89 925.48 918.42 902.08 891.20 880.35 870.35 861.95 851.72 841.26 829.55 809.11 802.81 813.89 823.65 823.38 823.53 816.64 806.34 788.51 764.42 731.88 739.48 738.71 727.13 723.70 713.78 701.86 694.42 680.20 671.66 668.58 664.67 659.45 655.05 651.25 647.69 644.74 640.32 635.87 625.92 625.58 627.58

```
3.4.6.22. Case 6 input file "intrchem.fil":
# file intrchem.fil
conservative
# end of file
3.4.6.23. Case 6 input file "inwelflo.fil":
# file inwelflo.fil
# Situation at time = 0
well 1
 shut in
 well 2
 shut in
 well 3
 shut in
 well 4
 shut in
 well 5
 inject 100.
 pressure 5.0e+07
 salinity .0
 enthalpy 4.2d+05
 tracers 1.d-06
 well 6
 shut in
 well 7
 shut in
 well 8
 shut in
well 9
 shut in
# Changes at time = ten days
 time 864000.
well 5
 shut in
# Changes at time = forty days
 time 3456000.
well 1
 produce 25.
 pressure 2.e+07
 well 2
 produce 25.
 pressure 2.e+07
 well 3
 produce 25.
 pressure 2.e+07
```

well 4 produce 25. pressure 2.e+07 well 5 inject 100. pressure 4.0e+07 salinity .02 enthalpy 4.2d+05 tracers 0 well 6 produce 25. pressure 2.e+07 well 7 produce 25. pressure 2.e+07 well 8 produce 25. pressure 2.e+07 well 9 produce 25. pressure 2.e+07 # end of file

3.4.6.24. Case 6 input file "inwelgeo.fil":

```
# file inwelgeo.fil
##### WELL 1
wellhead
13000.000 15915.147
                          # wellhead
-2000.
                          # datum level elevation
 0.
                          # skin factor
conductive
                             # electrical
cemented
                             # hydraulic
  .300
                             # diameter
13000.000 15915.147
                     0
                          # casing diameter reduction
                             # electrical
conductive
cemented
                             # hydraulic
 .250
                             # diameter
13000.000 15915.147 -1930
                          # slotted liner begins
conductive
                             # electrical
uncemented
                             # hydraulic
 .250
                             # diameter
13000.000 15915.147 -1990
                          # uncased section begins
insulated
                             # electrical
                             # hydraulic
uncemented
 .250
                             # diameter
13000.000 15915.147 -2010
                          # slotted liner begins
conductive
                             # electrical
                             # hvdraulic
uncemented
 .250
                             # diameter
13000.000 15915.147 -2070
                          # slotted liner ends
conductive
                             # electrical
cemented
                             # hydraulic
 .250
                             # diameter
13000.000 15915.147 -2140
                          # bottomhole
##### WELL 2
wellhead
13042.426 15957.574
                          # wellhead
                          # datum level elevation
-2000.
 0.
                          # skin factor
conductive
                             # electrical
                             # hydraulic
cemented
 .300
                             # diameter
13042.426 15957.574
                     0
                          # casing diameter reduction
conductive
                             # electrical
cemented
                             # hydraulic
 .250
                             # diameter
13042.426 15957.574 -1930
                          # slotted liner begins
conductive
                             # electrical
                             # hydraulic
uncemented
```

```
.250
                             # diameter
13042.426 15957.574 -1990
                           # uncased section begins
insulated
                             # electrical
uncemented
                             # hydraulic
 .250
                             # diameter
13042.426 15957.574 -2010
                           # slotted liner begins
conductive
                             # electrical
uncemented
                             # hydraulic
 .250
                             # diameter
13042.426 15957.574 -2070
                           # slotted liner ends
                             # electrical
conductive
cemented
                             # hydraulic
 .250
                             # diameter
13042.426 15957.574 -2140
                           # bottomhole
##### WELL 3
wellhead
13084.853 16000.000
                           # wellhead
-2000.
                           # datum level elevation
                           # skin factor
 0.
conductive
                             # electrical
                             # hvdraulic
cemented
                             # diameter
 .300
13084.853 16000.000
                     0
                           # casing diameter reduction
conductive
                             # electrical
cemented
                             # hydraulic
 .250
                             # diameter
13084.853 16000.000 -1930
                           # slotted liner begins
conductive
                             # electrical
uncemented
                             # hydraulic
 .250
                             # diameter
13084.853 16000.000 -1990
                           # uncased section begins
insulated
                             # electrical
uncemented
                             # hydraulic
 .250
                             # diameter
13084.853 16000.000 -2010
                           # slotted liner begins
conductive
                             # electrical
                             # hydraulic
uncemented
 .250
                             # diameter
13084.853 16000.000 -2070
                           # slotted liner ends
conductive
                             # electrical
cemented
                             # hydraulic
 .250
                             # diameter
13084.853 16000.000 -2140
                           # bottomhole
##### WELL 4
wellhead
12957.574 15957.574
                           # wellhead
                           # datum level elevation
-2000.
 0.
                           # skin factor
```

```
conductive
                             # electrical
cemented
                             # hydraulic
 .300
                             # diameter
12957.574 15957.574
                          # casing diameter reduction
                     0
conductive
                             # electrical
cemented
                             # hydraulic
 .250
                             # diameter
12957.574 15957.574 -1930
                          # slotted liner begins
conductive
                             # electrical
                             # hydraulic
uncemented
 .250
                             # diameter
12957.574 15957.574 -1990
                          # uncased section begins
insulated
                             # electrical
uncemented
                             # hydraulic
 . 250
                             # diameter
12957.574 15957.574 -2010
                          # slotted liner begins
conductive
                             # electrical
                             # hydraulic
uncemented
 .250
                             # diameter
12957.574 15957.574 -2070
                          # slotted liner ends
                             # electrical
conductive
cemented
                             # hydraulic
                             # diameter
 .250
12957.574 15957.574 -2140
                          # bottomhole
##### WELL 5
wellhead
13000.00 16000.00
                          # wellhead
-2000.
                          # datum level elevation
 0.
                          # skin factor
                             # electrical
conductive
cemented
                             # hydraulic
 .300
                             # diameter
13000.00 16000.00
                          # casing diameter reduction
                    0.
conductive
                             # electrical
cemented
                             # hydraulic
 .250
                             # diameter
13000.00 16000.00 -1990.
                          # uncased section begins
insulated
                             # electrical
uncemented
                             # hydraulic
 .250
                             # diameter
                          # uncased section ends
13000.00 16000.00 -2010.
conductive
                             # electrical
cemented
                             # hydraulic
 .250
                             # diameter
13000.00 16000.00 -2140.
                          # bottomhole
##### WELL 6
wellhead
13042.426 16042.426
                          # wellhead
```

```
# datum level elevation
-2000.
 0.
                             # skin factor
                                # electrical
conductive
cemented
                                # hydraulic
  .300
                                # diameter
13042.426 16042.426
                             # casing diameter reduction
                       0
conductive
                                # electrical
cemented
                                # hydraulic
  .250
                                # diameter
13042.426 16042.426 -1930
                             # slotted liner begins
conductive
                                # electrical
uncemented
                                # hydraulic
  .250
                                # diameter
13042.426 16042.426 -1990
                             # uncased section begins
insulated
                                # electrical
uncemented
                                # hydraulic
  .250
                                # diameter
13042.426 16042.426 -2010
                             # slotted liner begins
conductive
                                # electrical
uncemented
                                # hydraulic
 .250
                                # diameter
13042.426 16042.426 -2070
                             # slotted liner ends
                                # electrical
conductive
cemented
                                # hydraulic
  .250
                                # diameter
13042,426 16042,426 -2140
                             # bottomhole
##### WELL 7
wellhead
12915.147 16000.000
                             # wellhead
-2000.
                             # datum level elevation
 0.
                             # skin factor
conductive
                                # electrical
cemented
                                # hydraulic
  .300
                                # diameter
12915.147 16000.000
                             # casing diameter reduction
                       0
conductive
                                # electrical
cemented
                                # hydraulic
  .250
                                # diameter
12915.147 16000.000 -1930
                             # slotted liner begins
conductive
                                # electrical
uncemented
                                # hydraulic
 .250
                                # diameter
12915.147 16000.000 -1990
                             # uncased section begins
insulated
                                # electrical
uncemented
                                # hydraulic
  .250
                                # diameter
12915.147 16000.000 -2010
                             # slotted liner begins
conductive
                                # electrical
uncemented
                                # hydraulic
  .250
                                # diameter
```

```
12915.147 16000.000 -2070
                          # slotted liner ends
conductive
                             # electrical
cemented
                             # hydraulic
 .250
                             # diameter
12915.147 16000.000 -2140
                          # bottomhole
##### WELL 8
wellhead
12957.574 16042.426
                          # wellhead
-2000.
                          # datum level elevation
                          # skin factor
 0.
conductive
                             # electrical
cemented
                             # hydraulic
                             # diameter
 .300
12957.574 16042.426
                          # casing diameter reduction
                     0
conductive
                             # electrical
                             # hydraulic
cemented
 .250
                             # diameter
12957.574 16042.426 -1930
                          # slotted liner begins
conductive
                             # electrical
uncemented
                             # hydraulic
 .250
                             # diameter
12957.574 16042.426 -1990
                          # uncased section begins
                             # electrical
insulated
uncemented
                             # hydraulic
 .250
                             # diameter
12957.574 16042.426 -2010
                          # slotted liner begins
conductive
                             # electrical
uncemented
                             # hydraulic
 .250
                             # diameter
12957.574 16042.426 -2070
                          # slotted liner ends
conductive
                             # electrical
cemented
                             # hydraulic
 .250
                             # diameter
12957.574 16042.426 -2140
                          # bottomhole
##### WELL 9
wellhead
13000.000 16084.853
                          # wellhead
-2000.
                          # datum level elevation
                          # skin factor
 0.
conductive
                             # electrical
cemented
                             # hydraulic
 .300
                             # diameter
13000.000 16084.853
                     0
                          # casing diameter reduction
conductive
                             # electrical
cemented
                             # hydraulic
                             # diameter
 .250
13000.000 16084.853 -1930
                          # slotted liner begins
conductive
                             # electrical
```

```
uncemented
                                  # hydraulic
  .250
                                  # diameter
 13000.000 16084.853 -1990
                               # uncased section begins
 insulated
                                  # electrical
uncemented
                                  # hydraulic
  .250
                                  # diameter
13000.000 16084.853 -2010
                               # slotted liner begins
conductive
                                  # electrical
                                  # hydraulic
uncemented
  .250
                                  # diameter
13000.000 16084.853 -2070
                               # slotted liner ends
conductive
                                  # electrical
cemented
                                  # hydraulic
  .250
                                  # diameter
13000.000 16084.853 -2140
                               # bottomhole
# end of file
```

4. REFERENCES

- Adams, J. C., W. S. Brainerd, J. T. Martin, B. T. Smith and J. L. Wagener (1992), Fortran 90 Handbook: Complete ANSI/ISO Reference, McGraw-Hill, New York.
- Biot, M.A. (1941), General theory of three dimensional consolidation. *Journal of Applied Physics* **12**, 155-164.
- Biot, M.A. and D.G. Willis (1957), The elastic coefficients of the theory of consolidation. *Journal of Applied Mechanics* **24**, 594-601.
- Bruel, D. (2007), Using the migration of the induced seismicity as a constraint for fractured Hot Dry Rock reservoir modeling. *Int. J. of Rock Mechanics & Mining Sciences* **44**, 1106–1117.
- Budiansky, B. (1970), Thermal and thermoelastic properties of isotropic composites, *J. Composite Materials 4*, pp. 286–295.
- Carslaw, H. S. and J. C. Jaeger (1959), Conduction of Heat in Solids, Second Edition, Clarendon Press.
- DOE (2008), An evaluation of enhanced geothermal systems technology, U.S. Department of Energy.
- Garg, S.K., D.H. Brownell Jr., and J.W. Pritchett (1977), Dilatancy-induced fluid migration and the velocity anomaly. *Journal of Geophysical Research* **82(5)**, 855-864.
- Garg, S.K. (1987), On balance laws for fluid-saturated porous media. *Mechanics of Materials* **6**, 219-232.
- Ghassemi, A., A. Nygren, and A. Cheng (2008), Effects of heat extraction on fracture aperture: a poro-thermoelastic analysis. *Geothermics* **37(5)**, 525-539.
- Ishido, T. and H. Mizutani (1981), Experimental and theoretical basis of electrokinetic phenomena in rock-water systems and its application to geophysics, *J. Geophys. Res.* **86**, pp. 1763–1775.
- Ishido, T., and J. W. Pritchett (1999), Numerical simulation of electrokinetic potentials associated with subsurface fluid flow, *J. Geophys. Res.* **104**, pp. 15247–15259.
- Ishido, T. and J. W. Pritchett (2000), Using numerical simulation of electrokinetic potentials in geothermal reservoir management, *Proc. World Geothermal Congress 2000*, Beppu-Morioka, Japan, pp. 2629–2634.
- Ishido, T., and J. W. Pritchett (2003), Characterization of fractured reservoirs using continuous self-potential measurements, *Proc.* 28th Workshop on Geothermal Reservoir Engineering, Stanford University.

- Kohl, T. and R.J. Hopkirk (1995), "FRACTure" a simulation code for forced fluid flow and transport in fractured, porous rock. *Geothermics* **24**, 333-343.
- Kohl, T., K.F. Evans, R.J. Hopkirk, and L. Rybach (1995), Coupled hydraulic, thermal, and mechanical considerations for the simulation of hot dry rock reservoirs. *Geothermics* **24**, 345-359.
- Kohl, T. and T. Megal (2005), Coupled hydro-mechanical modeling of the GPK3 reservoir stimulation at the European EGS site Soultz-sous-Forets, *Proc.* 30th Workshop on Geothermal Reservoir Engineering, Stanford University.
- Kohl, T. and T. Megal (2007), Predictive modeling of reservoir response to hydraulic stimulations at the European EGS site Soultz-sous-Forets, *Int. J. Rock Mechanics and Mining Sciences* **44**, 1118-1131.
- Matthews, C. S. and D. G. Russell (1967), Pressure Buildup and Flow Tests in Wells, Monograph Volume 1, Henry L. Doherty Series, Society of Petroleum Engineers.
- Morland, L.W. (1972), A simple constitutive theory for a fluid-saturated porous solid. *Journal of Geophysical Research* 77, 890-900
- Nakanishi, S., J. W. Pritchett and T. Tosha (2001), Changes in ground surface geophysical signals induced by geothermal exploitation computational studies based on a numerical reservoir model for the Oguni geothermal field, Japan. *Transactions Geothermal Resources Council* **25**, 657–664.
- Noorishad, J. and C.-F. Tsang (1996), ROCMAS simulator: a thermohydromechanical computer code. In O. Stephansson, L. Jing and C.-F. Tsang (Eds.), Coupled thermohydro-mechanical processes of fractured media, pp. 551-558. Elsevier.
- Pritchett, J. W. and S. K. Garg (1980), Determination of effective well-block radii for numerical reservoir simulations, *Water Resources Research* **16(4)**, pp. 665-674.
- Pritchett, J. W. and S. K. Garg (1990), On similitude, heat conduction and two-phase flow in fractured porous media, *Proc.* 15th Workshop on Geothermal Reservoir Engineering, Stanford University.
- Pritchett, J. W. (1995), STAR: a geothermal reservoir simulation system, *Proc. World Geothermal Congress* 1995, Florence, Italy.
- Pritchett, J. W. (1997), Efficient numerical simulation of nonequilibrium mass and heat transfer in fractured geothermal reservoirs, *Proc.* 22nd Workshop on Geothermal Reservoir Engineering, Stanford University.
- Pritchett, J. W. (2003), Verification and validation calculations using the STAR geophysical postprocessor suite. Report No. SAIC-03/1040, Science Applications International Corporation, San Diego, California.

- Pritchett, J. W. and T. Ishido (2005), Hydrofracture characterization using downhole electrical monitoring, *Proc. World Geothermal Congress 2005*, Antalya, Turkey.
- Pritchett, J. W. (2008), Guide to the SPFRAC simulator, Science Applications International Corp. Report to DOE, Award DE-FG36-04GO14291, September.
- Pritchett, J. W. and T. Ishido (2010), Numerical simulation of underground electrical signals caused by hydrofracturing operations, *Proc. World Geothermal Congress* 2010, Bali, Indonesia.
- Pritchett, J. W. (2012), Estimating "technical capacity" for geothermal electricity generation in the United States, *Geothermal Resources Council Transactions* **36.**
- Pruess, K., S. Finsterle, G. Moridis, C. Oldenburg and Y.-S. Wu (1997), General-purpose reservoir simulators: the TOUGH2 family, *GRC Bulletin*, February, 53–57.
- Rutqvist, J., L. Borgesson, M. Chijimatsu, A. Kobayashi, T.S. Nguyen, L. Jing, J. Noorishad, and C.-F. Tsang (2001), Thermohydromechanics of partially saturated geological media: governing equations and formulation of four finite element models. *International Journal of Rock Mechanics and Mining Sciences* **38**, 105-127.
- Schenk, O. and K. Gärtner (2004), Solving unsymmetric sparse systems of linear equations with PARDISO, *Journal of Future Generation Computer Systems*, **20(3):**475--487, 2004
- Schenk, O. and K. Gärtner (2006), On fast factorization pivoting methods for symmetric indefinite systems, *Elec. Trans. Numer. Anal.*, **23:**158--179, 2006
- Shook, G. N. and J. L. Renner (2002), An inverse model for TETRAD: preliminary results, *Geothermal Resources Council Transactions* **26**, 119-122.
- Tester, J. W. et al. (2006), The future of geothermal energy, Massachusetts Institute of Technology.
- USGS (2008), Assessment of moderate- and high-temperature geothermal resources of the United States, *USGS Fact Sheet 2008-3082*.